

Electronic Thesis and Dissertation Repository

---

5-28-2012 12:00 AM

## In-Vivo Investigation of the Medial Longitudinal Arch of the Foot and Orthotic Interactions using Bi-Planar Fluoroscopy

Megan E.R. Balsdon  
*The University of Western Ontario*

Supervisor  
Dr. Thomas R. Jenkyn  
*The University of Western Ontario*

Graduate Program in Mechanical and Materials Engineering  
A thesis submitted in partial fulfillment of the requirements for the degree in Master of Engineering Science  
© Megan E.R. Balsdon 2012

Follow this and additional works at: <https://ir.lib.uwo.ca/etd>



Part of the [Biomechanical Engineering Commons](#)

---

### Recommended Citation

Balsdon, Megan E.R., "In-Vivo Investigation of the Medial Longitudinal Arch of the Foot and Orthotic Interactions using Bi-Planar Fluoroscopy" (2012). *Electronic Thesis and Dissertation Repository*. 570. <https://ir.lib.uwo.ca/etd/570>

This Dissertation/Thesis is brought to you for free and open access by Scholarship@Western. It has been accepted for inclusion in Electronic Thesis and Dissertation Repository by an authorized administrator of Scholarship@Western. For more information, please contact [wlsadmin@uwo.ca](mailto:wlsadmin@uwo.ca).

# IN-VIVO INVESTIGATION OF THE MEDIAL LONGITUDINAL ARCH OF THE FOOT AND ORTHOTIC INTERACTIONS USING BI-PLANAR FLUOROSCOPY

(SPINE TITLE: MEDIAL ARCH AND FOOT ORTHOTICS USING BI-PLANAR FLUOROSCOPY)

(Thesis format: Integrated Article)

by

Megan Elizabeth Rene Balsdon

Department of Mechanical and Materials Engineering  
Graduate Program in Engineering Science

Submitted in partial fulfillment  
of the requirements for the degree of  
Master of Engineering Science

The School of Graduate and Postdoctoral Studies  
Western University  
London, Ontario, Canada  
June, 2012

© Megan Elizabeth Rene Balsdon 2012

WESTERN UNIVERSITY  
SCHOOL OF GRADUATE AND POSTDOCTORAL STUDIES

**CERTIFICATE OF EXAMINATION**

Supervisor

---

Dr. Thomas R. Jenkyn, Ph.D., PEng.  
Department of Mechanical & Materials Engineering  
School of Kinesiology

Examiners

---

Dr. James Johnson, Ph.D., PEng.  
Department of Mechanical & Materials Engineering

---

Dr. Robert Klassen, Ph.D.  
Department of Mechanical & Materials Engineering

---

Dr. Jim Dickey, Ph.D.  
School of Kinesiology

The thesis by  
**Megan Elizabeth Rene Balsdon** entitled:

**IN-VIVO INVESTIGATION OF THE MEDIAL LONGITUDINAL ARCH OF THE  
FOOT AND ORTHOTIC INTERACTIONS USING BI-PLANAR FLUOROSCOPY**

is accepted in partial fulfilment of the requirements for the degree of  
Master of Engineering Science

Date \_\_\_\_\_

\_\_\_\_\_  
Chair of the Thesis Examination Board

## **ABSTRACT**

Orthotic devices are a conservative treatment for common disorders of the foot and ankle such as pes planus and pes cavus. It is thought that orthotics change the kinematics of the foot by applying forces and constraint on the plantar surface, which can act to change body biomechanics and correct for malalignment in the legs and trunk. This thesis compares the angle of the medial longitudinal arch (MLA) between three foot types: pes planus (low arch), pes cavus (high arch) and normal arch, during barefoot and shoed walking, and walking with orthotics. In-vivo bi-planar fluoroscopy was used with markerless radiostereometric analysis (RSA) to measure an angle that defines the MLA with the greatest accuracy to date. MLA angles were significantly smaller ( $p < 0.05$ ) in the planus group with the foam casted hard orthotic compared to walking barefoot, and in the subtalar joint neutral position compared to barefoot standing amongst all participants.

**Keywords:** biomechanics, fluoroscopy, radiostereometric analysis (RSA), foot, orthotics, subtalar joint neutral

## ACKNOWLEDGEMENTS

I would like to thank those who helped put this project together: firstly, the Western Engineering Machine shop, specifically Chris Vandelaar and Steve Arnold who helped design and fabricate the wooden platform used to collect all study data. Another key person who helped with this project immensely is Colin Dombroski, the pedorthist who fitted and provided all of the participants with orthotics. Thank you so much for giving up your time and energy for this project, not to mention donating the supplies and manpower needed to make the devices. Thanks very much to John Henry for your enthusiasm throughout our project. We couldn't have asked for a better x-ray technician to guide our patients through the testing protocol.

Thanks to my supervisor, Tom Jenkyn, for your guidance throughout my time at Western. I am pleased that this project was available and I enjoyed the challenges involved in completing this research – thank you for this opportunity.

To Anne-Marie and Angela – you two were most helpful through this entire process, responding to emails quickly and with so much detail, which was very helpful given you both live miles away. I'm very grateful for the help and insight you've provided from the very beginning. Thanks to Kristen for being an excellent person to work alongside – it was nice to always have someone to bounce ideas off of and tackle any issues that we encountered together.

Huge thanks to the WOBL lab manager, Ian Jones who has been extremely helpful throughout my entire experience at Western, for which I am truly grateful. I'd also like to thank those people in the lab who were always there for moral support and to help maintain my sanity: Sara, Sheila, Emily, Kristin, Dan, Angelo, Ashley and Kristyn. Special thanks to Sheila and Ashley who made it easy to coordinate and communicate with when sharing lab space and equipment.

I'd like to thank my girlfriends who always made time for a coffee or dinner date with me when I was available. Lastly, I'd like to thank my parents, Brian and Marylyn Balsdon, as well as Greg, Amy, and Shane who supported me in so many ways through the last few years. I'm sure you were wondering if I would ever finish this degree! Well I have, and I couldn't have done it without your love and support.

# TABLE OF CONTENTS

CERTIFICATE OF EXAMINATION.....	ii
ABSTRACT.....	iii
ACKNOWLEDGEMENTS.....	iv
TABLE OF CONTENTS.....	v
LIST OF FIGURES.....	viii
LIST OF TABLES.....	xi
LIST OF ABBREVIATIONS, SYMBOLS AND NOMENCLATURE.....	xii
CHAPTER 1 – INTRODUCTION.....	1
<b>1.1 KINEMATIC MEASUREMENT TECHNIQUES.....</b>	<b>1</b>
<b>1.1.1 Optical Tracking Systems.....</b>	<b>2</b>
<b>1.1.1.1 Soft Tissue Artifact.....</b>	<b>2</b>
<b>1.1.2 Medical Imaging.....</b>	<b>3</b>
<b>1.1.2.1 X-ray and fluoroscopic imaging.....</b>	<b>4</b>
<b>1.1.2.2 Computed Tomography (CT).....</b>	<b>5</b>
<b>1.2 Radiostereometric Analysis.....</b>	<b>6</b>
<b>1.2.1 Markerless Radiostereometric Analysis.....</b>	<b>7</b>
<b>1.2.2 RSA Calibration.....</b>	<b>8</b>
<b>1.2.2.1 Pin cushion distortion.....</b>	<b>10</b>
<b>1.2.2.2 Fluoroscope Calibration Model.....</b>	<b>13</b>
<b>1.2.2.3 Fluoroscope Algorithms.....</b>	<b>16</b>
<b>1.2.2.4 Experimental Set-up Recreation.....</b>	<b>16</b>
<b>1.2.2.5 3D Bone Model.....</b>	<b>18</b>
<b>1.2.2.6 Matching.....</b>	<b>19</b>
<b>1.3 FOOT ANATOMY.....</b>	<b>21</b>
<b>1.3.1 Bones and Articulations.....</b>	<b>21</b>
<b>1.3.1.1 Articulations and the Multi-Segment Foot Model.....</b>	<b>23</b>
<b>1.3.2 Medial Longitudinal Arch (MLA).....</b>	<b>24</b>
<b>1.3.2.1 MLA Function.....</b>	<b>24</b>
<b>1.3.2.2 MLA Measurements &amp; Angle.....</b>	<b>25</b>

1.3.2.2.1	<b>Calcaneus Coordinate System</b> .....	26
1.3.2.2.2	<b>MLA angle</b> .....	29
1.4	<b>ORTHOTICS</b> .....	29
1.4.1	<b>Custom and semi-custom orthotics</b> .....	30
1.4.2	<b>Clinical Assessment</b> .....	31
1.4.3	<b>Subtalar Joint Neutral Position</b> .....	32
1.4.4	<b>Orthotic Design &amp; Casting</b> .....	33
1.5	<b>RATIONALE</b> .....	33
1.6	<b>OBJECTIVES AND HYPOTHESIS</b> .....	34
1.7	<b>THESIS OVERVIEW</b> .....	35
1.8	<b>REFERENCES</b> .....	36
<b>CHAPTER 2 – STATIC BAREFOOT, NEUTRAL CUSHIONING RUNNING SHOE AND SUBTALAR JOINT NEUTRAL</b> .....		39
2.1	<b>INTRODUCTION</b> .....	39
2.2	<b>METHODS</b> .....	40
2.3	<b>RESULTS</b> .....	45
2.4	<b>DISCUSSION</b> .....	49
2.5	<b>REFERENCES</b> .....	52
<b>CHAPTER 3 – NEUTRAL CUSHIONING RUNNING SHOE COMPARED WITH NO SHOE DURING DYNAMIC GAIT</b> .....		54
3.1	<b>INTRODUCTION</b> .....	54
3.2	<b>METHODS</b> .....	55
3.3	<b>RESULTS</b> .....	58
3.4	<b>DISCUSSION</b> .....	61
3.5	<b>REFERENCES</b> .....	64
<b>CHAPTER 4 – FOAM CASTED HARD AND SOFT ORTHOTICS, PLASTER HARD AND SOFT ORTHOTICS AND PFO COMPARED WITH BAREFOOT WALKING</b> .....		65
4.1	<b>INTRODUCTION</b> .....	65
4.2	<b>METHODS</b> .....	67
4.3	<b>RESULTS</b> .....	70
4.4	<b>DISCUSSION</b> .....	73
4.5	<b>REFERENCES</b> .....	76

CHAPTER 5 – TWO-DIMENSIONAL VERSUS THREE-DIMENSIONAL ANALYSIS .....	77
5.1 INTRODUCTION .....	77
5.2 METHODS .....	78
5.3 RESULTS .....	82
5.4 DISCUSSION .....	89
5.5 REFERENCES.....	92
CHAPTER 6 – GENERAL DISCUSSION AND CONCLUSIONS.....	93
6.1 SUMMARY .....	93
6.2 STRENGTHS AND LIMITATIONS.....	96
6.3 RECOMMENDATIONS AND FUTURE DIRECTIONS .....	98
6.4 SIGNIFICANCE .....	99
6.5 REFERENCES.....	100
APPENDICES .....	101
APPENDIX A – SEGMENTATION USING OSIRIX.....	102
APPENDIX B – MATLAB CODE .....	110
APPENDIX C – ETHICS APPROVAL .....	116
APPENDIX D – CRIC APPROVAL .....	117
APPENDIX E – RAW DATA & STATISTICS.....	118
APPENDIX F – CURRICULUM VITAE.....	126



## LIST OF FIGURES

Figure 1.1: Calibration frame orientation for bi-planar fluoroscopic RSA of the foot. Frame axes x, y and z are shown in red, green and blue, respectively. ....	10
Figure 1.2: Distortion grid and attachment to fluoroscope B. Precisely constructed grid of stainless steel beads embedded in plastic that is used to correct for image distortion. ....	11
Figure 1.3: (a) Sample image taken of the distortion grid by fluoroscope A, and (b) close up view of the distortion grid and numbering used for MATLAB algorithms.....	12
Figure 1.4: Perspective Projection Model illustrating the projection coordinate system, the calibration frame coordinate system, a calibration point (Calib. Pt) and an image point (Im. Pt). Modified from (Rougee et al., 1993). ....	14
Figure 1.5: Imported calibration frame points (F1/C1) into laboratory coordinate system of recreated experimental set-up of fluoroscope B in Rhinoceros (Rhinoceros; Robert McNeel & Associates, Seattle, WA, USA).....	17
Figure 1.6: Image depicting final experimental set-up of both fluoroscopes in Rhinoceros (Rhinoceros; Robert McNeel & Associates, Seattle, WA, USA). ....	18
Figure 1.7: An image of the left calcaneus foot bone with digitized bony landmarks in both (a) 3D Volume Rendering, and (b) 3D Surface Rendering settings in OsiriX (Pixmeo, Geneva, Switzerland). ....	19
Figure 1.8: Manual matching trial showing three bones of the foot – first metatarsal, navicular and calcaneus in red, purple and blue, respectively, with shading settings (Rhinoceros, Robert McNeel & Associates, Seattle, WA, USA). ....	20
Figure 1.9: Manual matching trial for three bones of the foot – first metatarsal, navicular and calcaneus in red, purple and blue, respectively, with digitized bony landmarks in Rhinoceros (Rhinoceros, Robert McNeel & Associates, Seattle, WA, USA). ....	21
Figure 1.10: Medial view of the right foot showing three of four foot segments of the multi-segment foot model by Jenkyn & Nicol (2007) – Dark grey (medial forefoot), medium grey (midfoot) and light grey (rearfoot). Modified from (Norden & Frankel, 2001).....	22
Figure 1.11: Left calcaneus with bony landmarks defined in red on the medial process (MP), sustentaculum tali (ST) and lateral surface (LS) as well as the defined coordinate system and axes. Modified from (Kimball, 2011). ....	27
Figure 1.12: Medial view of a left foot showing the angle theta ( $\theta$ ) of the medial longitudinal arch between the navicular tuberosity (NT), medial process of the calcaneus (MP) and first metatarsal head (MH). Modified from (Kimball, 2011). ....	28

Figure 2.1: (a) Solid Works drawing of fluoroscope configuration and proposed platform design, and (b) photograph of erected plywood platform designed for bi-planar fluoroscopy of the foot.....	41
Figure 2.2: Pes cavus participant static barefoot image from the (a) lateral view (fluoroscope A), and (b) anterior-posterior oblique view (fluoroscope B).....	43
Figure 2.3: Mean arch angle differences for normal, cavus and planus foot types of the subtalar neutral (STN) position and neutral cushioning running shoe from the barefoot case. Error bars are +/- 1SD from the mean of each group. ....	48
Figure 2.4: Arch angle differences with respect to barefoot stance for subjects for three different foot types in the subtalar neutral position. ....	48
Figure 2.5: Arch angle differences for subjects with three different foot types: normal, pes cavus and pes planus, while wearing running shoes with respect to barefoot stance. ....	49
Figure 3.1: Photograph of the neutral cushioning running shoes used for all subjects, New Balance model 882 (New Balance Athletic Shoe Inc., Boston, MA, USA). ....	56
Figure 3.2: Matching neutral cushioning running shoe for a ‘normal’ participant. ....	58
Figure 3.3: MLA angles at the instant of foot-flat in dynamic walking gait – a comparison of barefoot and neutral cushioning running shoes. ....	59
Figure 3.4: MLA angle differences with subjects in a neutral cushioning shoe compared with no shoe at the instant of foot-flat in dynamic walking gait. Data points are shown in blue, red and green for normal, pes cavus and pes planus foot types, respectively. ....	60
Figure 4.1: (a) Custom soft material (plastazote) orthotic, (b) custom hard material (subortholen) orthotic, and (c) proprioceptive feedback-type orthotic (PFO) with different foam inserts.....	68
Figure 4.2: (a) Participant walking on wooden platform during data collection (left), and (b) calibration of both fluoroscopes with a calibration frame with axes x, y, z, denoted by red, green and blue, respectively.....	69
Figure 4.3: A comparison of MLA angle differences while walking with five orthotic conditions compared to barefoot walking.....	71
Figure 4.4: Comparison of MLA angle changes from barefoot walking for five conditions – foam casted hard and soft orthotics, plaster casted hard and soft orthotics, and PFO. ....	72
Figure 5.1: Lateral fluoroscopic view of the foot showing (a) the process of selecting bony landmarks following matching process in Rhinoceros using script ‘ExportPoints.rvb’, and (b) the calcaneal-first metatarsal angle calculation (CFMA) defined by Murley et al. (2009). ....	81

Figure 5.2: Comparison of two- and three-dimensional analyses of six participants in the barefoot condition. Error bars for each subject are represented by the standard deviation of each foot type.....	83
Figure 5.3: Comparison of two- and three-dimensional analyses of six participants in the foam casted soft orthotic condition. Error bars for each subject are represented by the standard deviation of each foot type. ....	83
Figure 5.4: Comparison of two- and three-dimensional analyses of six participants in the foam casted hard orthotic condition. Error bars for each subject are represented by the standard deviation of each foot type. ....	84
Figure 5.5: Comparison of two- and three-dimensional analyses of six participants in the PFO condition. Error bars for each subject are represented by the standard deviation of each foot type.....	84
Figure 5.6: Comparison of 3D and 2D analyses of calculated mean MLA and CFMA angles (respectively) in the normal group. Error bars for each subject are represented by the standard deviation of that condition between the two subjects.....	85
Figure 5.7: Comparison of 3D and 2D analyses of calculated MLA and CFMA angles (respectively) for the cavus group. Error bars for each subject are represented by the standard deviation of that condition between the two subjects.....	86
Figure 5.8: Comparison of 3D and 2D analyses of calculated MLA and CFMA angles (respectively) for the planus group. Error bars for each subject are represented by the standard deviation of that condition between the two subjects.....	86
Figure 5.9: Bland-Altman plot for both subjects of normal foot type. The mean difference in arch angle is represented by the solid line, with $\pm 2SD$ represented by the dotted lines.....	87
Figure 5.10: Bland-Altman plot for both subjects of pes cavus foot type. The mean difference in arch angle is represented by the solid line, with $\pm 2SD$ represented by the dotted lines.....	88
Figure 5.11: Bland-Altman plot for both subjects of pes planus foot type. The mean difference in arch angle is represented by the solid line, with $\pm 2SD$ represented by the dotted lines.....	88

## LIST OF TABLES

Table 2.1: Mean MLA angle measurements during static stance conditions: barefoot, subtalar neutral position and neutral cushioning running shoe.....	47
Table 2.2: Mean, maximum, minimum and range measurements of static barefoot MLA angles for three foot types – normal, pes cavus and pes planus.....	47
Table 2.3: Mean vector magnitudes (NTMH and NTMP) normalized to foot length and compared between pathological groups. These are the two vectors that comprise the medial longitudinal arch angle. ....	49
Table 3.1: Mean and standard deviations of MLA angles at the instant of foot-flat in dynamic walking for barefoot and neutral cushioning running shoe conditions. ....	60
Table 4.1: MLA angle differences from barefoot walking of five different conditions along with the mean and standard deviation, separated by foot type. ....	72
Table 5.1: Differences between 3D and 2D arch angle analyses for each subject ( $\Delta\theta$ ) ...	85
Table 5.2: Mean differences, overall mean and standard deviation of all conditions within each pathological group between 3D and 2D analyses ( $\Delta\theta$ ).....	87

## LIST OF ABBREVIATIONS, SYMBOLS AND NOMENCLATURE

° – degree(s)

$\theta$  – (Theta) rotation about the vertical axis of the image

$\varphi$  – (Phi) rotation about the horizontal axis of the image

$\psi$  – (Psi) about the perpendicular to the image

2D – two-dimensional

3D – three-dimensional

ANOVA – analysis of variance

AI – arch index

C – 2D image plane coordinate system horizontal axis as defined by the distortion grid

c – C coordinates of an image point in the image plane coordinate system

$c_s$  – C coordinates of the projected x-ray source in the image plane coordinate system

CAD – computer aided-design

CPedC – Canadian Certified Pedorthist

cm – centimetre(s)

$\cos^{-1}$  – inverse cosine

CT – computed tomography

d – distance from S to S' (mm)

durometer – measure of hardness of a material

EVA – type of ThermoLyn® thermoplastic

fRSA – fluoroscopic radiostereometric analysis

II – image intensifier

ISB – International Society of Biomechanics

JCS – Joint Coordinate System

kV – kilovolt

L – 2D image plane coordinate system vertical axis as defined by the distortion grid

l – L coordinate of an image point in the image plane coordinate system

$l_s$  – L coordinate of the projected x-ray source in the image plane coordinate system

LS – lateral anterior surface of the calcaneus

mA – milliampere

MH – metatarsal head of the first metatarsal

MLA – medial longitudinal arch  
mm – millimetre(s)  
MP – medial process of the calcaneus  
mpeg – moving picture experts group  
mRSA – markerless radiostereometric analysis  
NT – navicular tuberosity  
NTSC – National Television System Committee  
O – origin vector  
obj – object file  
 ${}^xP_y$  – point location in terms of y coordinates with respect to x  
pes cavus – (cavus) participants with high arches  
pes planus – (planus) participants with flat feet or low arches  
PFO – proprioceptive feedback-type orthotic  
PTTD – posterior tibialis tendon dysfunction  
R – roentgen  
R – calibration frame coordinate system or laboratory coordinate system (O, X, Y, Z)  
R' – the projection coordinate system (S, X', Y', Z')  
RCH-500 – type of ThermoLyn® thermoplastic  
RSA – radiostereometric analysis  
S – position of the x-ray source  
S' – position of the projected x-ray source on the image plane  
s – second(s)  
SD – Standard deviation  
 $s_p$  – pixel size (mm)  
ST – sustentaculum tali (calcaneus)  
STA – soft tissue artifact (aka skin motion artifact)  
STJ – subtalar joint  
STN – subtalar joint neutral  
 $T_y^x$  – transformation matrix expressing y with respect to x (4 by 4 dimensions)  
TKR – total knee replacement  
TIFF – tagged image file format

$\mu\text{R}$  – micro roentgen

WOQIL - Wolf Orthopaedic Quantitative Imaging Laboratory

$x'$  – x coordinate of a calibration point in the projection coordinate system

$x_i$  – x coordinate of the 3D calibration point 'i' in the calibration frame coordinate system

$x_s$  – x coordinate of the x-ray source in the calibration frame coordinate system

$X$  – axis in the calibration frame coordinate system

$X'$  – axis in the projection coordinate system

$X^{\text{cal}}$  – calcaneus coordinate system vector

$y'$  – y coordinate of a calibration point in the projection coordinate system

$y_i$  – y coordinate of 3D calibration point 'i' in the calibration frame coordinate system

$y_s$  – y coordinates of x-ray source in the calibration frame coordinate system

$Y$  – axis in the calibration frame coordinate system

$Y'$  – axis in the projection coordinate system

$Y^{\text{cal}}$  – calcaneus coordinate system vector

$z'$  – z coordinate of a calibration point in the projection coordinate system

$z_i$  – z coordinate of 3D calibration point 'i' in the calibration frame coordinate system

$z_s$  – z coordinate of x-ray source in the calibration frame coordinate system

$Z$  – axis in the calibration frame coordinate system

$Z'$  – axis in the projection coordinate system

$\hat{Z}^{\text{cal}}$  – unit vector created from LS to MP

## **CHAPTER 1 – INTRODUCTION**

### **1.1 KINEMATIC MEASUREMENT TECHNIQUES**

Biomechanics is the application of classical mechanics to the analysis of biological and physiological systems (Norden & Frankel, 2001). Different aspects of biomechanics employ different parts of applied mechanics. For example, the principles of statics have been applied to analyze the magnitude and nature of forces involved in various joints and muscles of the musculoskeletal system. The principles of dynamics have been utilized for motion description, gait analysis, and segmental motion analysis and have many applications in sports mechanics (Norden & Frankel, 2001). Research for this thesis applies the principles of dynamics to analyze specific movements of the musculoskeletal system. There are different types of movement analysis: anatomical contributions to the movement (functional anatomy), describing the characteristics of motion (kinematics) and determining the cause of the motion (kinetics) (Hamill & Knutzen, 2003). In this thesis the characteristics of the motion are most important, thus it will focus on quantifying the kinematics of the bones of the human body.

There are different ways to measure these kinematic movements – using photographic or video analysis methods, optical tracking systems and medical imaging methods, to name a few. Capturing kinematics with high speed photographic or video camera methods is a fairly simple procedure as there are no wires or equipment restraining the subject from operating normally and so they are free to perform the any movement or motion of interest. The standard National Television System Committee (NTSC) video rate is 60 interlaced frames per second and can be collected with various shutter speeds. This equipment is portable, relatively inexpensive and the video data can be digitized using a biomechanical analysis program. An obvious limitation to single camera video analysis is that it is not able to capture any out of plane motion, and many biomechanical movements, such as rowing, occur in three dimensions (Bechard, Nolte, Kedgley, & Jenkyn, 2009).



### **1.1.1 Optical Tracking Systems**

Camera-based optical tracking systems are the most common method of quantifying three-dimensional joint kinematics (Kedgley, Birmingham, & Jenkyn, 2009a). Reflective markers are placed on the skin over anatomical landmarks to reconstruct a three-dimensional model of the subject being tested. The optical motion capture cameras emit visible red light that reflect off these markers and back into the cameras. A direct linear transform algorithm reconstructs the three-dimensional locations of these reflective markers and therefore is able to calculate joint angles, rotations and translations. This method is used regularly as it is a quick and efficient tool to collect and assess the gait and other motions of all different patients in real time, with close to immediate feedback on their kinematics. Optical motion analysis is mostly common for kinematics of knee, hip and upper body; however, it generally treats the foot as a rigid segment, represented with only three markers on the lateral malleolus, second metatarsal and calcaneus (heel).

A multi-segment foot model developed by Jenkyn and Nicol separates the foot into four segments in order to track them individually (Jenkyn & Nicol, 2007). These four segments are the lateral forefoot (fifth metatarsal), medial forefoot (first metatarsal), midfoot (dorsal navicular tuberosity and 2<sup>nd</sup> & 3<sup>rd</sup> cuneiforms) and hindfoot (calcaneus). This method is a non-invasive way to determine foot and ankle kinematics, specifically pronation and supination in the frontal plane, as well as movements in the sagittal and transverse planes. This model showed excellent agreement with four studies when comparing hindfoot motion in the frontal plane (11° range of motion compared to 10° and 12°); however; it does not target specific articulations between two foot bones and it still has some small error due to soft tissue artefact (or skin motion artefact).

#### **1.1.1.1 Soft Tissue Artifact**

Soft tissue artifact (STA) is the error on marker trajectories that arises due to the relative movement between the markers and the underlying bone (Leardini, Chiari, Della Croce, & Cappozzo, 2005). Studies have been performed to quantify this particular error using optical tracking in conjunction with external fixators for fracture fixation devices, percutaneous markers and 2D or 3D fluoroscopy. As far as technique is concerned, some

drawbacks to the external fixation method are associated with the condition of the soft tissue in these patients, as they have likely suffered a trauma of some sort, and therefore their motion may be non-physiological due to wearing this device. The percutaneous skeletal trackers clamped to the epiphyses can allow assessment of the STA in healthy subjects; however, there are limitations associated with sliding restrictions of the skin, imposed by the pins, typically mounted in traditional skin marker locations (epicondyles and malleoli). Previous studies using intra-cortical pins have been able to quantify the STA error by comparing the locations of the intra-cortical pins with respect to skin markers during various activities. Magnitudes of skin mounted markers were found to exhibit displacements between 10-20mm and some rotations greater than  $10^\circ$  with respect to the underlying bone (Leardini et al., 2005). The use of intra-cortical and percutaneous pins for quantifying STA on normal volunteers is somewhat invasive and therefore quite limited for ethical reasons.

The techniques based on fluoroscopy are minimally invasive, provide a complete 3D measurement of the STA and enable analyses of a large number of skin markers; however, this method is limited to a single joint at a time and extensive image data processing is required. The summary of the results in Leardini et al. (2005) conclude that STA error is greater than the error from the use of the optical tracking systems, and that the STA is also greater when analyzing the thigh compared to any other lower limb segment. Each technique in determining skeletal kinematics has both advantages and disadvantages, and therefore should be chosen according to the specific applications and research incentives.

### **1.1.2 Medical Imaging**

Medical imaging of the human body requires some form of energy, and this energy used must be capable of penetrating tissues in order to produce the required radiological image. This penetration or interaction with the tissues through the body (e.g. absorption, attenuation) results in the detected energy containing useful information regarding the internal anatomy of the patient being scanned (Bushberg, Seibert, Leidholdt, & Boone, 2002). In order for the medical image to be useful in diagnostics, the technical quality of the images and the conditions of their acquisition must be optimized.

Therefore, the quality of these images requires a compromise between patient safety and radiation dosage. Though better x-ray images can be made with a high dose of radiation, excessive patient exposure to radiation in order to achieve a clearer image is not acceptable.

### **1.1.2.1 X-ray and fluoroscopic imaging**

Radiography was the first medical imaging technology when Wilhelm Roentgen discovered x-rays in 1895. Radiography (or roentgenography) defined the field of radiology, and gave rise to radiologists – physicians who specialize in the interpretation of medical images. Collecting images in radiography involves an x-ray source on one side of the patient, and an x-ray detector on the other side. Radiographic images are typically formed by a short duration pulse of x-rays that are emitted by the x-ray tube (less than  $\frac{1}{2}$  second). A large fraction of the x-rays are absorbed by the patient; however, some pass through the patient and reach the detector to form the radiographic image (Bushberg et al., 2002).

Fluoroscopy refers to the continuous acquisition of a sequence of x-ray images, essentially a real-time x-ray movie of the patient. Digital fluoroscopy can provide visual assistance to surgeons for the placement of catheters, guide wires and pacemakers in cardiac catheterization laboratories. Additionally, it can be used for dynamic studies of other complex internal organs. Fluoroscopic images are typically acquired at rates of 60 interlaced frames per second (of 30 true frames per second), as per the standard television frame rate in North America. The x-ray dose per frame can be as low as one one-thousandth of that used during serial image acquisition.

The principal component of the imaging chain that distinguishes fluoroscopy from radiography is the image intensifier. The outputted image of a fluoroscopic imaging system is a projection of a radiographic image. Due to the sheer number of images that must be produced to depict motion, for radiation dose reasons, fluoroscopic systems should produce a usable image with relatively few x-ray photons; therefore, a very sensitive detector is needed. Image intensifiers are several thousand times more sensitive than a standard 400-speed screen-film cassette and therefore, in principle, can produce images using several thousand times less radiation. For example, standard fluoroscopy

uses about 1 to 5  $\mu\text{R}$  (micro roentgen) incident upon the image intensifier per image, whereas the screen-film system requires exposure of about 600  $\mu\text{R}$  to achieve an optical density of 1.0 (Bushberg et al., 2002). Total exposure will vary with how many images are required, as well as the tissue-dosage conversion factor, which depends on the absorption level of the anatomy being imaged.

Fluoroscopy is most frequently used during medical surgeries to place stents in clogged arteries or advancing catheters during angiographic procedures, assuring the correct position of the catheter before contrast media is injected into the desired vessel or body cavity (Bushberg et al., 2002). Surgery guided with fluoroscopy provides a real-time video or still image for physicians and allows them to know the precise location of their work, while keeping the surgery non-invasive for the patient.

#### **1.1.2.2 Computed Tomography (CT)**

Computed Tomography (CT) became clinically available in the early 1970s and is the first medical imaging modality made possible by the computer. CT images are produced by passing x-rays through the body, at a large number of angles, by rotating the x-ray tube around the body. One or more linear detector arrays, opposite the x-ray source, collect the transmission projection data. The numerous data points collected in this manner are synthesized by a computer into a tomographic image of the patient (tomo-meaning 'slice' and -graphy meaning 'picture'). The advantage of this type of image over projection image is its ability to display the anatomy in a slice of tissue in the absence of over- or underlying structures. CT has reduced the need for exploratory surgery by acquiring 60 images at a thickness of 5mm in 10 seconds, and thus revealing the presence of cancer, subdural hematomas, aneurysms and other pathologies (Bushberg et al., 2002).

CT images can also be used in biomedical engineering to create three-dimensional (3D) models of a particular bone, muscle or joint, and use them in finite element analyses as well as implant research and design. CT images are also used in conjunction with single and dual plane fluoroscopy in radiostereometric analysis (RSA).

## 1.2 Radiostereometric Analysis

Radiostereometric analysis (RSA), also known as Roentgen stereophotogrammetry, is the science of obtaining reliable three-dimensional measurements from a pair of two-dimensional radiographs in order to determine primarily geometric characteristics of an object (Selvik, 1990). It is an accurate technique for measuring three-dimensional (3D) position of an object in space using roentgen rays or x-rays (Selvik, 1989). Historically, the first detailed description of precise localization and measurement using roentgen rays was published by Davidson in 1898. This researcher designed an apparatus so the geometry could be reconstructed from the time of roentgen exposure, with the two x-rays represented by silk threads (Selvik, 1990). This apparatus consisted of an x-ray tube fixed to a horizontal bar in order to explore the same object from two different known positions. The laboratory coordinate system was represented by placing two perpendicular metal wires on the object in order to replicate its exact position on the table. Two silk threads were also fixed at the same position representing the x-ray focus and then the position of the object was reconstructed by stretching the threads between the x-ray focus and the image on the developed film. The location where both threads cross in space determines the position of the x-rayed object (Bottner et al., 2005).

Current RSA systems are computerized and semi-automated to track radiographic localizations of landmarks in the human body. In order to track landmark positions through various movements, artificial landmarks have been introduced, using metallic implants or inserting tantalum beads. Tantalum has the two crucial properties required for metallic implantation: high inertness to body tissue and bone, as well as high absorption of x-rays (Selvik, 1990). An implantation instrument such as a spring loaded steel cannula is used to place these tantalum beads directly into the cortical bone. Three non-collinear markers are to be inserted to each segment of interest; however, approximately 5-9 beads are typically inserted to compensate for loose or invisible markers (Bottner et al., 2005). Traditionally, these beads have been inserted into orthopaedic implants, including the polyethylene lining and have been proven useful in determining migration and wear of the implant. For in-vivo testing, consent from the patient as well as approval from the ethics board is required to implant these beads into the patient's bone. Almost

all bead implantations are done during a scheduled surgery on the joint of interest since it would otherwise require an unnecessary surgery for the study participant.

### **1.2.1 Markerless Radiostereometric Analysis**

Standard RSA is an accurate method in determining migration and wear of orthopaedic implants such as a total hip arthroplasties (Bottner et al., 2005) as well as total or uni-compartmental knee arthroplasty (Karrholm, 1989). Tantalum beads are not only implanted into the patient's bone(s) during surgery, but they are incorporated into the design of the implant as well. This may incur some additional expenses associated with redesigning the implant, assuring it equates the strength and properties of a standard device. Though RSA has been proven accurate for this specific application, when the kinematics of healthy individuals is required, this method poses a major ethical problem as a painful and unnecessary surgery would be needed to implant the tantalum beads into the bone(s). Therefore, standard RSA limits the subject population to patients already undergoing surgical intervention on the joint of interest, eliminating them from the 'healthy' category. In response to this issue, markerless radiostereometric analysis (markerless RSA) was developed and validated by Anne-Marie Allen (2009) for the Wolf Orthopaedic Quantitative Imaging Laboratory (WOQIL) at Western University.

This study used a phantom bone model of the glenohumeral joint (Sawbones; Pacific Research Laboratories, Vashon, USA) on a cross slide-table to quantify kinematic translations by comparing known translated measures (accuracy of  $1\mu\text{m}$ ) to markerless RSA measurements. Joint rotations were compared with the 'gold standard', a standard RSA system, which has an accuracy of  $0.121^\circ$  (Kedgley et al., 2009a). The average root mean squared errors of this markerless RSA system for translation and rotation were  $0.082\text{mm}$  and  $1.18^\circ$ , respectively. Though markerless RSA methods are relatively new in their application to three-dimensional in-vivo biomechanics, they have also been used, along with standard RSA, in analyzing wear and migration of orthopaedic implants such as in total knee arthroplasty (Zuffi, Leardini, Catani, Fantozzi, & Cappello, 1999). This study used model-based kinematics of total knee replacements (TKR) using single-plane fluoroscopic images to evaluate the accuracy of this system by taking multiple static, single plane images of the TKR in both in vitro and in-vivo testing scenarios. The total

knee replacement hardware was developed into a three-dimensional model using CAD software in order to match the location of the implant to the fluoroscopic images.

Markerless RSA is synonymous in the literature with model-based RSA (Zuffi et al., 1999), image-based RSA (de Bruin et al., 2008), and optimized image matching RSA method (Bingham & Li, 2006). All of these studies of markerless RSA, or roentgen stereophotogrammetrical analysis, differ slightly by the algorithms that each one uses in their data analysis. One thing these methods have in common is that they do not require the use of tantalum markers in the implant or bone, and therefore they are all non-invasive techniques that can be conducted on healthy and non-surgical individuals.

Though there have been both traditional and markerless RSA studies looking at the knee, hip and shoulder joints, there have not yet been any three-dimensional studies analyzing the foot and its complex skeletal kinematics. Using traditional RSA to quantify this motion would be very invasive and the subject population even smaller than the knee or hip as surgery of the foot is quite rare in terms of arthroplasty and fracture repair. Therefore, only markerless RSA is a suitable technique to assess skeletal foot kinematics of a healthy population. The markerless RSA system in this thesis uses two C-arm fluoroscopes to collect both lateral and anterior-posterior oblique images of the foot.

### **1.2.2 RSA Calibration**

A calibration technique is required to determine the experimental set-up parameters, specifically the x-ray foci locations and the image plane pose. A calibration frame (or cage) establishes a coordinate system for the region of interest in the bi-planar RSA set up and determines the locations of the two imaging devices. In order for this to be achieved, each x-ray or fluoroscope must ‘see’ two planes of the calibration frame – a fiducial and a control plane (Kedgley & Jenkyn, 2009b). The fiducial plane creates a transformation from the image coordinate system to the laboratory coordinate system – represented by the calibration frame itself, and the control plane determines the focal point from which the x-rays originate. Calibration frames for bi-planar RSA set ups are generally designed with the assumption that the imaging devices will be at right angles to one another. Therefore, calibration frames were created to have pairs of fiducial and control planes at 90° to each other as well (Valstar et al., 2005).

Though bi-planar radiostereometric analysis (RSA) traditionally uses two imaging devices (x-rays or fluoroscopy image intensifiers) placed perpendicularly to one another, Kedgley and Jenkyn (2009b) challenged this idea. These researchers demonstrated that the RSA accuracy was not affected when the relative angles of the image intensifiers of the fluoroscopes were less than  $135^\circ$ . Therefore, RSA may be performed with the imaging devices at relative angles other than  $90^\circ$  while calibrating with a calibration object with pairs of fiducial and control planes oriented orthogonally to each other (Kedgley & Jenkyn, 2009b).

Fluoroscopy calibration for this thesis is required before executing the experimental protocol by imaging a calibration frame with embedded beads at known locations (Allen, 2009). In the case of RSA calibration for imaging the foot, the wooden platform designed for data collection has a detachable top, specifically designed to perform calibration with a tripod, to get the calibration frame in an optimal position for both fluoroscopes (Figure 1.1). This frame was designed by Kedgley (2009c) and defines the laboratory coordinate system for this thesis, with the axes x, y and z coloured in red, green and blue, respectively.



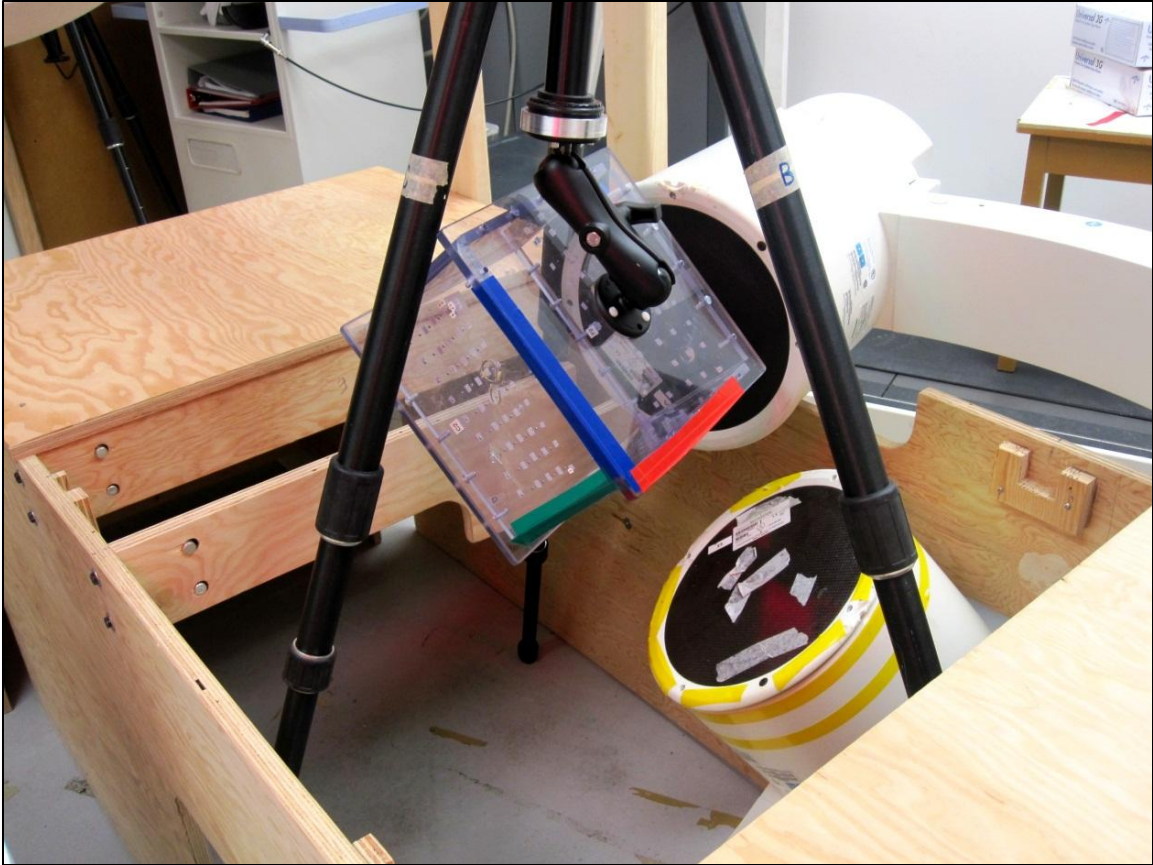


**Figure 1.1:** Calibration frame orientation for bi-planar fluoroscopic RSA of the foot. Frame axes x, y and z are shown in red, green and blue, respectively.

### 1.2.2.1 Pin cushion distortion

The combination of both the curved design of the image intensifier and the limitations of electron focusing, result in a non-uniform magnification of the peripheral aspect of the image – this notion is commonly referred to as ‘pin-cushion’ distortion (Wearing et al., 2005). Following executing the experimental protocol on each testing day, the calibration images of the fluoroscope need to be corrected for pin cushion distortion. Distortion correction is performed by imaging a distortion grid, made of plexiglass with stainless steel beads embedded at known locations, also designed by Kedgley (2009c), and is shown in Figure 1.2.

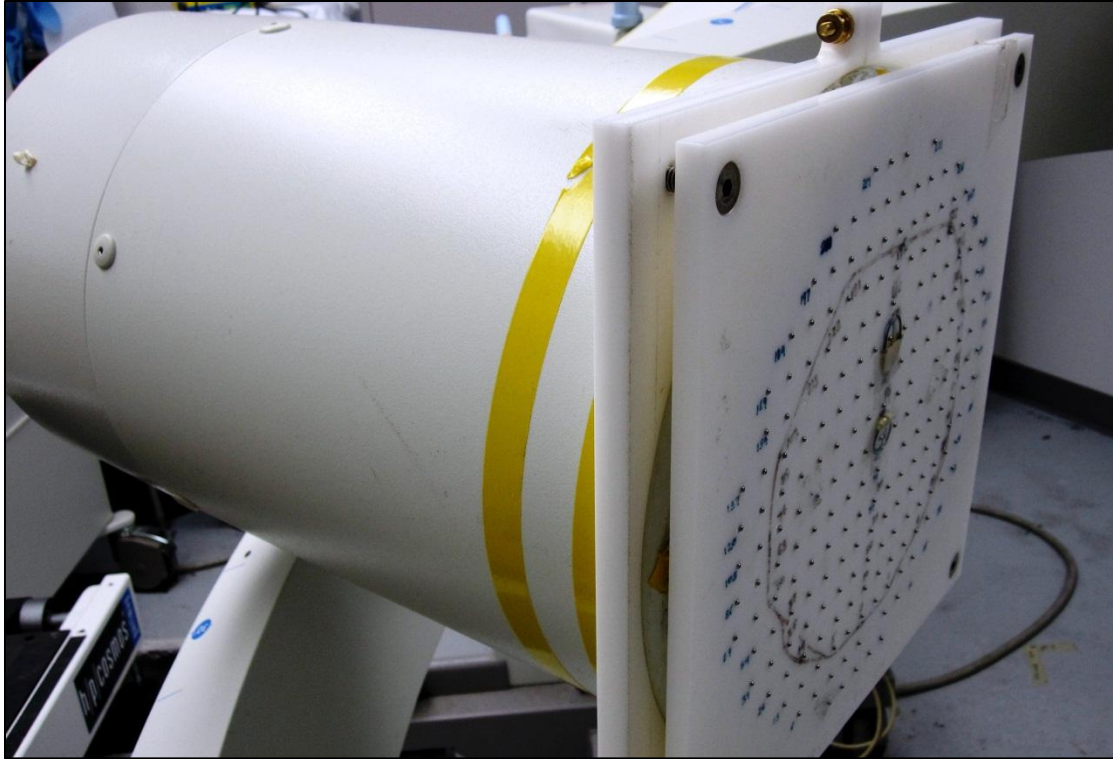


**Figure 1.2: Distortion grid and attachment to fluoroscope B. Precisely constructed distortion grid of stainless steel beads embedded in plastic that is used to correct for image distortion.**

The distortion grid is oriented so that sequential numbers of the beads appear horizontal in the image taken by the fluoroscopes. The center bead denoted with a circular wire is bead #70 which is also represents the centre of the image plane (Figure 1.3(a) and (b)).

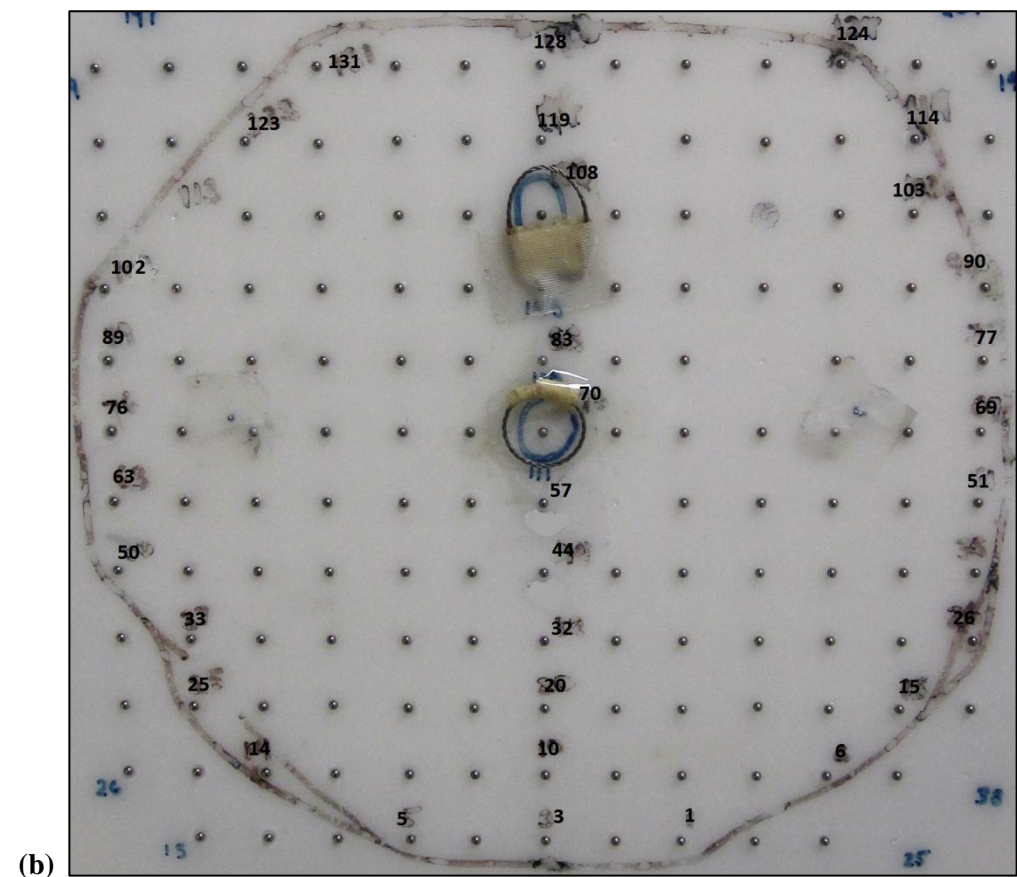
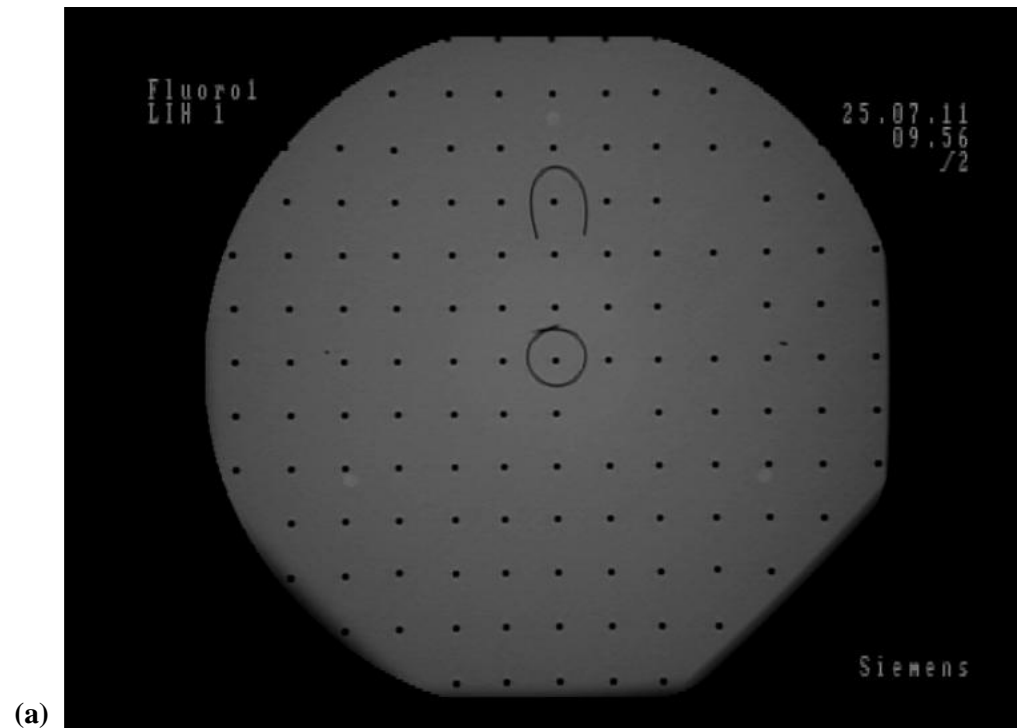


Figure 1.3: (a) Sample image taken of the distortion grid by fluoroscope A, and (b) close up view of the distortion grid and numbering used for MATLAB algorithms.

Using an algorithm in MATLAB developed by Kedgley (2009c), the points of both the calibration frame image and the distortion grid image are picked sequentially and their two-dimensional locations inputted into a spreadsheet. With their known two-dimensional locations, the selected distortion grid image points are first corrected for distortion using a global approach that employs a fourth-order polynomial fit (Kedgley, 2009c). In this global approach, the distortion vector at each point is calculated and these data points are then used to determine an overall expression for the distortion within the image. This may be calculated according to the Cartesian coordinates of the image. The positions of the beads in the image are related to their known positions according to a fourth order polynomial. These coefficients of this polynomial are then used to correct the calibration frame points for distortion, resulting in the two-dimensional calibration frame points coordinates as they are projected onto the image plane.

#### **1.2.2.2 Fluoroscope Calibration Model**

The calibration algorithm, created by Kedgley (2009c) was based on a model developed by Rougee et al. (1993). Each fluoroscope is modelled as a pinhole camera, with the calibration frame as a perspective projection onto the image intensifier (Rougee, Picard, Ponchut, & Troussset, 1993). It is assumed that x-rays are straight lines and originate from a single point source. This perspective projection model can be represented by Figure 1.4 where:

O = the origin of the calibration frame

S = the position of the x-ray source

S' = the position of the projection of the x-ray source onto the image plane

R = (O, X, Y, Z) the calibration frame coordinate system (also referred to as the laboratory coordinate system)

R' = (S, X', Y', Z') the projection coordinate system.

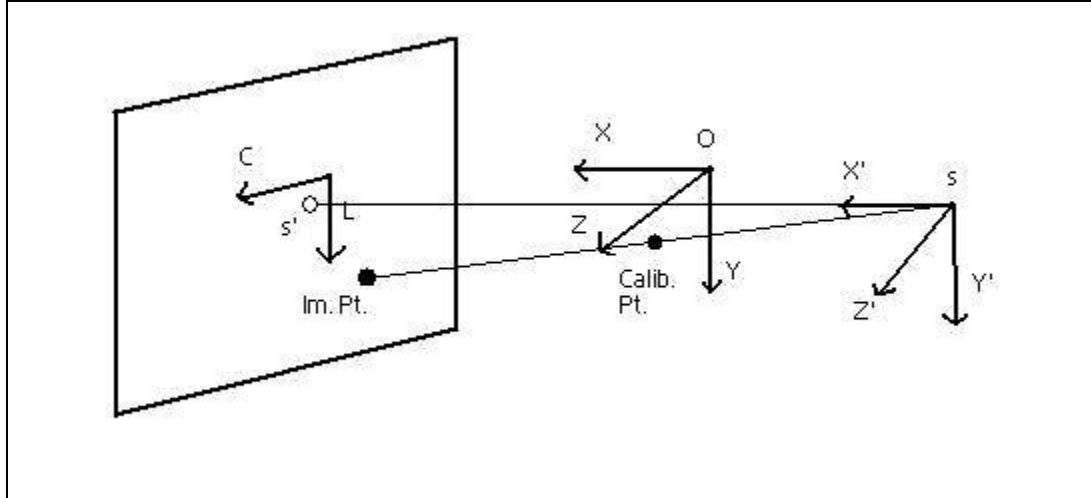


**Figure 1.4: Perspective Projection Model illustrating the projection coordinate system, the calibration frame coordinate system, a calibration point (Calib. Pt) and an image point (Im. Pt). Modified from (Rougee et al., 1993).**

The C and L axes define the coordinate system of the 2D image plane and are parallel to the Z' and Y' axes, respectively. It should be noted that all measurements are in mm, except for measurements in the image plane coordinate systems, which are in pixels. A calibration bead or point and its corresponding image plane projected point are also shown in Figure 1.4. By viewing this projection model in the Y' and Z' directions, a relationship can be determined between the coordinates of a calibration bead in R' – the projection coordinate system (x', y', z') and its projected image plane coordinates (c, l). This relationship can be reflected in matrix form:

$$\frac{x'}{d} \begin{bmatrix} C \\ l \\ 1 \end{bmatrix} = \begin{bmatrix} \frac{c_s}{d} & 0 & \frac{1}{s_p} \\ \frac{l_s}{d} & \frac{1}{s_p} & 0 \\ \frac{1}{d} & 0 & 0 \end{bmatrix} \begin{bmatrix} x' \\ y' \\ z' \end{bmatrix} \quad \text{Equation 1.1}$$

and matrix P(c<sub>s</sub>, l<sub>s</sub>, d) is defined as:

$$P(c_s, l_s, d) = \begin{bmatrix} \frac{c_s}{d} & 0 & \frac{1}{s_p} \\ \frac{l_s}{d} & \frac{1}{s_p} & 0 \\ \frac{1}{d} & 0 & 0 \end{bmatrix} \quad \text{Equation 1.2}$$

where:

$d$  = the distance from S to S' (mm)

$s_p$  = pixel size (mm)

$(c, l)$  = coordinates of an image point (pixels)

$(c_s, l_s)$  = coordinates of the source (pixels), and

$(x', y', z')$  = coordinates of a calibration point in the projection coordinate system (mm).

Pixel size is considered a known quantity in the fluoroscope model using a custom MATLAB code for the fluoroscopes in the WOQIL (Kedgley, 2009c). The average pixel size for fluoroscopes A and B are 0.3847 mm and 0.3819 mm, respectively.

The coordinates of a calibration point in R' can be derived from their known coordinates in the laboratory coordinate system (R) using an Euler angle rotation sequence and using the coordinate of the x-ray source in the calibration frame coordinate system  $(x_s, y_s, z_s)$ .

$$\begin{bmatrix} x' \\ y' \\ z' \end{bmatrix} = R(\theta, \varphi, \psi) \begin{bmatrix} x - x_s \\ y - y_s \\ z - z_s \end{bmatrix} \quad \text{Equation 1.3}$$

The sequence of rotations are such that the first rotation occurs about the vertical axis of the image, the second about the horizontal axis of the image, and the third and final rotation occurs about the perpendicular axis to the image plane. The angles are denoted by theta ( $\theta$ ), phi ( $\varphi$ ), and psi ( $\psi$ ) and in the case of Figure 1.4, corresponding axes are Y, Z and X respectively. These rotations, along with a total of 9 calibration parameters, provide the relationship between the 3D calibration points and their 2D projections. The remaining mathematics associated with this relationship is described extensively by Allen (2009).

### 1.2.2.3 Fluoroscope Algorithms

As far as determining these results, standard RSA code is first applied to calculate the locations of the x-ray source(s) using MATLAB algorithms (The MathWorks; Natick, MA, USA) (Kedgley, 2009c). Following the acquisition of the x-ray source positions, an additional series of algorithms are used to determine the 9 calibration parameters of each fluoroscope which represent the orientation and location of the image plane with respect to the x-ray source. This series of three additional algorithms not only determines the three Euler angle rotations and the distance ‘d’ from the source to the image plane, but it optimizes these parameters, assuring the lowest possible error value, giving the user a guideline for precision.

The symbolic equations are determined based on the orientation of the calibration frame with each fluoroscope (shown in Figure 1.4) and are calculated in mathematics operation software called Maple (Maplesoft; Waterloo, ON, Canada). The P-matrix (Equation 1.2) is defined based on the experimental and calibration set up, followed by a series of rotations and translations that result in expressions for both ‘c’ and ‘l’. These expressions are copied from Maple and pasted into an existing function, which is then called up by custom MATLAB algorithms. In addition to the 3D calibration points ( $x_i$ ,  $y_i$ ,  $z_i$ ) and their 2D projected coordinates ( $c_i$ ,  $l_i$ ), the initial Euler angle rotations and fluoroscope distance can be estimated. This calibration and optimization routine is performed for each fluoroscope separately.

### 1.2.2.4 Experimental Set-up Recreation

After acquiring the final fluoroscope parameters in MATLAB, the experimental set-up is recreated in solid modelling software (Rhinoceros; Robert McNeel & Associates, Seattle, WA, USA). This virtual set-up is required in order to match the imported bone model with both fluoroscope images simultaneously. Following instructions in Appendices E and F of Anne-Marie Allen’s thesis (2009), the set-up for each testing date is recreated given the acquired calibration parameters and x-ray source location. Starting with the Euler angle sequence, the fluoroscope coordinate system is first rotated to the correct orientation. After plotting a point representing the x-ray focus coordinates, a vector of length ‘d’ is created in line with the axis about which the last

rotation occurred, and then joined to the x-ray source point. The image plane is then defined by creating a plane orthogonal to the vector. The image plane size is calculated based on the known value of pixel size and the known dimensions of the fluoroscopic images (540x720 pixels). Using the image of the calibration frame, and importing the 3D calibration frame points of the corresponding fiducial and control planes, the final image plane correction can be made, which results in the calibration points to line up between the camera and the target (Figure 1.5).

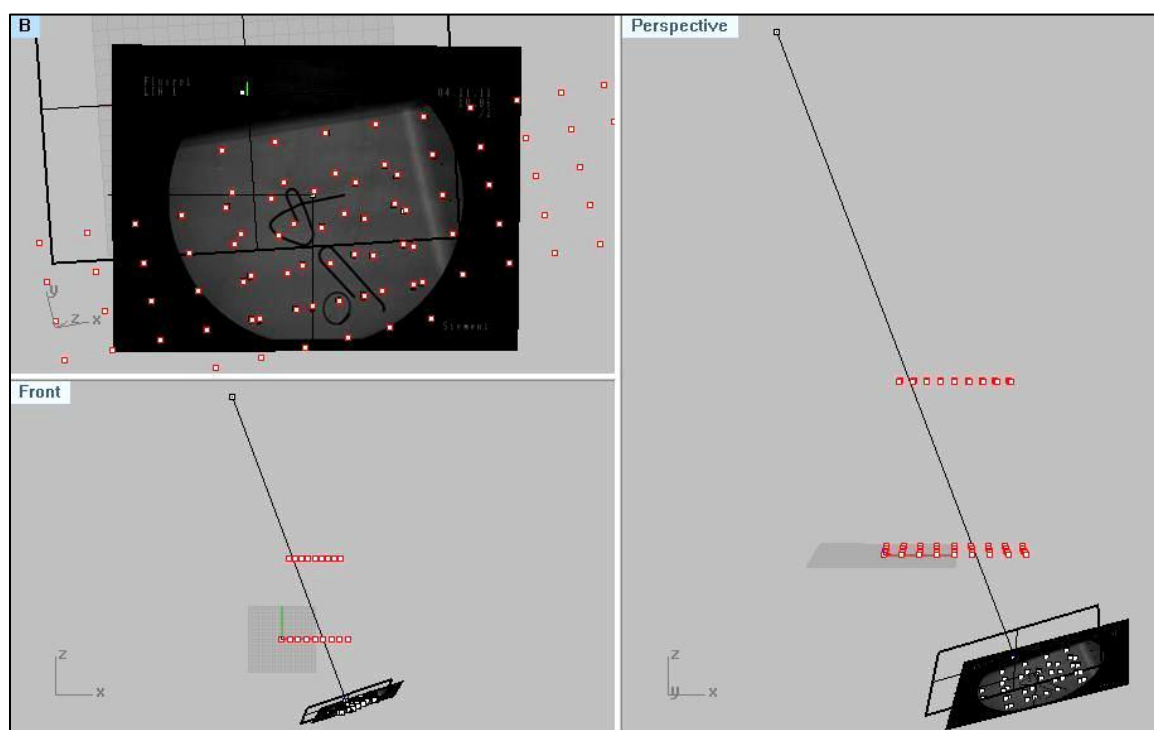


**Figure 1.5: Imported calibration frame points (F1/C1) into laboratory coordinate system of recreated experimental set-up of fluoroscope B in Rhinoceros (Rhinoceros; Robert McNeel & Associates, Seattle, WA, USA).**

When both x-ray foci and image planes are positioned correctly in separate files, the virtual experimental set-up of one fluoroscope is imported into the other and combined into one modelling file (Figure 1.6). This set-up allows for each image plane to be viewed by its corresponding x-ray source, therefore in the precise location to match the imported bone model to the two 2D images.



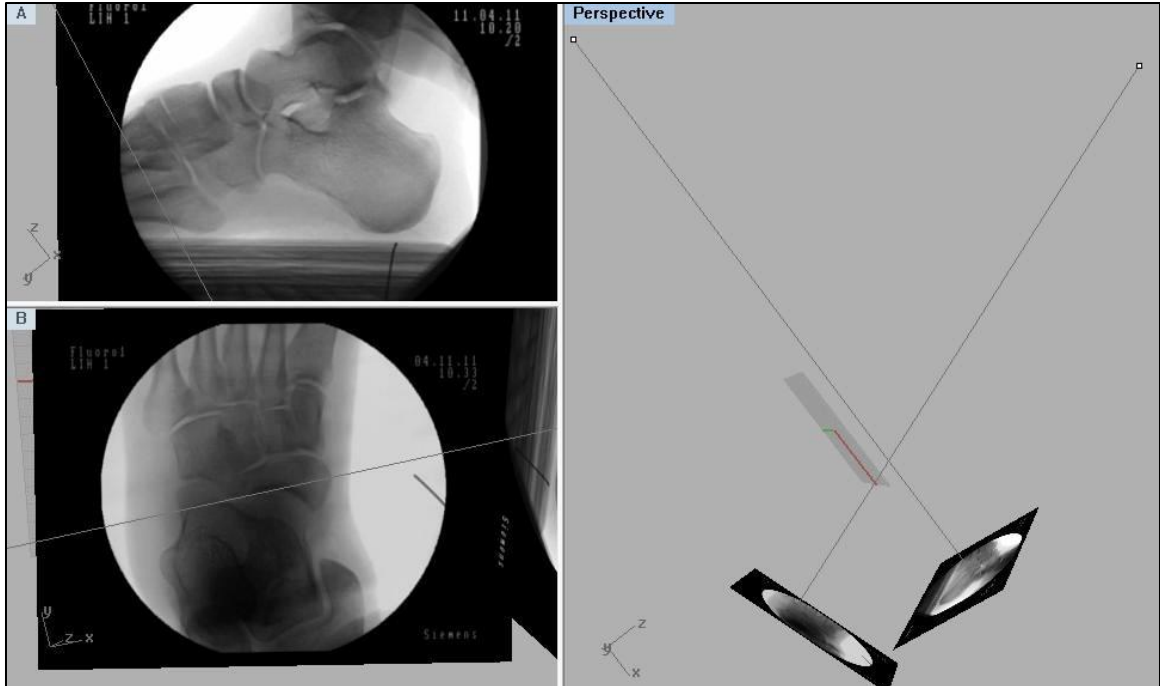


**Figure 1.6: Image depicting final experimental set-up of both fluoroscopes in Rhinoceros (Rhinoceros; Robert McNeel & Associates, Seattle, WA, USA).**

### 1.2.2.5 3D Bone Model

In order to complete the image matching process, a computed tomography (CT) scan is required for each study participant. For this thesis, the CT was to be taken of the left foot, from the ends of the toes to slightly proximal to the talar dome. The CT's are acquired with the following settings: 0.625mm thickness, bone window with a 3D reconstruction.

In order to convert these CT's into three-dimensional (3D) models, the images are imported and manipulated into open source image processing and DICOM viewing software called OsiriX (Pixmeo, Geneva, Switzerland). Each bone of interest is segmented individually in order to be imported as a separate entity in Rhinoceros to complete the manual matching process (section 1.2.2.6). The settings are changed from '3D Volume' to '3D Surface Rendering' where bony landmarks are located and marked in red (Figure 1.7(a)) and then a 'soft' bone filter is applied to smooth the surface of the bone (Figure 1.7(b)). Each bone is exported as an object file (.obj) so that the model can be imported into Rhinoceros to complete the manual matching process. Refer to Appendix A for complete detailed instructions on creating a 3D bone model in OsiriX.

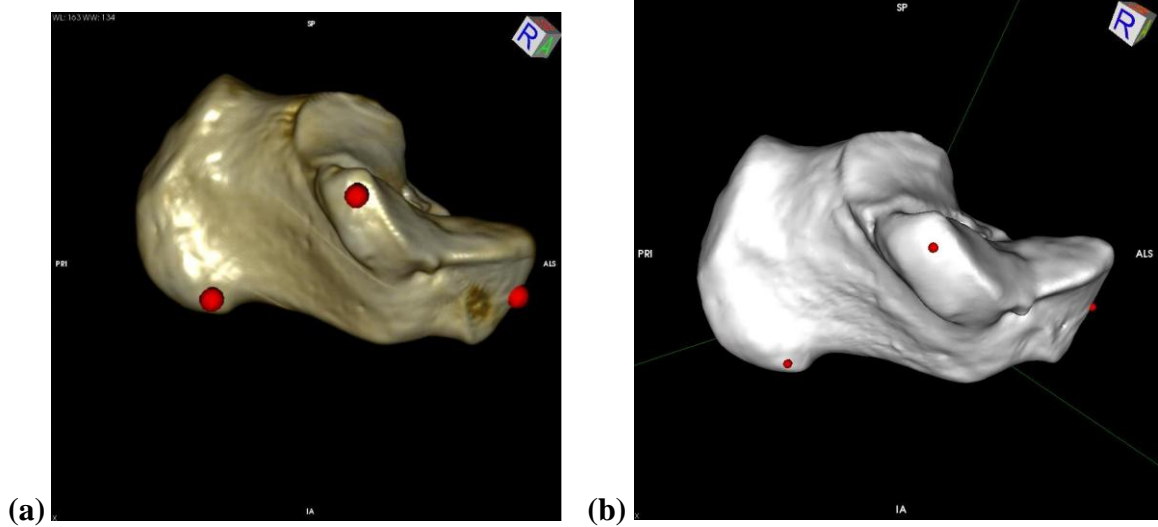


**Figure 1.7:** An image of the left calcaneus foot bone with digitized bony landmarks in both (a) 3D Volume Rendering, and (b) 3D Surface Rendering settings in OsiriX (Pixmeo, Geneva, Switzerland).

### 1.2.2.6 Matching

The goal of the manual matching procedure is to recreate the position and orientation of the objects captured by both fluoroscopes. The models of all the bones are first imported into the recreated experimental set-up (Rhinoceros) where they can be rotated and translated in three dimensions. Before being manipulated, points are placed on the chosen bony landmarks of each bone, denoted by a small black meshes exported from OsiriX. Initially, the three bones of interest are grouped in order to be translated and rotated together, to get an initial main reference position. The shaded viewpoint function can be used to get a better idea of the bones' initial orientation, as the curves and indentations of the bones are visible (Figure 1.8).

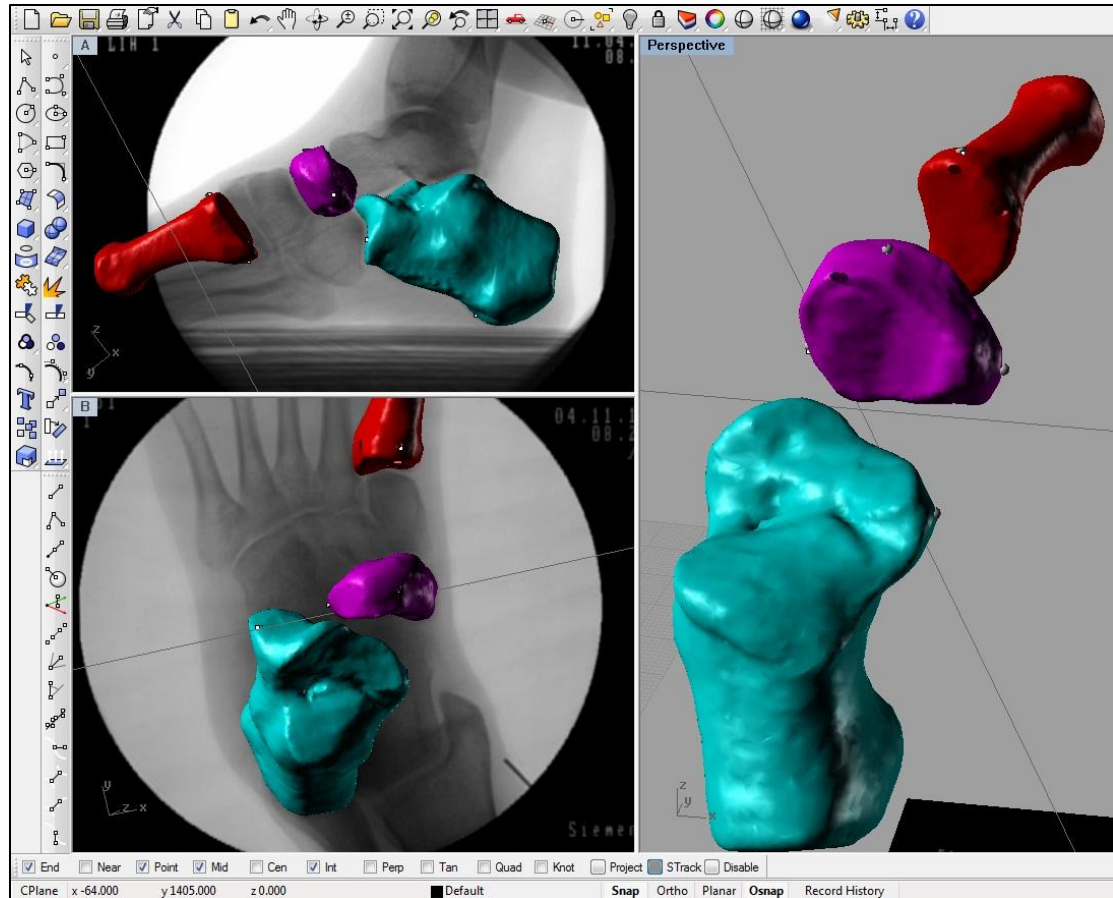


**Figure 1.8: Manual matching trial showing three bones of the foot – first metatarsal, navicular and calcaneus in red, purple and blue, respectively, with shading settings (Rhinceros, Robert McNeel & Associates, Seattle, WA, USA).**

The bones are then ungrouped and manually rotated and translated individually by no more than  $1^\circ$  or 1mm, as per the method described by Allen (2009), in order to get the bones in the exact orientation with respect to both image planes. Specific landmarks for each bone are used to match the bones in these final stages, such as the outline of the lateral calcaneus or the first metatarsal shaft, until the bone's silhouette matches the outline of the landmarks on the image. Fine tuning the position of the bones occurs by manually translating images as little as 0.05mm in one direction until the bones' silhouettes match the x-ray images of both image planes (Figure 1.9). Once the silhouettes are manually matched, the coordinates of the bony landmarks, denoted by the black mesh points, are exported into a spreadsheet using custom RhinoScript created by Allen (2009) (Rhinceros, Robert McNeel & Associates, Seattle, WA, USA). For each

different frame and/or condition, the new images are uploaded onto the respective image planes and the bones are then re-matched.

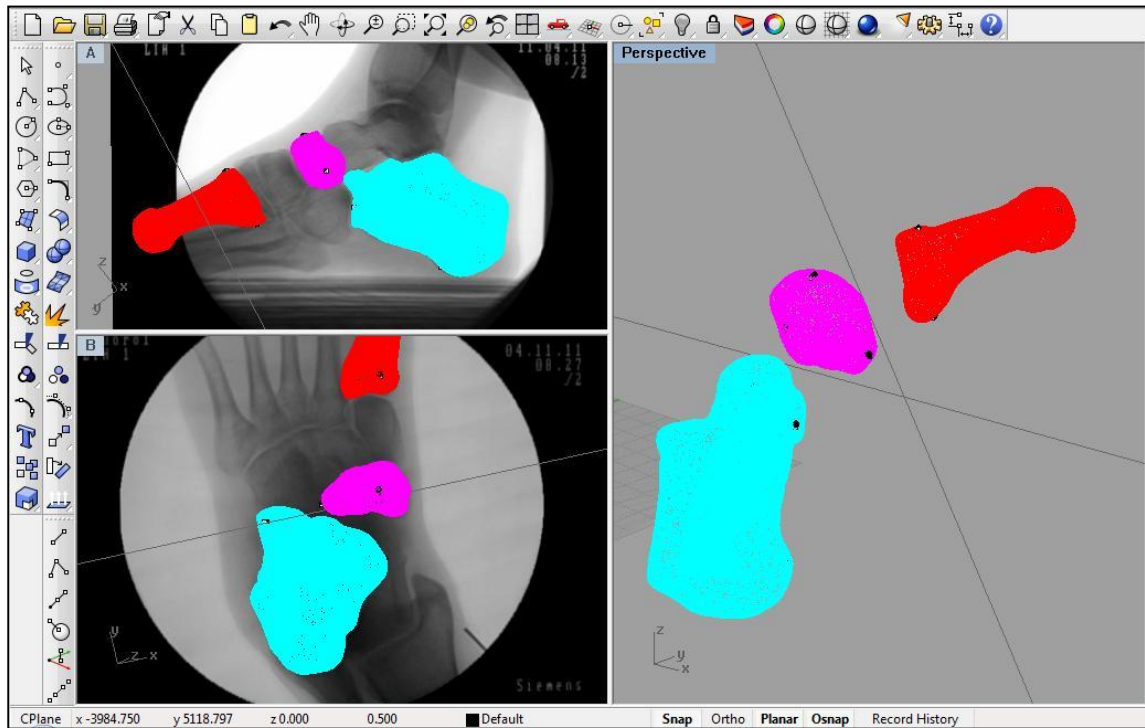


**Figure 1.9: Manual matching trial for three bones of the foot – first metatarsal, navicular and calcaneus in red, purple and blue, respectively, with digitized bony landmarks in Rhinoceros (Rhinoceros, Robert McNeel & Associates, Seattle, WA, USA).**

## 1.3 FOOT ANATOMY

### 1.3.1 Bones and Articulations

The foot is composed of 28 bones (including sesamoids) whose motions are closely interrelated (Figure 1.10). The unique qualities of the foot allow it to be rigid when necessary, as in ballet dancing on point, or flexible, as in walking barefoot on sand. Other structures that make up the anatomy of the foot are a plethora of tendons, ligaments and the plantar fascia. The plantar fascia originates on the medial process of the calcaneus and spans the transverse tarsal, tarsometatarsal, and metatarsophalangeal joints to insert on the metatarsophalangeal plantar plates and collateral ligaments as well as the hallucal sesamoids (Norden & Frankel, 2001).

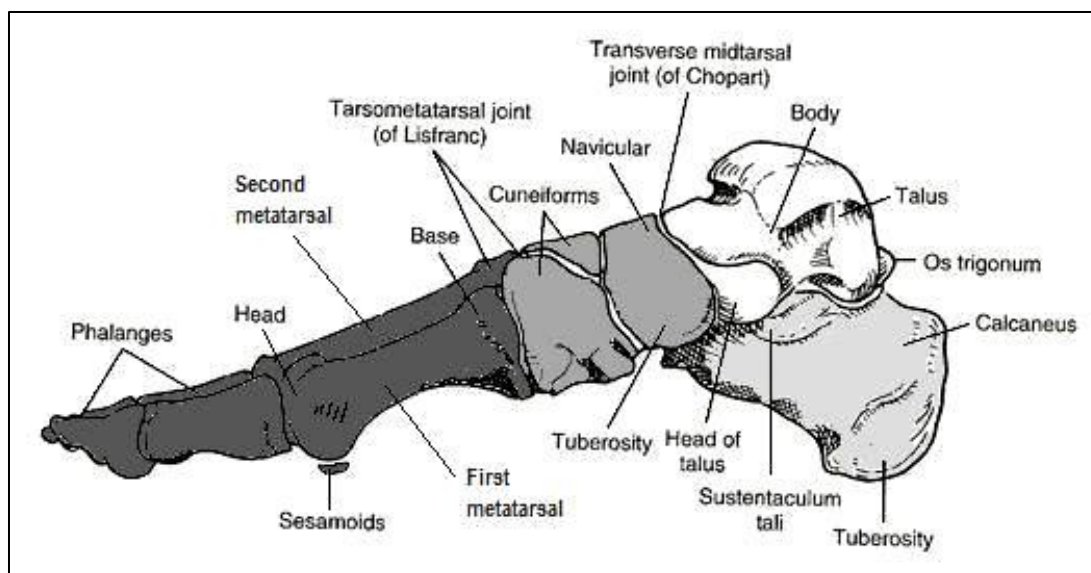


**Figure 1.10: Medial view of the right foot showing three of four foot segments of the multi-segment foot model by Jenkyn & Nicol (2007) – Dark grey (medial forefoot), medium grey (midfoot) and light grey (rearfoot). Modified from (Norden & Frankel, 2001).**

Overall motion of the bones of the foot is complex and occurs around three axes and in three planes. Flexion-extension occurs in the sagittal plane, abduction-adduction occurs in the horizontal or transverse plane, and inversion-eversion occurs in the coronal or frontal plane.

Even though the foot's motion during gait occurs in three planes, it is often considered to be a 'rigid segment' when determining kinematics during gait analysis. When using the 'Helen Hayes' passive reflective marker configuration in optical tracking systems, there are three markers that make up the foot and ankle complex: the lateral malleolus, the calcaneus (or heel) and the second metatarsal. Therefore, the heel and metatarsal markers make up the foot as if it was a rigid beam, allowing only the motion with respect to the ankle joint. Quantifying the kinematics of the foot in this way assumes that there are no additional movements that occur within the foot. Therefore, motion such as pronation of the midfoot, flexing of the medial longitudinal arch or inversion of the rearfoot cannot be quantified. This omission not only requires that each individual has the same foot structure and function (which is not the case), but also that the kinematics of the bones within the foot do not have any affect on a person's overall kinematics (which

is also not the case). Complete understanding of the biomechanics of the foot requires that the foot be treated as several interconnected segments.

### **1.3.1.1 Articulations and the Multi-Segment Foot Model**

The foot has many other movements and articulations that cannot be measured using standard optical gait analysis techniques. Non-standard, ‘multi-segment foot models’ have been created in order to divide the foot into four or five segments about that can be tracked individually. As mentioned in section 1.1.1, the four segments determined by Jenkyn & Nicol are the lateral forefoot (fifth metatarsal), medial forefoot (first metatarsal), midfoot (dorsal navicular tuberosity and 2<sup>nd</sup> & 3<sup>rd</sup> cuneiforms) and hindfoot (calcaneus) (Jenkyn & Nicol, 2007). The tarsals in the midfoot segment were assumed to be rigid in this analysis. This study quantified six joint motions between four foot segments and one lower limb segment using optical motion capture. Clusters of three non-collinear reflective markers were placed on each segment to determine how the different segments moved with respect to one another during gait. The talus orientation, though not directly tracked, was reconstructed using the adjacent lower leg and midfoot segments.

Pronation and supination of the foot are terms commonly used to describe positioning of the plantar surface of the foot and occur primarily at the subtalar (talocalcaneal) joint. At times, these motions are described in a simple manner, for example: during supination, the sole of the foot faces medially and during pronation, the sole faces laterally. However, as mentioned previously, these foot motions represent combined movements that occur in all three anatomical planes: abduction/adduction in the transverse plane, dorsi- and plantar flexion in the sagittal plane and inversion/eversion in the frontal plane (Hamill & Knutzen, 2003). Therefore, supination of the foot is a combination of inversion, adduction and plantar flexion whereas pronation is a combination of eversion, abduction and dorsiflexion. The multi-segment foot model described by Jenkyn and Nicol (2007) defines the motions of the foot and ankle complex with a bit more detail. For example, the subtalar (talocalcanealnavicular) joint was defined as the midfoot segment rotation with respect to the talus about the vector 2-axis

of the Subtalar Joint Coordinate System (JCS) defined by the International Society of Biomechanics (ISB) (Wu, et al., 2002).

ISB has published defined joint coordinate systems for most of the joints by defining anatomical axes to use as a standard for comparing movements and orientations about the particular joint (ISB, 2011). Though the anatomical axis for the ankle has been defined and gives reference to the calcaneus, there have been no standardized coordinate systems defined for the other joints of the foot complex.

### **1.3.2 Medial Longitudinal Arch (MLA)**

For this thesis, we are interested in the overall motion of the foot in all three anatomical planes, but specifically the movement of the medial longitudinal arch (MLA). The MLA is a concave arch that is located along the medial aspect of the foot between the head of the first metatarsal and the calcaneal tuberosity – the highest part of the arch being the talonavicular and naviculocuneiform joints. Another main structure that makes up the MLA is the plantar fascia (Norden & Frankel, 2001).

#### **1.3.2.1 MLA Function**

The development of the MLA had two major effects on the evolution of bipedal human gait: first, it provides the plantar flexors enough mechanical advantage to lift the weight of the body during the stance phase of gait, and secondly, it provides the foot with the capacity to absorb some of the increased shock cause by upright striding (Saltzman, Nawoczinski, & Talbot, 1995).

The movement of the MLA itself is complex and is explained in different ways, including using a term called the ‘windlass mechanism’ – described as dorsi-flexion of the metatarsophalangeal joints which generates traction on the plantar fascia and causes the arch to elevate. During toe-off in the gait cycle, the toes are dorsi-flexed passively as the body passes over the foot and the plantar fascia tightens and acts to shorten the distance between the metatarsal head and the heel (Norden & Frankel, 2001). This motion creates a rigid structure, in preparation of foot propulsion and this increased foot rigidity is reflected by the increase in arch height, as the forefoot is drawn in and closer to the rearfoot. Other studies have modeled the arch mechanically as a simple truss, which

predicts lower strain energy storage and more resultant injuries for both low- and high-arched individuals, as compared to those with normally arched feet (Simkin & Leichter, 1990).

The MLA is of considerable interest in recent research, as evidence suggests that arch structure can directly affect the kinematics of an individual. For example, one study compared leg stiffness in high and low arched runners. This study showed that high arched individuals had increased vertical ground reaction forces, largely due to decreased flexion at the knee, which led to increased knee stiffness (Williams III, Davis, Scholz, Hamill, & Buchanan, 2004). The arch has also been of interest in looking at its relationship with chronic plantar fasciitis, a condition of inferior heel pain where the insertion of the plantar fascia develops micro tears that are quite painful. One study did not find any relationship between plantar fasciitis and arch height nor excessive arch elongation when observing the arch in two dimensions with videofluoroscopy (Wearing et al., 2004).

Measuring in-vivo kinematics using two-dimensional videofluoroscopy does not capture the complex three-dimensional motions of the MLA. Typically, only motion in the sagittal plane is measured, and therefore any motions in the transverse and frontal planes, such as inversion apparent in a high arched foot or abduction in a flat foot, will not be taken into account. Capturing skeletal kinematics of the foot in all three planes, while performing dynamic gait, has not been reported in the literature to date. This thesis quantifies the motions of the MLA in all three dimensions using bi-planar fluoroscopic RSA during unrestrained, weight-bearing walking gait.

### **1.3.2.2 MLA Measurements & Angle**

As mentioned previously, the joint coordinate systems of the foot have not been defined or standardized by the International Society of Biomechanics (ISB). Therefore, there is a lack of standard when reporting on the kinematics of the foot segments, as well as a lack of standard for the local axis system in each articulating bone. With no 'gold standard' for measuring kinematics of the foot joints, their minute motions can only be compared within each subject and with similar studies in the literature. In three dimensions, a multi-segment foot model, as mentioned previously, measures the relative



movement of foot segments with respect to one another. Using a multi-segment foot model by Tome et al. (2006), in addition to marker clusters on five foot segments, a single marker was placed on the skin over the navicular tuberosity. This marker, along with the digitized points on the posterior calcaneus and first metatarsal head were used to generate the MLA angle (Tome, Nawoczenski, Flemister, & Houck, 2006). The dot product of the two 3-dimensional vectors from the navicular to the metatarsal head and navicular to the posterior heel was used to calculate the angle, which resulted in a planar representation of the MLA angle irrespective of foot position. A larger MLA angle indicates a decrease or lowering of the arch, whereas a smaller, more acute angle indicates an elevation of the MLA.

In measuring kinematics, it is almost impossible to place any set of markers in the same place for each subject, whether reflective markers for optical tracking or tantalum beads in standard RSA. Therefore, to quantify joint motion in skeletal kinematics, the position and orientation of one bone with respect to the other is required. For bi-planar fluoroscopy, since definite markers don't exist, bony landmarks must be digitized on a three-dimensional model in order to define the coordinate system for each bone. The same method applies to the bones in the medial longitudinal arch – the calcaneus, the navicular and the first metatarsal.

Coordinate systems are first created by taking a three-dimensional model of the bones of interest, typically developed from a CT scan. The models are created in a program called OsiriX and then each landmark is digitized with a point, denoted as a 'mesh' as described in section 1.2.4. The digitization process must be done carefully as choosing an incorrect landmark will create fixed errors in the bone coordinate system, throwing off the entire arch angle calculation.

#### **1.3.2.2.1 Calcaneus Coordinate System**

In order to create the coordinate system of the calcaneus, three bony landmarks are to be digitized (Figure 1.11). These points are the superior medial surface or the sustentaculum tali (ST), the medial process (MP) and the lateral anterior surface (LS). A unit vector was created from LS to MP and is defined as  $\hat{Z}^{cal}$ . An oblique vector, both inferior-superior and slightly posterior-anterior, was created from MP to ST. The cross

product of  $-\hat{Z}^{\text{cal}}$  and the vector MPST was taken to give an anteriorly and slightly medial pointed vector  $Y^{\text{cal}}$ . Finally, the cross product of  $Z^{\text{cal}}$  and  $Y^{\text{cal}}$  gives  $X^{\text{cal}}$ , which is an axis pointed proximally and slightly medial.

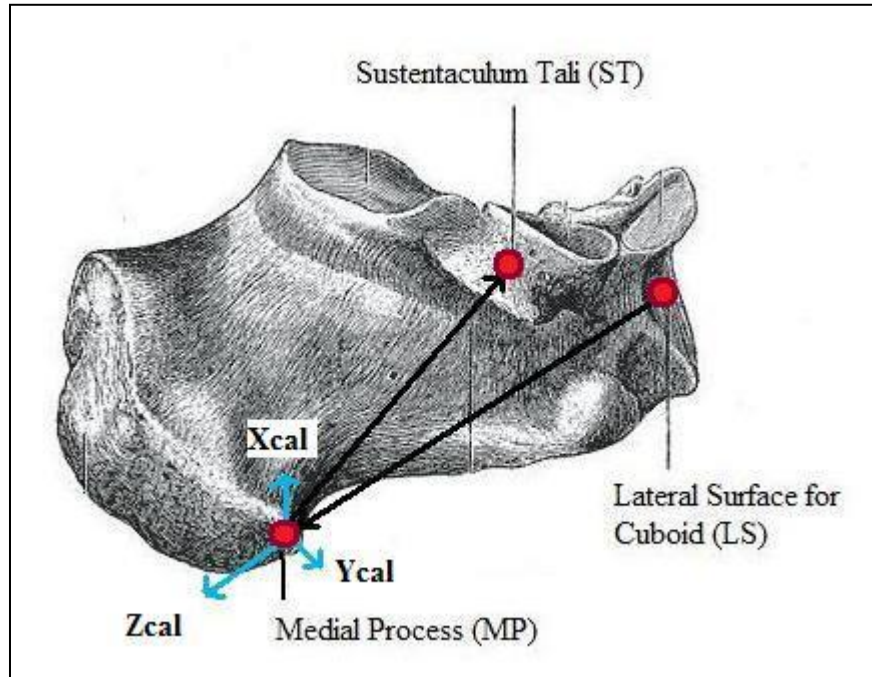


**Figure 1.11: Left calcaneus with bony landmarks defined in red on the medial process (MP), sustentaculum tali (ST) and lateral surface (LS) as well as the defined coordinate system and axes. Modified from (Kimball, 2011).**

The origin of the calcaneus coordinate system is established as the medial process (MP). Therefore a transformation matrix of the calcaneus coordinate system with respect to the laboratory coordinate system is written as:

$$T_{\text{cal}}^{\text{lab}} = \begin{vmatrix} x^{\text{cal}} & y^{\text{cal}} & z^{\text{cal}} & | & o^{\text{cal}} \\ 0 & 0 & 0 & | & 1 \end{vmatrix} \quad \text{Equation 1.4}$$

The specific orientations of the navicular and the first metatarsal with respect to the laboratory coordinate system are not required to calculate the angle of the medial longitudinal arch. Calculating the angle of the MLA requires the positions of the navicular and the first metatarsal with respect to the calcaneus coordinate system. Therefore, only two additional bony landmarks were also digitized – one on the navicular

tuberosity (NT), and one on the head of the first metatarsal (MH) (Figure 1.12). Please note that this figure shows the locations of the points in two dimensions; for example, the point on the metatarsal head is digitized at the very tip where it articulates with the phalange.

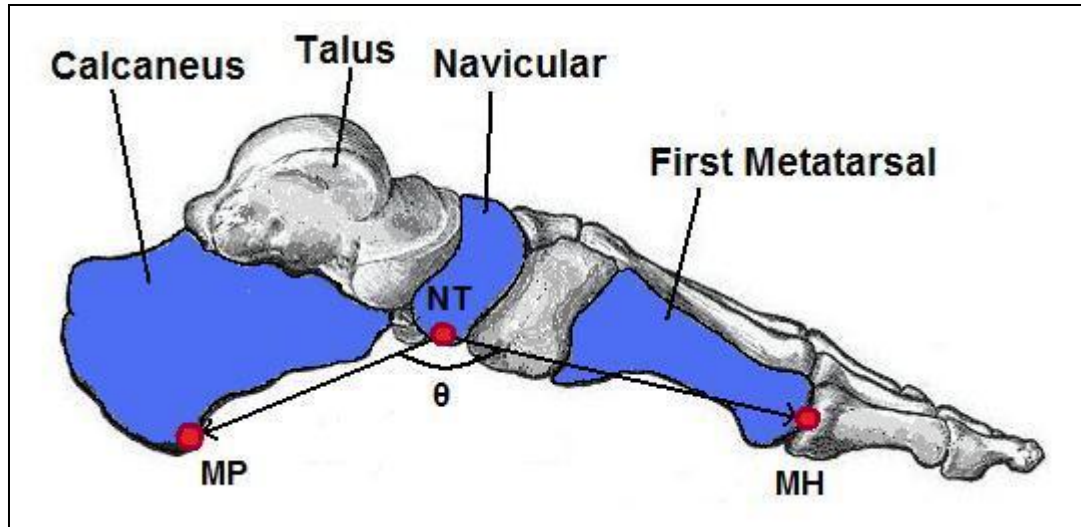


**Figure 1.12: Medial view of a left foot showing the angle theta ( $\theta$ ) of the medial longitudinal arch between the navicular tuberosity (NT), medial process of the calcaneus (MP) and first metatarsal head (MH). Modified from (Kimball, 2011).**

The inverse of the initial transformation matrix results in the transformation matrix of the lab with respect to the calcaneus, which is required in order to determine the coordinates of the two digitized points, NT and MH with respect to the calcaneus (Equation 1.5). Both matrices of these point coordinates must be augmented ('concatenated' function in MATLAB) with an additional '1' value as the last row of the matrix so that the matrix dimensions agree when performing matrix multiplication (Equations 1.6 and 1.7).

$$T_{lab}^{cal} = [T_{cal}^{lab}]^{-1} \quad \text{Equation 1.5}$$

$${}^{cal}P_{NT} = T_{lab}^{cal} * {}^{lab}P_{NT} \quad \text{Equation 1.6}$$

$${}^{cal}P_{MH} = T_{lab}^{cal} * {}^{lab}P_{MH} \quad \text{Equation 1.7}$$

### 1.3.2.2.2 MLA angle

Vectors are created from the navicular tuberosity (NT) to medial process (MP) and the metatarsal head (MH), all within the calcaneus coordinate system.

$$\overrightarrow{NTMP} = {}^{cal}P_{MP} - {}^{cal}P_{NT} \quad \text{Equation 1.8}$$

$$\overrightarrow{NTMH} = {}^{cal}P_{MH} - {}^{cal}P_{NT} \quad \text{Equation 1.9}$$

The lengths of the two vectors in the calcaneus coordinate system are determined ( $|NTMP|$  and  $|NTMH|$ ). The dot product of the two vectors is calculated and then inserted into the equation to determine theta ( $\theta$ ) as shown below and demonstrated in Figure 1.10.

$$\theta = \cos^{-1} \left[ \frac{(\overrightarrow{NTMP} \cdot \overrightarrow{NTMH})}{(|NTMP| \cdot |NTMH|)} \right] \quad \text{Equation 1.10}$$

This angle in 3D represents a measure of the height of the medial longitudinal arch. A smaller theta ( $\theta$ ) will represent a higher and more restricted arch, whereas a larger angle represents more of a flat arch, as the navicular is closer to the ground, and creating a greater span between those two vectors. This angle is calculated using custom MATLAB code ‘MLA\_Kinematics.m’ shown in Appendix B1.

## 1.4 ORTHOTICS

Any pathological change in foot structure or motion, however subtle, may have a profound impact on the foot’s shock-absorbing, propulsive, and stabilizing roles. Footwear in Western society can vary from a rigid ski boot to a soft moccasin. Some of these externally restrictive materials may alter normal foot and ankle biomechanics and ultimately cause the development of some pathological conditions (Norden & Frankel, 2001). However, footwear restriction may also contribute to stopping the progression of some lower limb musculoskeletal disorders; more specifically, the use of orthotics aids in restricting the motion of the medial longitudinal arch (MLA) during stance phase of gait

by constraining and supporting the bones of the medial column of the foot and limiting the elongation of the arch, alleviating stress on soft tissue of the lower limb.

#### **1.4.1 Custom and semi-custom orthotics**

The functional foot orthosis, or orthotic, is a conservative treatment for many musculoskeletal disorders. Most commonly, they are prescribed for foot pathologies such as pes planus (flat foot) and pes cavus (high arch). These conditions can cause people to have other musculoskeletal problems associated with their lower back, upper and lower legs, as well as general foot pain and discomfort (Edelstein & Bruckner, 2002).

In Canada, a physician typically refers a patient to a certified pedorthist, who then fits that patient with a pair of custom orthotics, tailored to the patient's specific biomechanical needs. Custom foot orthotics are quite pricey and are not always covered by extended health insurance plans; therefore, people may purchase off-the-shelf devices that have minimal foam padding, non-custom support or provide external stimulus to the foot such as a proprioceptive feedback-type orthotic (PFO) (Barefoot Science, Mississauga, Ontario, Canada). A PFO has a raised soft dimple under the middle of the plantar surface of the forefoot, which is supposed to encourage the intrinsic muscles of the foot to contract during gait. The purpose of the PFO device is to help strengthen the foot over time, with interchangeable levels of stimuli under the plantar surface of the forefoot. The PFO does not appear to have a rigid arch support built-in, or a heel cup to control rearfoot motion. This lack of support and robust structure is fairly typical for most off-the-shelf devices as they are not tailored to specific foot types.

In response to the issue of cost and function, a number of foot orthotic laboratories have developed semi-custom orthotics. Based on a range of height, length and width measures from selected landmarks of the foot, a finite number of molds can be designed. When the laboratory receives a negative impression (cast, foam, etc.), specific measurements are taken and the mold of best fit is chosen from a library of functional orthotic shapes. The devices are made from this mold and are therefore a compromise between cost and shape as it significantly reduces the time and expense of fabrication (Zifchock & Davis, 2008). Zifchock & Davis (2008) compared custom to semi-custom orthotics in both high and low-arched individuals using optical motion capture. This

study showed that the semi-custom device was a reasonable alternative to the custom device in terms of comfort and ability to control rearfoot motion. The effects that either of these devices had on the medial longitudinal arch were not examined in this study due to the relative motion between the markers and underlying bone. The kinematics of the medial longitudinal arch are still unknown with the use of orthotics, and therefore the proceeding studies will compare the effect of custom orthotics and a specific off-the-shelf device, the PFO, on volunteers with normal and extreme arch heights.

#### **1.4.2 Clinical Assessment**

Despite the abundance of studies on the anatomy of the medial longitudinal arch (MLA), there still remains some dispute about how to classify arch structure of different foot types. Some methods include physically measuring the arch height directly using anthropometric and radiographic techniques along with indirect approaches such as photographic and footprint methods (Saltzman et al., 1995). Other methods may have a clinician look at where the individual bears most of their weight. In normally arched feet, the weight-bearing is distributed evenly on all five metatarsal heads. In the extremely high arched foot characteristic of pes cavus, weight-bearing is distributed unevenly along the lateral border of the foot (Franco, 1987). People with pes planus often demonstrate a flat-footed gait with no toe-off, often associated with a large plantar weight-bearing surface with the main source of weight-bearing on the first and second metatarsals. For the purposes of this thesis, classifying the subject volunteers by arch structure and gait mechanics will be based on a series of comprehensive tests completed by a Canadian certified pedorthist (CPedC).

First, the patient will remove all shoes and socks, and roll up their pants so the pedorthist can see the patients' entire foot and ankle joint. The patient then stands in double limb weight-bearing stance so the pedorthist can examine overall navicular height with respect to the ground. The patient then rotates their hips to one side, and then the other to determine how the degree to which the arch is flexible or rigid. Similarly, the patient then completes a double and then single legged squat to determine the overall movement of the arch and its flexibility. Finally, the patient walks down a laneway and

back a few times so the pedorthist can determine the individual's inversion/eversion, forefoot adduction/abduction and their ankle plantar and dorsiflexion during gait.

From these specific tests, the pedorthist would decide to which group the individual belonged – a high navicular height combined with rearfoot inversion, forefoot adduction, ankle plantar flexion and a rigid arch in general, the individual would be in the pes cavus (high arch) group. Conversely a low navicular height combined with rearfoot eversion, forefoot abduction and ankle dorsiflexion, the individual would be in the pes planus group. Exclusion criteria for this thesis include a rigid pes planus individual determined by no movement of the arch during the hip rotation test.

### **1.4.3 Subtalar Joint Neutral Position**

The subtalar joint (STJ) is composed of the articulations between the talus and the calcaneus and its neutral position is defined as the position where the joint is neither supinated nor pronated (Pierrynowski & Smith, 1997; Elveru, Rothstein, Lamb, & Riddle, 1988). It is the most widely used reference point for the clinical measurement of the relationship of rearfoot to forefoot. This clinical measure can also be used to categorize individuals into groups based on forefoot position relative to the rearfoot, to determine whether it is everted or inverted relative to the calcaneus.

This subtalar joint neutral (STN) position provides the clinician with a relative zero measure from which to measure the STJ range of motion. The STN position is also used for casting of foot orthotics. The reliability of the STN position has been in question for quite some time. Previous studies have shown inconsistencies from experienced foot care specialists assessing patients and placing them in the STN position in the standing, seated, and prone position (laying face down on an examination table with leg projected beyond the back edge). The greatest variability occurred in the standing position compared with the other two positions ( $\pm 2.85$  degrees); however, the six raters examined in this study were more familiar with the seated and prone positions (Pierrynowski & Smith, 1997). The pedorthist for the proceeding studies is most familiar with the standing position for assessing the STJ and uses its neutral position in standing to cast the foot for orthotics using the foam box method.

#### **1.4.4 Orthotic Design & Casting**

The overall purpose of a foot orthotic is to aid in placing the foot in such a position as to encourage as near normal foot alignment and function as possible (Chuter, Payne, & Miller, 2003). Orthotics are prescribed and created from a cast of the patient's foot. The main purpose of an orthotic device is to provide support on the plantar aspect of the foot in an attempt to readjust the foot into a more appropriate weight-bearing position (Franco, 1987).

The orthotic is structurally made of four units: the shell or cast of the foot, the post (correcting platform), the forefoot extension and the cover. The cast of the foot is moulded by a Canadian certified pedorthist (CPedC) and represents the positive cast of the foot. The post or correcting platform holds the shell in the functional position desired by the clinician. The fore-foot extension consists of a piece of cushioning or supportive material that spans the width and length of the forefoot. The cover is the interface between the shell of the orthotic and the foot (Phillips, 1995). The cover and post are made of various materials, depending on the patient's specific biomechanical needs.

There are two different types of casting were used for the purposes of this thesis – plaster and foam casting. The plaster cast is created using strips of plaster material soaked in water and then placed on the foot while the patient is in the prone position (described previously). The plaster hardens while the clinician holds the individual in their subtalar joint neutral position. The volunteer is to be lying down on a table with their torso facing down with their feet over the end. The foam casting methods is completed while standing where the clinician presses their foot into a foam box while placing them in the subtalar neutral (STN) position.

### **1.5 RATIONALE**

The rationale for this study was developed from a few previous accomplishments in our laboratory. The markerless fluoroscopic RSA system, validated by Anne-Marie Allen at the Wolf Orthopaedic Quantitative Imaging Laboratory, can now be used for measuring in-vivo kinematics. The foot was chosen as the structure of study since there is a lack of knowledge on measuring its skeletal kinematics during weight-bearing, dynamic walking gait. Though the multi-segment foot model used with an optical motion capture



system gives an indication of the relative movement between the foot's segments, it is unable to capture the minute changes in specific foot bone positions and orientations during stance phase since it uses skin mounted optical markers. But the minute kinematics of the foot bones are of interest since abnormal foot structure and function is known to contribute clinically to certain lower limb musculoskeletal injuries and disorders. Capturing these minute bone motions can only be measured with 3D fluoroscopy and RSA. Additionally, any type of footwear and orthotics can be tested with bi-planar fluoroscopy and RSA without needing any alterations to the shoe or orthotic. Therefore, shoe integrity is maintained and the biomechanics of the shoed foot can be measured as it would normally be used. Also, fluoroscopic RSA allows for easy footwear changes during data collection, so that a range of footwear and orthotic types can be tested with a single testing session.

The introduction of a foot coordinate system with respect to the calcaneus is used for the bones that comprise the medial longitudinal arch – the calcaneus, navicular and first metatarsal. This relationship provides insight on a useful method to measure the medial longitudinal arch through various conditions. Additionally, there exists a lack of information on how foot orthotic interventions affect the foot with respect to skeletal kinematics. More specifically, it is not clear how the different types of orthotics affect the medial longitudinal arch in both static and dynamic scenarios.

## **1.6 OBJECTIVES AND HYPOTHESIS**

The primary objective of this thesis was to design and implement the experimental setup for using bi-planar fluoroscopic RSA on the foot during normal weight-bearing walking gait. The objectives of the subsequent studies were:

1. To directly measure the positions and orientations of the bones of the medial longitudinal arch (MLA) in static barefoot stance and compare these with the subtalar joint neutral position,
2. To compare MLA bone kinematics for barefoot static weight-bearing stance and dynamic walking gait to the same conditions in a neutral cushioning running shoes,

3. To quantify the changes in MLA angle between five different orthotic conditions using fluoroscopic markerless RSA, and
4. To compare the three-dimensional (3D) MLA angle measure with a two-dimensional (2D) measure of the MLA from the same data set using a method in the literature defined for use with single plane fluoroscopy.

All of the above studies are compared among three patient groups with different foot types: normal arch, pes planus (low arch), and pes cavus (high arch).

It was hypothesized that:

1. The static comparison of the subtalar neutral joint and neutral cushioning running shoe would show a decrease in arch angle across all subjects compared with barefoot, and that the decrease would be greater in the subtalar neutral position,
2. In dynamic gait, the running shoe condition would show a slightly smaller absolute arch angle compared with barefoot walking in all three subject groups,
3. A consistent angle decrease would be seen for all subjects with different orthotic interventions, and the pes planus group would respond better to the orthotics overall. Therefore, it was expected that the MLA angle would decrease the most for the planus group and the least amount for the cavus group. Furthermore, it was hypothesized that the firm orthotic will have a slightly greater effect in magnitude compared with the soft orthotic, and
4. The arch angles calculated would be different from 2D to 3D for each foot type, but that the changes between the calculated 2D and 3D angles would be consistent across all conditions for each participant.

## **1.7 THESIS OVERVIEW**

Chapter 2 describes the design of the wooden platform used for all subsequent chapters, as well as the effect of both the subtalar joint neutral position and neutral cushioning running shoes on the angle of the medial longitudinal arch. Chapter 3 shows how the neutral cushioning running shoes affect the medial longitudinal arch during dynamic gait by comparing the trials to barefoot walking. Chapter 4 compares the medial longitudinal arch using different orthotics during dynamic gait, both for overall effect of

the orthotics within subject groups as well as between subject groups (pes planus, pes cavus and normal). Chapter 5 presents an overall analysis of the findings using bi-planar fluoroscopic RSA and comparing them to a single plane fluoroscopic two-dimensional analysis. Chapter 6 summarizes the conclusions drawn from this work, outlines its significance, discusses possible limitations and suggests potential future work in this area of research.

## 1.8 REFERENCES

- Allen, A.-M. (2009). *Development and Validation of a Markerless Radiostereometric Analysis (RSA) System*. London, Canada: Western University.
- Bechard, D. J., Nolte, V., Kedgley, A. E., & Jenkyn, T. R. (2009). Total kinetic energy production of body segments is different between racing and training paces in elite Olympic rowers. *Sports Biomechanics*, 8(3), 199-211.
- Bingham, J., & Li, G. (2006). An Optimized Image Matching Method for Determining In-Vivo TKA Kinematics with a Dual-Orthogonal Fluoroscopic Imaging System. *Transactions of the ASME*, 128, 588-595.
- Bottner, F., Su, E., Nestor, B., Azzis, B., Sculco, T., & Bostrom, M. (2005). Radiostereometric Analysis: The Hip. *HSS Journal*, 1(1), 94-99.
- Bushberg, J. T., Seibert, J. A., Leidholdt, E. M., & Boone, J. M. (2002). *The Essential Physics of Medical Imaging: Second Edition*. Philadelphia: Lippincott Williams & Wilkins.
- Chuter, V., Payne, C., & Miller, K. (2003). Variability of Neutral-Position Casting of the Foot. *Journal of the American Podiatric Medical Association*, 93(1), 1-5.
- de Bruin, P., Kaptein, B., Stoel, B., Reiber, J., Rozing, P., & Valstar, E. (2008). Image-based RSA: Roentgen stereophotogrammetric analysis based on 2D-3D image registration. *Journal of Biomechanics*(41), 155-164.
- Edelstein, J. E., & Bruckner, J. (2002). *Orthotics: A Comprehensive Clinical Approach*. SLACK Incorporated.
- Elveru, R. A., Rothstein, J. M., Lamb, R. L., & Riddle, D. L. (1988). Methods for Taking Subtalar Joint Measurements. A Clinical Report. *Physical Therapy*, 68, 678-682.
- Franco, A. H. (1987). Pes Cavus and Pes Planus - Analyses and Treatment. *Physical Therapy*, 67(5), 688-694.

- Hamill, J., & Knutzen, K. M. (2003). *Biomechanical Basis of Human Movement: Second Edition*. Baltimore: Lippincott Williams & Wilkins.
- ISB. (2011). *Standards*. Retrieved October 20, 2011, from International Society of Biomechanics: <http://isbweb.org/information-services/standards>
- Jenkyn, T., & Nicol, A. (2007). A multi-segment kinematic model of the foot with a novel definition of forefoot motion for use in clinical gait analysis during walking. *Journal of Biomechanics*(40), 3271-3278.
- Karrholm, J. (1989). Roentgen stereophotogrammetry: Review of orthopedic applications. *Acta Orthopaedica Scandinavica*, 60(4), 491-503.
- Kedgley, A. (2009c). *Development of a Fluoroscopic Radiostereometric analysis system with an application to glenohumeral joint kinematics*. London, ON: School of Graduate and Postdoctoral Studies, Western University.
- Kedgley, A. E., Birmingham, T., & Jenkyn, T. R. (2009a). Comparative accuracy of radiostereometric and optical tracking systems. *Journal of Biomechanics*(42), 1350-1354.
- Kedgley, A., & Jenkyn, T. R. (2009b). RSA calibration accuracy of a fluoroscopy-based system using nonorthogonal images for measuring functional kinematics. *Medical physics*, 36(7), 3176-3180.
- Kimball, R. (2011). *Osteology of the Foot*. Retrieved January 2012, from Podiatry Boards Part 1 Review: <http://podiatryboards.web.officelive.com/footbones.aspx>
- Leardini, A., Chiari, L., Della Croce, U., & Cappozzo, A. (2005). Human movement analysis using stereophotogrammetry Part 3. Soft tissue artifact assessment and compensation. *Gait and Posture*, 212-225.
- Norden, M., & Frankel, V. H. (2001). *Basic Biomechanics of the Musculoskeletal System: Third Edition*. Baltimore: Lippincott Williams & Wilkins.
- Phillips, J. (1995). *The Functional Foot Orthosis* (2nd ed.). Churchill Livingstone.
- Pierrynowski, M. R., & Smith, S. B. (1997). Effect of Patient Position on the Consistency of Placing the Rearfoot at the Subtalar Neutral. *Journal of the American Podiatric Medical Association*, 87(9), 399-406.
- Rougee, A., Picard, C., Ponchut, C., & Troussset, Y. (1993). Geometrical Calibration of X-ray Imaging Chains for Three-Dimensional Reconstruction. *Computerized Medical Imaging and Graphics*, 17(4/5), 295-300.
- Saltzman, C. L., Nawoczenski, D. A., & Talbot, K. D. (1995). Measurement of the Medial Longitudinal Arch. *Archives of Physical Medicine and Rehabilitation*, 76(1), 45-49.

- Selvik, G. (1989). Roentgen stereophotogrammetry. A method for the study of the kinematics of the skeletal system. *Acta orthopaedica Scandinavica*, 232, 1-51.
- Selvik, G. (1990). Roentgen Stereophotogrammetric Analysis. *Acta Radiologica*, 31(2), 113-126.
- Simkin, A., & Leichter, I. (1990). Role of the calcaneal inclination in the energy storage capacity of the human foot - a biomechanical model. *Medical & Biological Engineering & Computing*, 28, 149-152.
- Tome, J., Nawoczenski, D. A., Flemister, A., & Houck, J. (2006). Comparison of Foot Kinematics Between Subjects with Posterior Tibialis Tendon Dysfunction and Healthy Controls. *Journal of Orthopaedic & Sports Physical Therapy*, 36(9), 635-644.
- Valstar, E. R., Gill, R., Ryd, L., Flivik, G., Borlin, N., & Karrholm, J. (2005). Guidelines for standardization of radiostereometry (RSA) of implants. *Acta Orthopaedica*, 76(4), 563-572.
- Wearing, S. C., Smeathers, J. E., Yates, B., Sullivan, P. M., Urry, S. R., & Dubois, P. (2004). Sagittal Movement of the Medial Longitudinal Arch Is Unchanged in Plantar Fasciitis. *Medicine & Science in Sports & Exercise*, 1761-1767.
- Wearing, S. C., Smeathers, J. E., Yates, B., Sullivan, P. M., Urry, S. R., & Dubois, P. (2005). Errors in measuring sagittal arch kinematics of the human foot with digital fluoroscopy. *Gait and Posture*, 21, 326-332.
- Williams III, D. S., Davis, I. M., Scholz, J. P., Hamill, J., & Buchanan, T. S. (2004). High-arched runners exhibit increased leg stiffness compared to low-arched runners. *Gait and Posture*, 19, 263-269.
- Wu, G., Siegler, S., Allard, P., Kirtley, C., Leardini, A., Rosenbaum, D., . . . Stokes, I. (2002). Letter to the editor: ISB recommendation on definitions of joint coordinate system of various joints for the reporting of human joint motion - part I: ankle, hip, and spine. *Journal of Biomechanics*, 35, 543-548.
- Zifchock, R. A., & Davis, I. (2008). A comparison of semi-custom and custom foot orthotic devices in high- and low-arched individuals during walking. *Clinical Biomechanics*, 23, 1287-1293.
- Zuffi, S., Leardini, A., Catani, F., Fantozzi, S., & Cappello, A. (1999). A model-based method for the reconstruction of total knee replacement kinematics. *IEEE Transactions on Medical Imaging*, 18(10), 981-991.
- zunzun.com*. (n.d.). Retrieved 2011, from Online Curve Fitting - User Selectable Polynomial: [www.zunzun.com](http://www.zunzun.com)

## **CHAPTER 2 – STATIC BAREFOOT, NEUTRAL CUSHIONING RUNNING SHOE AND SUBTALAR JOINT NEUTRAL**

### **2.1 INTRODUCTION**

Markerless RSA is an accurate method to quantify skeletal kinematics. By integrating x-ray fluoroscopy with RSA, the combined method enables the collection of dynamic in-vivo data by capturing moving x-ray images. A study was completed by Allen (2009) as described in section 1.2.1 to validate the markerless fluoroscopic RSA (fRSA) system for the Wolf Orthopaedic Quantitative Imaging Laboratory (WOQIL). The following study demonstrates the clinical use of this validated markerless RSA system to measure in-vivo skeletal kinematics without the requirement of embedding tantalum markers into each bone. To the best of the author's knowledge, using markerless fRSA to quantify the motions of the foot bones and more specifically, the medial longitudinal arch (MLA) has not been performed to date.

Despite the abundance of studies evaluating the anatomy and biomechanics of the medial longitudinal arch (MLA), there still remains some dispute about how to classify arch structure. Some methods include physically measuring the arch height directly using anthropometric and radiographic techniques along with indirect approaches such as photographic and footprint methods (Saltzman et al., 1995). Others use arch index (AI), a measurement that uses a caliper device to measure the dorsum height at 50% of total foot length and dividing that value by the truncated foot length measured from the heel to the first metatarsal head (Williams & McClay, 2000). Molloy et al. (2009) used the AI to initially classify individuals by arch height but then analyzed both mean plantar contact area and mean plantar pressure differences between low- and high-arched feet across three different shoed conditions.

The MLA is of considerable interest in recent research, as evidence suggests that arch structure can affect an individual's overall kinematics. Using optical motion capture, previous researchers found an increase in leg stiffness in high arch compared to low arch runners due to increased knee flexion and peak ground reaction forces (Williams III et al., 2004). In order to look at the structure and function of the foot itself, and not just its effect on the rest of the body, multi-segment foot models have been developed to

quantify the motion of different foot segments using optical motion capture. Traditional motion capture considers the foot to be a rigid segment and so multi-segment models were developed to provide more insight on foot function and kinematics (Jenkyn & Nicol, 2007).

A version of a multi-segment foot model has been used by researchers to determine the change in MLA angle in posterior tibialis tendon dysfunction (PTTD) (Tome et al., 2006). In this study, researchers added a reflective marker on the skin overlying the navicular tuberosity, in addition to marker clusters placed on the posterior calcaneus and first metatarsal head, to calculate an angle in three dimensions using the dot product of two vectors from the navicular to both the metatarsal head and the posterior calcaneus. This angle measurement was calculated using optical motion capture, therefore error due to skin mounted markers is probable.

The purpose of this study was to quantify the medial longitudinal arch (MLA) angle using a similar angle measure to Tome et al. (2006) in static weight-bearing stance and compare this angle between three foot types for three conditions. The three different foot types studied were normal arch, pes cavus (high arch) and pes planus (low arch), and the three static stance conditions were no shoe (barefoot), neutral cushioning running shoes and barefoot while being held in the subtalar joint neutral (STN) position. It was hypothesized that the cavus and planus groups would show the smallest and largest mean MLA angle, respectively. It also was hypothesized that both the running shoe and STN position would show an angle decrease from barefoot stance, with the STN position showing a greater decrease in MLA angle for all subjects.

## **2.2 METHODS**

In order to capture the desired view of the foot in each fluoroscope, a platform was designed and created out of plywood in order to raise the participants to a level where the fluoroscopes could take an x-ray of their left foot. Prior to the development of this platform, the fluoroscopy machines were positioned correctly to assure the proper view of the foot, and therefore the platform could be built to fit that precise fluoroscope configuration.

A sketch was made initially to include the measurements and dimensions of the platform and it was then drafted by staff at Western University's machine shop in Solid Works (Dassault Systèmes SolidWorks Corporation, Waltham, MA, USA), illustrated in Figure 2.1(a). Following approval of the sketch and 3D model, the platform was then built in such a way that it could be erected and dismantled with ease and in a timely manner. A railing was later added for the safety of the volunteers, as the platform stands above the ground by approximately one meter (Figure 2.1(b)).

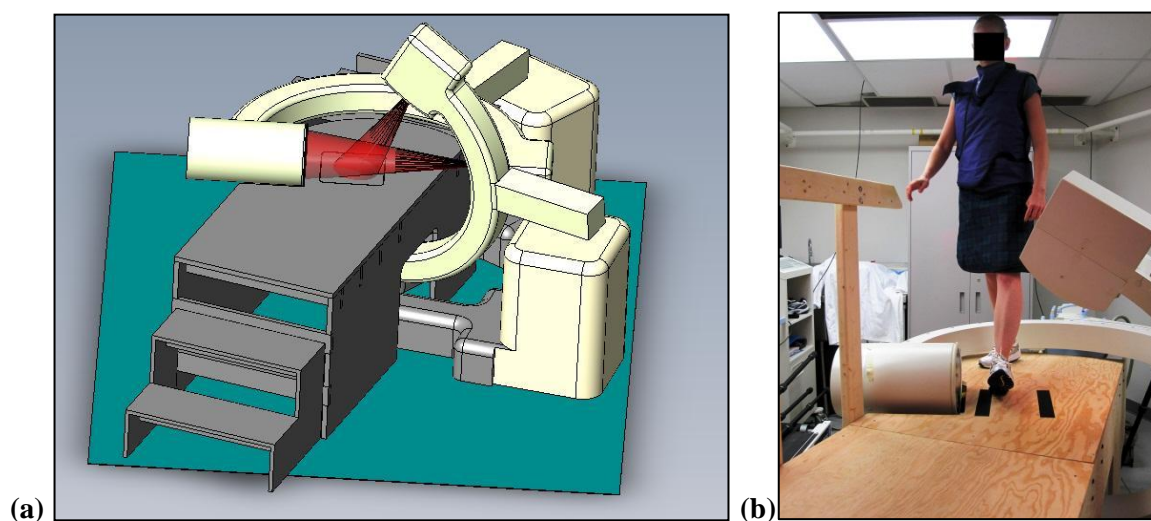


**Figure 2.1: (a) Solid Works drawing of fluoroscope configuration and proposed platform design, and (b) photograph of erected plywood platform designed for bi-planar fluoroscopy of the foot.**

Sixteen participants (mean age 27.4 years) were recruited from the Fowler Kennedy Sports Medicine Clinic by a Canadian certified pedorthist (CPedC). The participants consisted of 6 normal arch, 5 pes planus and 5 pes planus, and among those were 8 males and 8 females. The pedorthist performed a clinical assessment of the participants' gait patterns and the structure and function of their medial longitudinal arch to assure they fit in either the normal arch, pes cavus (high arch) or pes planus (low arch) group. Participants in the normally arched group were asymptomatic with no history of foot or ankle problems. The detailed clinical assessment is described in section 1.4.2.

The image intensifiers of two fluoroscopes (SIREMOBIL Compact (L); Siemens Medical Solutions USA Inc., Malvern, PA, USA) were set-up up at approximately 120° to one another and were positioned to capture a sagittal plane, lateral view of the left foot



and an oblique anterior-posterior view to capture rearfoot position. For each condition, simultaneous images were taken with the fluoroscopes, which are 720 pixels by 540 pixels in size. The voltage and current settings were approximately 50 kV and 0.3 mA for each testing date.

Fluoroscope calibration was performed before executing the experimental protocol by imaging a calibration frame designed by Kedgley (2009c) with embedded beads at known locations. The calibration frame was in a position for each fluoroscope to capture an image with visible beads on both fiducial and control planes (described in section 1.2.2). Calibration was performed once at the beginning of testing, and once following the recording of the fluoroscopic images in order to account for any accidental bumping or kicking of the fluoroscopes during data collection.

Participants stood in quiet (single limb) full weight-bearing stance and a static image was then taken of the left foot. Three static conditions were looked at for this study – barefoot, neutral cushioning running shoe and subtalar neutral (STN) position. Each participant was held in the STN position by the same Canadian certified pedorthist that initially assessed their foot structure and function. A detailed description of this position is described in section 1.4.3. For each static trial, it was ensured that the hindfoot, navicular, first cuneiform and the base of the first metatarsal were visible in both fluoroscopes for a more accurate matching procedure (Figure 2.2).

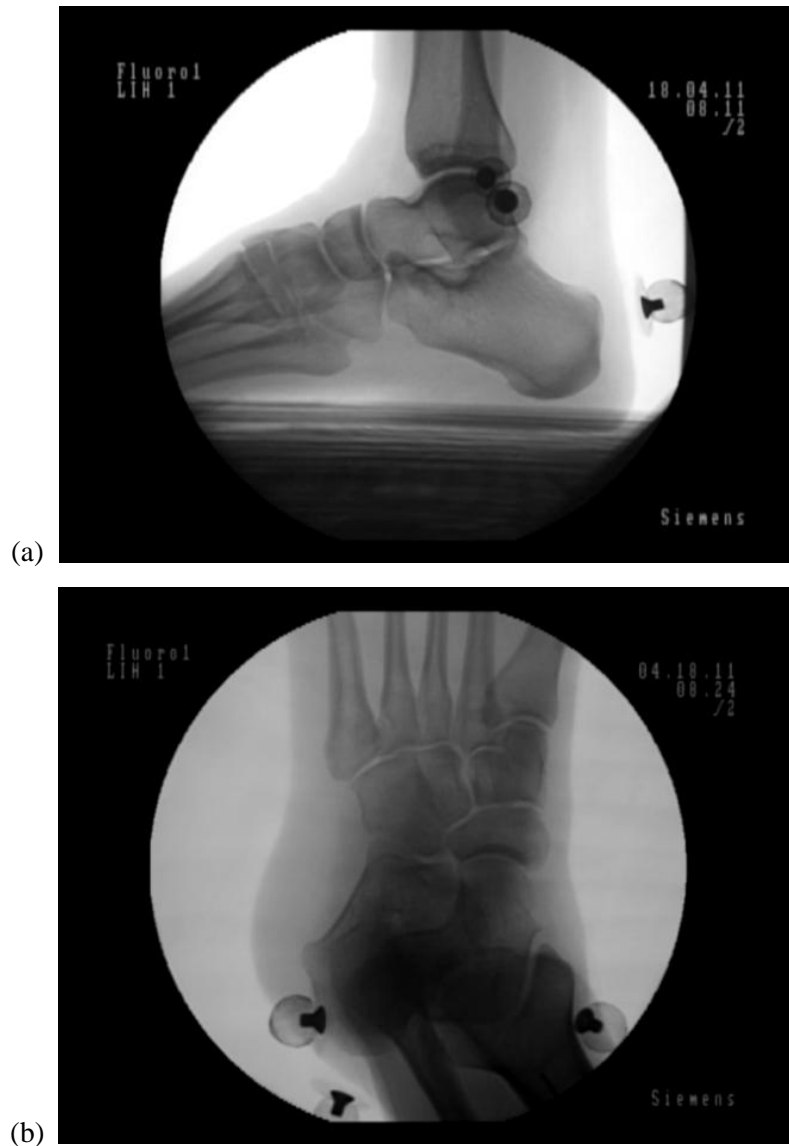


**Figure 2.2: Pes cavus participant static barefoot image from the (a) lateral view (fluoroscope A), and (b) anterior-posterior oblique view (fluoroscope B).**

Following data collection, the calibration images of the fluoroscope were corrected for pin cushion distortion by imaging a distortion grid as described in section 1.2.2. The distortion grid image was taken by both fluoroscopes separately, following data collection and calibration.

Once these images are taken by both fluoroscopes, the locations of the beads in both images were determined using a calibration algorithm in MATLAB (The MathWorks, Natick, MA, USA). This algorithm allows the user to pick each point in

numerical order, and imports the image coordinates of the selected points into a spreadsheet. After selecting the points on the image and using their known two-dimensional locations, the points were then corrected for distortion (described in section 1.2.2.1). Finally, the relationship between these points and the known 3D locations of the calibration frame beads determined the location of the x-ray foci.

Following the acquisition of the x-ray source positions, an additional series of MATLAB algorithms were used to determine the parameters of each fluoroscope – meaning the orientation and location of the image plane with respect to the x-ray focus. This series of three additional algorithms not only determines the three Euler angle rotations, but optimizes these parameters, assuring a root mean squared error (RMSE) of less than 0.5 giving the user a guideline for accuracy.

The symbolic equations for  $l_p$  and  $c_p$  were determined in Maple (Maplesoft, Waterloo, ON, Canada) as described in 1.2.2.2 by creating the perspective projection model for this study's specific calibration and fluoroscope orientation. The P-matrix was then defined and then a series of rotations and translations resulted in expressions for both ' $c_p$ ' and ' $l_p$ ', which were then copied into an existing MATLAB function. This function was used in conjunction with a custom algorithm, along with the 3D calibration points (x, y, z) and their 2D projected coordinates (c, l) to determine the initial estimates of the Euler angle rotations and fluoroscope distances (Allen, 2009). Each calibration and optimization routine was performed for each fluoroscope separately.

After acquiring the final parameters in MATLAB, the experimental set-up for each fluoroscope was recreated in a solid modelling program (Rhinceros; Robert McNeel & Associates, Seattle, WA, USA). Using instructions from Appendices E and F of Anne-Marie Allen's thesis (2009), the set-up for each testing date was recreated with the acquired calibration parameters and x-ray foci positions for each fluoroscope. This set-up allowed for each image plane to be viewed by its corresponding x-ray source, the precise location to match the 3D bone model to the two 2D images.

The matching procedure recreated the pose of the objects captured by both fluoroscopes. The 3D models of all three bones, along with their designated bony landmarks, were imported into the recreated experimental set-up where they were rotated and translated in three dimensions. The bony landmarks were used to manually match the

bones in these final stages, until the silhouette's bones match the outline of the landmarks on the image, translating images as little as 0.05mm in one direction.

A similar angle calculation to the one used by Tome et al. (2006) was used for this study to quantify the MLA of the foot. Once the bones were manually matched, the locations of the first metatarsal head, the medial process of the calcaneus, and the navicular tuberosity in three-dimensional space were exported to an Excel file using RhinoScript created by Allen (2009). Custom MATLAB code was then employed ('MLA\_Kinematics.m' – Appendix B1) to calculate the medial longitudinal arch angle using vector and matrix mathematics (see Section 1.3.2). The output of this algorithm was an angle in three-dimensional space (in degrees) which was compared among the three conditions by calculating the changes in angle from barefoot stance.

Statistical analysis was performed using SPSS (IBM Corporation, Armonk, New York, USA). A repeated measures analysis of variance test (ANOVA) with Bonferroni correction was used to detect the statistical differences in the measured arch angle for the three conditions across all subjects. An additional analysis was completed using a multivariate general linear model to determine if there was a significant difference between foot types (normal, planus and cavus). Statistical significance was set at  $p < 0.05$ . Where appropriate, Tukey's post-hoc analyses were used to evaluate statistical differences.

## 2.3 RESULTS

The mean medial longitudinal arch (MLA) angles of the three foot types are shown in Table 2.1 along with the standard deviations (SD). In barefoot static stance, the planus group (low arch) had the greatest mean arch angle ( $127.8^{\circ} \pm 13.7^{\circ}$ ) and the smallest mean angle was seen by the normal group ( $98.7^{\circ} \pm 17.0^{\circ}$ ). The pes cavus (high arch) group had an average arch angle of  $110.9^{\circ} \pm 15.8^{\circ}$ . Maximum and minimum arch angles are shown in Table 2.2, which also shows the range between these values in each patient group during static barefoot stance.

Figure 2.3 shows the average angle differences within each patient group – normal, pes cavus and pes planus. The largest difference occurred in the planus group, with an average angle decrease of  $-13.7^{\circ} \pm 3.2^{\circ}$  in the STN position with respect to the

barefoot condition. The average angle decreases were  $-10.8^{\circ} \pm 4.2^{\circ}$  and  $-9.6^{\circ} \pm 3.5^{\circ}$  for the normal and cavus groups, respectively.

The STN position demonstrated a decrease in arch angle across all subjects ranging from  $-4.20^{\circ}$  to a maximum angle arch decrease of  $-19.01^{\circ}$ . Figure 2.4 shows the arch angle differences for each subject in the STN position as compared with the barefoot condition, along with the mean difference of  $-11.3^{\circ} \pm 3.8^{\circ}$  as well as two lines representing  $\pm 1$  SD from the mean. It should be noted that the two subjects with the greatest change in arch angle across all subjects (difference of more than -1 standard deviation from the mean) were from the normal and planus groups. The two subjects that showed the least amount of decrease in arch angle belong to the normal and cavus groups.

Comparing the neutral cushioning running shoe to barefoot stance, the difference in arch angle between subjects was slightly more variable, with the range of arch angle differences spanning from a decrease of  $-13.24^{\circ}$  to an increase of  $5.07^{\circ}$  (Figure 2.5). Thirteen of sixteen participants fell within  $\pm 1$  SD from the mean arch angle difference of  $-1.92^{\circ} \pm 6.9^{\circ}$  as seen in Figure 2.5. Two of the planus participants showed an angle decrease of more than one standard deviation from the mean.

These results across all subjects were significant ( $p < 0.05$ ) in the subtalar neutral position (STN) as compared with barefoot stance whereas the neutral cushioning running shoe did not demonstrate a significant change over all subjects compared with barefoot ( $p > 0.05$ ). Statistical significance was also apparent when looking at the differences between group means ( $p < 0.05$ ). With the use of Tukey's post-hoc analysis, results showed a significant difference between the normal and the planus groups in both the barefoot and the subtalar neutral positions ( $p = 0.02$ ,  $p = 0.034$ ).

An interesting finding was discovered when calculating the lengths of the vectors used to form the MLA angle and comparing them amongst pathological foot types. This was completed after the unexpected results of the barefoot arch angles of the cavus group. The mean distances from the navicular tuberosity (NT) to both the metatarsal head (MH) and the medial process (MP) of the calcaneus were calculated using the static barefoot trials of fifteen of the same participants, five from each group. The vectors were then normalized for foot length (L) and then averaged within each group – values are

shown in Table 2.3. The scalar NTMP/L was significantly different for the cavus foot type ( $p < 0.05$ ) when compared with both planus and normal foot types using a one-way analysis of variance (ANOVA) and Tukey's post-hoc test.

**Table 2.1: Mean MLA angle measurements during static stance conditions: barefoot, subtalar neutral position and neutral cushioning running shoe.**

MLA Angle (degrees)	Normal (6 Total)		Cavus (5 Total)		Planus (5 Total)	
	Mean	SD	Mean	SD	Mean	SD
Barefoot	98.7 <sup>a</sup>	16.0	110.9	15.8	127.8 <sup>b</sup>	13.7
STN	87.9 <sup>a,c</sup>	14.7	101.3 <sup>c</sup>	18.3	114.0 <sup>b,c</sup>	11.5
Shoe	100.7	11.9	106.6	17.3	123.4	19.0
Change from Barefoot	Mean	SD	Mean	SD	Mean	SD
STN	-10.8	4.2	-9.6	3.5	-13.7	3.2
Shoe	2.04	4.1	-4.3	3.0	-4.3	7.9

<sup>a</sup> Significantly different versus the planus group ( $p < 0.05$ )

<sup>b</sup> Significantly different versus the normal group ( $p < 0.05$ )

<sup>c</sup> Significantly different versus barefoot static stance ( $p < 0.05$ )

**Table 2.2: Mean, maximum, minimum and range measurements of static barefoot MLA angles for three foot types – normal, pes cavus and pes planus.**

	MLA Angle (degrees)			
	Mean	Maximum	Minimum	Range
<b>Normal</b>	99	129	84	45
<b>Cavus</b>	111	128	88	40
<b>Planus</b>	128	139	104	35

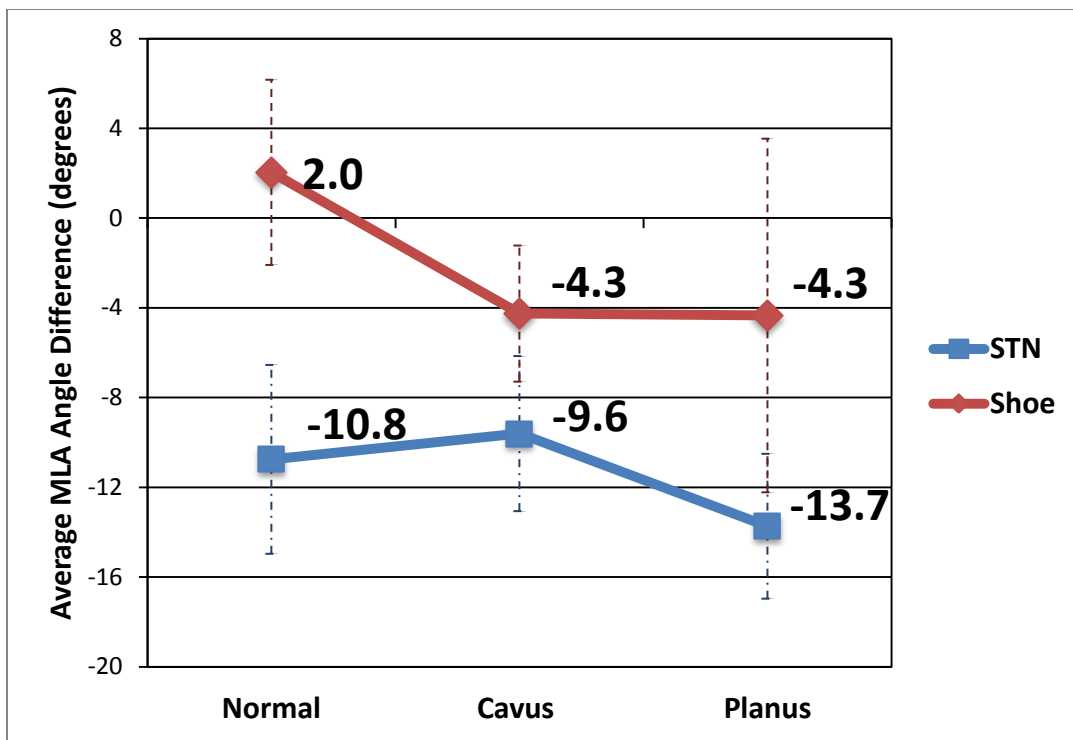


Figure 2.3: Mean arch angle differences for normal, cavus and planus foot types of the subtalar neutral (STN) position and neutral cushioning running shoe from the barefoot case. Error bars are +/- 1SD from the mean of each group.

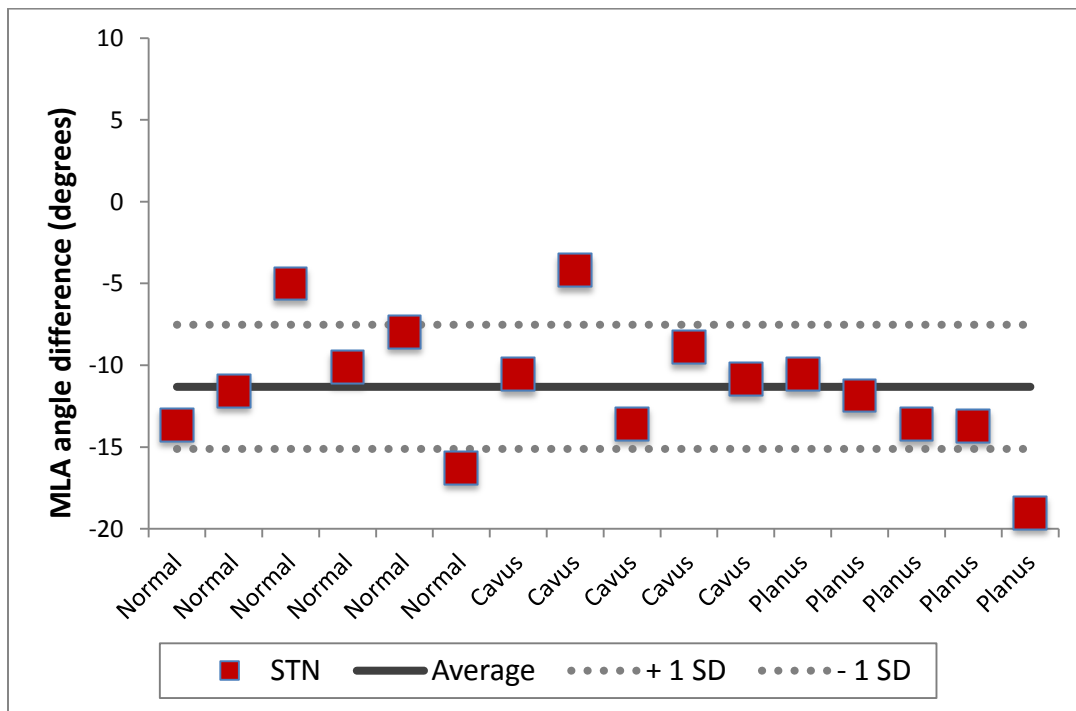
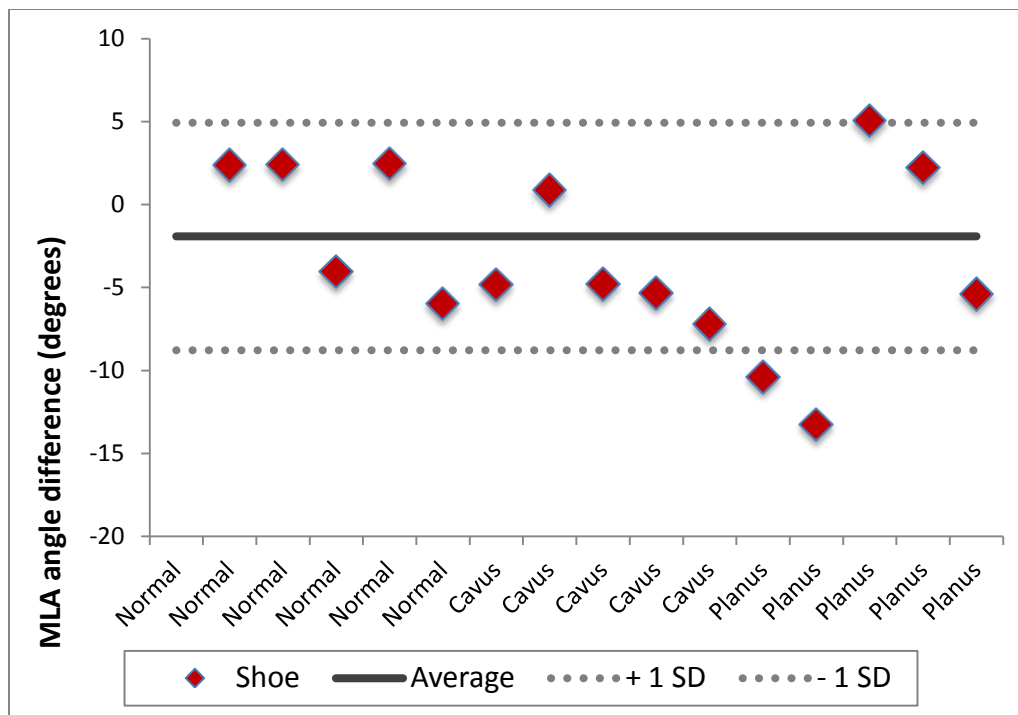


Figure 2.4: Arch angle differences with respect to barefoot stance for subjects for three different foot types in the subtalar neutral position.



**Figure 2.5: Arch angle differences for subjects with three different foot types: normal, pes cavus and pes planus, while wearing running shoes with respect to barefoot stance.**

**Table 2.3: Mean vector magnitudes (NTMH and NTMP) normalized to foot length and compared between pathological groups. These are the two vectors that comprise the medial longitudinal arch angle.**

	NTMH/L	SD	NTMP/L	SD
<b>Normal</b>	0.389	0.012	0.445	0.080
<b>Planus</b>	0.382	0.020	0.451	0.035
<b>Cavus</b>	0.399	0.014	0.591 <sup>a</sup>	0.049

<sup>a</sup> Significantly different versus normal and planus groups ( $p < 0.05$ )

## 2.4 DISCUSSION

The purpose of this study was to quantify the medial longitudinal arch (MLA) angle in static weight-bearing stance and compare this angle between three foot types for three conditions. The three different foot types studied were normal arch, pes cavus (high arch) and pes planus (low arch), and the three static stance conditions were no shoe (barefoot), neutral cushioning running shoes and barefoot while being held in the subtalar



joint neutral (STN) position. As hypothesized, the greatest mean MLA angle during barefoot static stance was measured in the pes planus group and it was significantly different versus the mean barefoot angle of the normal arch group. This outcome was expected because a pes planus patient should have a greater barefoot arch angle than a normal patient since by definition, they will show increased pronation of the forefoot and eversion of the rearfoot, flattening the arch (Franco, 1987).

The normal group showed the smallest mean barefoot arch angle, which was not coincident with the hypothesis. The mean MLA angle for the cavus group was greater than the normal group, which was a surprising result given the cavus foot type will typically have the highest (visible) arch height of the three groups. This is because the cavus foot structure is typically considered to be oversupinated while supporting most of the weight with the lateral side of the foot causing rearfoot inversion (Xiong, Goonetilleke, Witana, Weerasinghe, & Au, 2010). Based on this expected foot position, it was thought that these items would translate into a smaller calculated MLA angle. Since this initial measure did not reflect the hypothesis, magnitudes were calculated for the two vectors that form the MLA angle. The normalized length of the vector from the navicular tuberosity to the medial process of the calcaneus was found to be significantly greater in the pes cavus group compared with the mean vector magnitudes of the other two pathological groups. By definition, the rearfoot of a pes cavus is inverted, and the forefoot is supinated at the transverse tarsal joint (Franco, 1987). Therefore, this significantly larger distance from the navicular tuberosity to the calcaneus may indicate that the position of the calcaneus is in a slightly different orientation than expected and is perhaps more everted than previously thought. It is recommended that the osseous structure of a larger sample of pes cavus patients be investigated further to determine if there is a trend in foot structure that is causing this longer vector and thus, resulting in a greater than expected MLA angle.

The secondary hypothesis for this study was supported since an overall MLA angle decrease was seen in both the subtalar neutral (STN) position and with neutral cushioning running shoes. A greater decrease in angle was measured in the STN position and it was statistically significant across all study participants as compared with barefoot static stance. As noted in the results, the two largest angle decreases ( $-19.0^{\circ}$  and  $-16.8^{\circ}$ )

were seen in subjects from the pes planus and normal groups, respectively. These larger angle decreases were likely the result of greater initial (barefoot) arch angles for these two participants, meaning an increase in pronation of the forefoot and eversion of the rearfoot. The subtalar neutral (STN) position is used by clinicians when creating the cast of a patient's foot for orthotic fabrication by placing the foot in the 'neutral' position and serves as a reference point for other lower extremity measurements (Elveru, Rothstein, Lamb, & Riddle, 1988). Therefore, the clinician likely requires a greater adjustment for the participants with a larger barefoot MLA angle in order to get them into the STN position. This large adjustment was not expected from a participant in the normal group since the normal foot type would usually have a fairly neutral barefoot arch angle, and therefore, the change to the subtalar joint neutral position would be smaller. However, in this particular case, the normal subject's MLA angle in barefoot stance was approximately 129°, similar to the mean planus group MLA angle. This large barefoot angle likely accounts for the large adjustment and consequently, an MLA angle decrease, to get this normal participant into the STN position.

Results demonstrated a large MLA angle range across all subjects when comparing static barefoot stance with the neutral cushioning running shoe. As hypothesized, a smaller mean decrease in arch angle was measured for all subjects when compared with the subtalar neutral condition results. Both the cavus and planus groups showed a small decrease in arch angle when wearing cushioning shoes compared with barefoot, though neither change was considered significant. In the normal group, the mean MLA angle change was in the positive direction, showing a small MLA angle increase. These findings indicate that the cushioning shoe gave added support for the planus and cavus participants, therefore elevating the arch slightly, restricting its ability to elongate during flatfoot of stance phase. This restriction is indicated by less movement of the medial midfoot and thus, a slightly smaller degree of pronation for patients with pes planus and pes cavus. In contrast, wearing running shoes and weight-bearing may have allowed the arch to elongate further in the normal group, increasing pronation slightly and resulting in a greater overall MLA angle of the foot.

Strengths of this study lie in the consistency of evaluating each participant by using the same clinician. Additionally, the evaluation performed by this clinician was

completed in a regular clinical setting. This same clinician (pedorthist) was also the individual who placed each participant in the STN position during testing. Keeping the clinician consistent eliminates any error due to slight differences in examination style, however, the reliability of this particular clinician has not been studied specifically, therefore errors may exist that cannot be quantified for this study.

Due to the nature of the extensive experimental protocol and time constraints of the study, only a small number of subjects in each group were tested. Another possible limitation to the study may be reflected in the variability in the absolute arch angles. It was expected that participants in the cavus group would have the smallest mean arch angle and the planus group to have the largest (with the normal group in between) but this was not the case. An interesting calculation discovered a difference in vector magnitudes between groups, which may explain this arch angle discrepancy in terms of foot structure. However, variability in arch angle measures may also be attributed to some participants having appeared to function as a pes cavus or a normal patient, but their absolute arch angle may not have reflected their overall foot function, causing slightly inconsistent angles and differences between conditions. Further analysis should include comparing the subtalar joint neutral angle with the use of orthotics since the ultimate goal of orthotics are to restrict the medial longitudinal arch and maintain close to neutral position through flatfoot in gait.

## 2.5 REFERENCES

- Allen, A.-M. (2009). *Development and Validation of a Markerless Radiostereometric Analysis (RSA) System*. London, Canada: Western University.
- Elveru, R. A., Rothstein, J. M., Lamb, R. L., & Riddle, D. L. (1988). Methods for Taking Subtalar Joint Measurements. A Clinical Report. *Physical Therapy*, 68, 678-682.
- Franco, A. H. (1987). Pes Cavus and Pes Planus - Analyses and Treatment. *Physical Therapy*, 67(5), 688-694.
- Jenkyn, T., & Nicol, A. (2007). A multi-segment kinematic model of the foot with a novel definition of forefoot motion for use in clinical gait analysis during walking. *Journal of Biomechanics*(40), 3271-3278.

- Kedgley, A. (2009c). *Development of a Fluoroscopic Radiostereometric analysis system with an application to glenohumeral joint kinematics*. London, ON: School of Graduate and Postdoctoral Studies, Western University.
- Molloy, J. M., Christie, D. S., Teyhen, D. S., Yeykal, N. S., Tragord, B. S., Neal, M. S., . . . McPoil, T. (2009). Effect of Running Shoe Type on the Distribution and Magnitude of Plantar Pressures in Individuals with Low- or High-Arched Feet. *Journal of the American Podiatric Medical Association*, 99(4), 330-338.
- Saltzman, C. L., Nawoczenski, D. A., & Talbot, K. D. (1995). Measurement of the Medial Longitudinal Arch. *Archives of Physical Medicine and Rehabilitation*, 76(1), 45-49.
- Tome, J., Nawoczenski, D. A., Flemister, A., & Houck, J. (2006). Comparison of Foot Kinematics Between Subjects with Posterior Tibialis Tendon Dysfunction and Healthy Controls. *Journal of Orthopaedic & Sports Physical Therapy*, 36(9), 635-644.
- Williams III, D. S., Davis, I. M., Scholz, J. P., Hamill, J., & Buchanan, T. S. (2004). High-arched runners exhibit increased leg stiffness compared to low-arched runners. *Gait and Posture*, 19, 263-269.
- Williams, D. S., & McClay, I. S. (2000). Measurements used to characterize the foot and the medial longitudinal arch: Reliability and validity. *Physical Therapy*, 80(9), 864-871.
- Xiong, S., Goonetilleke, R. S., Witana, C. P., Weerasinghe, T. W., & Au, E. Y. (2010). Foot Arch Characterization: A Review, A New Metric, and a Comparison. *Journal of the American Podiatric Medical Association*, 100(1), 14-24.
- zunzun.com*. (n.d.). Retrieved 2011, from Online Curve Fitting - User Selectable Polynomial: [www.zunzun.com](http://www.zunzun.com)

## **CHAPTER 3 – NEUTRAL CUSHIONING RUNNING SHOE COMPARED WITH NO SHOE DURING DYNAMIC GAIT**

### **3.1 INTRODUCTION**

The structural behaviour of the foot has a direct effect on the biomechanics of the rest of the body. The foot is the interface between the body and the ground during any weight-bearing activity such as walking gait. Upon contact with the ground, the foot distributes the large forces resulting from ground contact and acts to dissipate a portion of the forces from the ground through the tarsal joints before they reach the long bones of the leg (Hamill & Knutzen, 2003; Norden & Frankel, 2001). When performing gait analysis using optical motion capture, the foot typically has only two markers attached to it – one on the heel and one on the second metatarsal. This means the foot is assumed to be a rigid segment, articulating only at the ankle with the lower leg. Such an analysis does not allow for the measurement of clinically relevant motions within the structure of the foot, such as midfoot motion with respect to the rearfoot, representing the function of the arches of the foot. In response to this deficiency, multi-segment foot models have been developed for use with optical motion capture to measure the motion of segments within the structure of the foot during normal walking. One such model tracks the medial and lateral forefoot, the midfoot and the hindfoot (Jenkyn, Anas, & Nichol, 2009). Though multi-segment foot models can measure relative motion between foot segments, there still exists some motion of the bones that cannot be measured with any confidence by skin mounted markers, since skin mounted markers are susceptible to soft tissue artifact error (also known as skin motion artifact error) as discussed in section 1.1.1. Changes in plantar pressure reflect differences in arch structure when comparing mean contact pressure of the midfoot to that of the entire foot. These measures were compared between high- and low-arched individuals in an attempt to quantify the degree of pronation between foot types (Molloy, et al., 2009). The medial longitudinal arch (MLA) is an integral structure in the foot and the height of the MLA has been shown to affect gait biomechanics. However, the change in arch height has not been quantified in terms of an arch angle when looking at running shoes compared with no shoe. This arch angle

measurement is a useful method to compare arch height for various conditions while accounting for positioning and motion of the arch in three dimensions.

In order to observe and quantify the small motions of individual foot bone kinematics, x-ray fluoroscopy can be used. Previous studies performed on the foot have used single plane fluoroscopy and external bone markers for reference (Wrbaskic & Dowling, 2007). Additional studies have used single plane fluoroscopy in conjunction with plantar pressure measurements to determine the distribution of weight on the foot (Gefen, Megido-Ravid, Itzhak, & Arcan, 2000).

The current study will track three bones of the foot using markerless fluoroscopic RSA (fRSA): the calcaneus, navicular and first metatarsal. These three bones define the medial longitudinal arch (MLA) of the foot. Using a similar MLA arch measure to one developed by Tome et al. (2006), bony landmarks from these three bones are digitized to quantify arch angle, where a larger MLA angle represents a lower arch height and a smaller angle represents a higher arch. The goal is to measure the kinematics of the medial longitudinal arch during walking gait when wearing a neutral cushioning running shoe and compare this measure to walking with no shoe. Before measuring the MLA with orthotics, it is important to know how the shoe affects the arch angle, since orthotics cannot be worn without shoes. Neutral cushion running shoes were chosen for footwear since they are recommended by clinicians to be worn with orthotics. Different foot types are likely to respond uniquely to each static condition, therefore, three pathological groups will be analyzed: pes planus (low arch), pes cavus (high arch) and normal arch.

It was hypothesized that the medial longitudinal arch angle would decrease with the addition of neutral cushioning running shoes as compared with the no shoe condition. It was also hypothesized that the cavus and planus groups would show the smallest and largest mean arch angle, respectively.

### **3.2 METHODS**

Six female subjects (mean 27.3 years of age) participated in this study, two from each group of normally arched, pes cavus and pes planus. Each participant was assessed as described in section 1.4.2 by a certified Canadian pedorthist in order to assure each participant fit the required specifications. Participants were excluded if they had other

foot abnormalities such as hallux valgus, if they had previous foot and/or ankle fractures or if they were considered to have a rigid pes planus, meaning their arch showed limited flexibility during the hip rotation test.

A wooden platform was used for participants to walk on, consistent with the previously mentioned static study (section 2.2). The participants were asked to walk along the platform past the laterally placed fluoroscope at their preferred pace, aligning their left heel with a mark on the platform. This mark assured that the fluoroscope underneath the platform would capture a proper anterior posterior view of the foot in motion. Two conditions were compared for this dynamic study – barefoot and neutral cushioning running shoes. The same make and model of the running shoes were used for every participant (Figure 3.1). Two trials were collected for each condition to ensure proper gait and to make sure the calcaneus, navicular and first metatarsal were visible in both fluoroscopic videos through stance phase of gait.



**Figure 3.1: Photograph of the neutral cushioning running shoes used for all subjects, New Balance model 882 (New Balance Athletic Shoe Inc., Boston, MA, USA).**

Prior to testing, a calibration frame designed by Kedgley (2009c) was positioned such that each fluoroscope would take an image of corresponding fiducial and control planes. Following testing, a distortion grid was placed on the image intensifier of each fluoroscope to correct for pin cushion distortion. The fluoroscopes were calibrated and corrected for distortion on each day of data collection.

The position of the beads on both the calibration and distortion images were manually located using the custom written algorithm designed by Kedgley (2009c) described in Section 1.2 (MATLAB; The MathWorks, Natick, MA, USA). Following distortion correction of the calibration image(s), a series of custom written algorithms developed by Allen (2009) were used to determine the location of both the x-ray foci and the fluoroscope parameters used to recreate the experimental set-up, also described in section 1.2. Each fluoroscope collected images at 30 frames per second, and produced x-ray images that were the clearest during midstance as the foot supports the body's weight. The fluoroscopes were synchronised by collecting the dynamic x-ray videos for each fluoroscope simultaneously with the same computer hardware (ViewCast Corporation; Plano, TX, USA). For both conditions (barefoot and cushion shoe), all frames were extracted to TIFF format (tagged image file format) from the dynamic fluoroscopic video. Four images at the instant of the foot-flat during gait were selected for each condition and then averaged in order to quantify the arch angle when the left foot would be bearing the most weight.

The matching process (section 1.2.2.6) was completed for all four frames for each condition. Following matching, custom RhinoScript written by Allen (2009) was used to export the locations of the bony landmarks into a spreadsheet (Rhinoceros; Robert McNeel & Associates, Seattle, WA, USA). From there, custom written MATLAB code was used to determine the angle of the MLA by calculating the dot product between the vectors from the navicular tuberosity to the medial process of the calcaneus and the navicular tuberosity and the first metatarsal head.



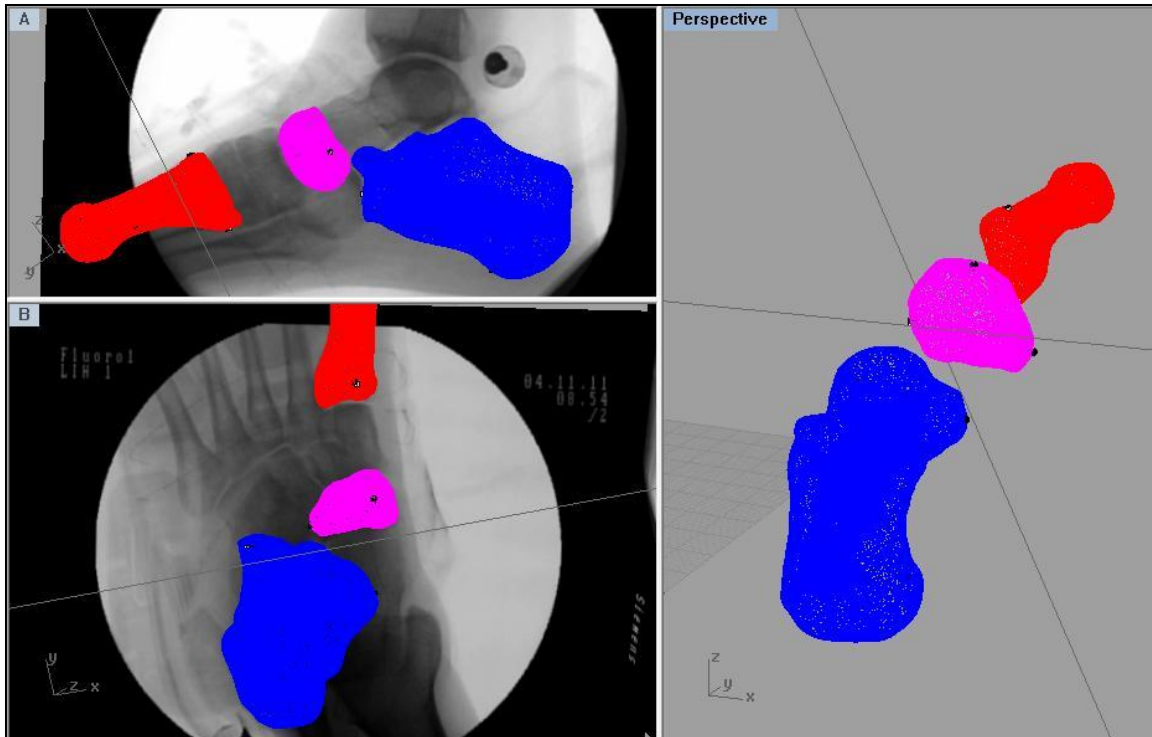


**Figure 3.2: Matching neutral cushioning running shoe for a ‘normal’ participant.**

Statistical analysis was performed using SPSS (IBM Corporation, Armonk, NY, USA). Paired t-tests were used to detect the statistical differences in the measured arch angle of the six subjects for the two conditions, as well as for the two subjects within each group. An additional analysis was completed using a multivariate general linear model to determine if there was a significant difference between subject groups (normal, pes planus and pes cavus). Statistical significance was set at  $p < 0.05$ . Where appropriate, Tukey’s post-hoc analyses were used to evaluate statistical differences.

### 3.3 RESULTS

The average angles for all six subjects are shown in Figure 3.3 for both barefoot and neutral cushioning running shoe conditions at the instant of foot-flat in the gait cycle. The mean MLA angles for each foot type and each condition are shown in Table 3.1. The mean and standard deviations of arch angles within each group are listed, with the normal group showing the smallest arch angles of all three groups. The mean barefoot angles were calculated at  $100.7^{\circ} \pm 3.5^{\circ}$  in the normal group,  $124.9^{\circ} \pm 7.6^{\circ}$  in the cavus group and

$132.6^{\circ} \pm 12.4^{\circ}$  in the planus group. With neutral cushioning running shoes, the mean values were  $98.0^{\circ} \pm 8.8^{\circ}$  in the normal group,  $125.4^{\circ} \pm 12.2^{\circ}$  in the cavus group and  $127.2^{\circ} \pm 12.6^{\circ}$  in the planus group.

The MLA angle differences are shown in Figure 3.4, which represents the change in arch angle from barefoot to running shoes during dynamic gait. Two subjects, one from the normal and cavus groups, showed an arch angle increase with the use of the running shoes; however, both subjects in the planus group demonstrated a decrease in MLA angle in neutral running shoes compared with walking barefoot.

The differences in mean arch angle for the two subjects of the planus group were statistically significant ( $p < 0.05$ ) when comparing barefoot and running shoe means using a paired t-test. No other significant differences were found in measured angles between conditions, or between subject group analyses.

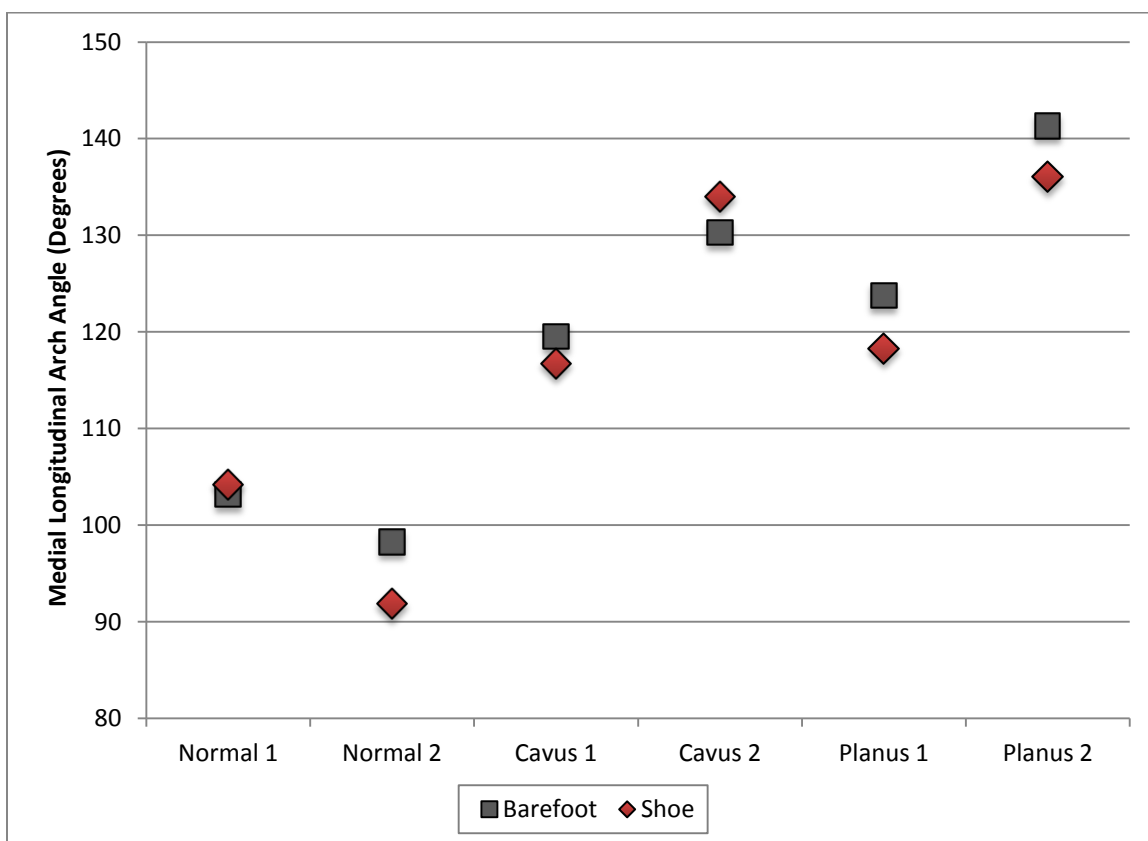


**Figure 3.3: MLA angles at the instant of foot-flat in dynamic walking gait – a comparison of barefoot and neutral cushioning running shoes.**

**Table 3.1: Mean and standard deviations of MLA angles at the instant of foot-flat in dynamic walking for barefoot and neutral cushioning running shoe conditions.**

	Foot Type	Mean	Std. Deviation	N
<b>Barefoot</b>	Normal	100.7	3.5	2
	Cavus	124.9	7.6	2
	Planus	132.6	12.4	2
	<b>Total</b>	<b>119.4</b>	<b>16.3</b>	<b>6</b>
<b>Shoe</b>	Normal	98.0	8.8	2
	Cavus	125.4	12.2	2
	Planus	127.2	12.6	2
	<b>Total</b>	<b>116.9</b>	<b>17.0</b>	<b>6</b>

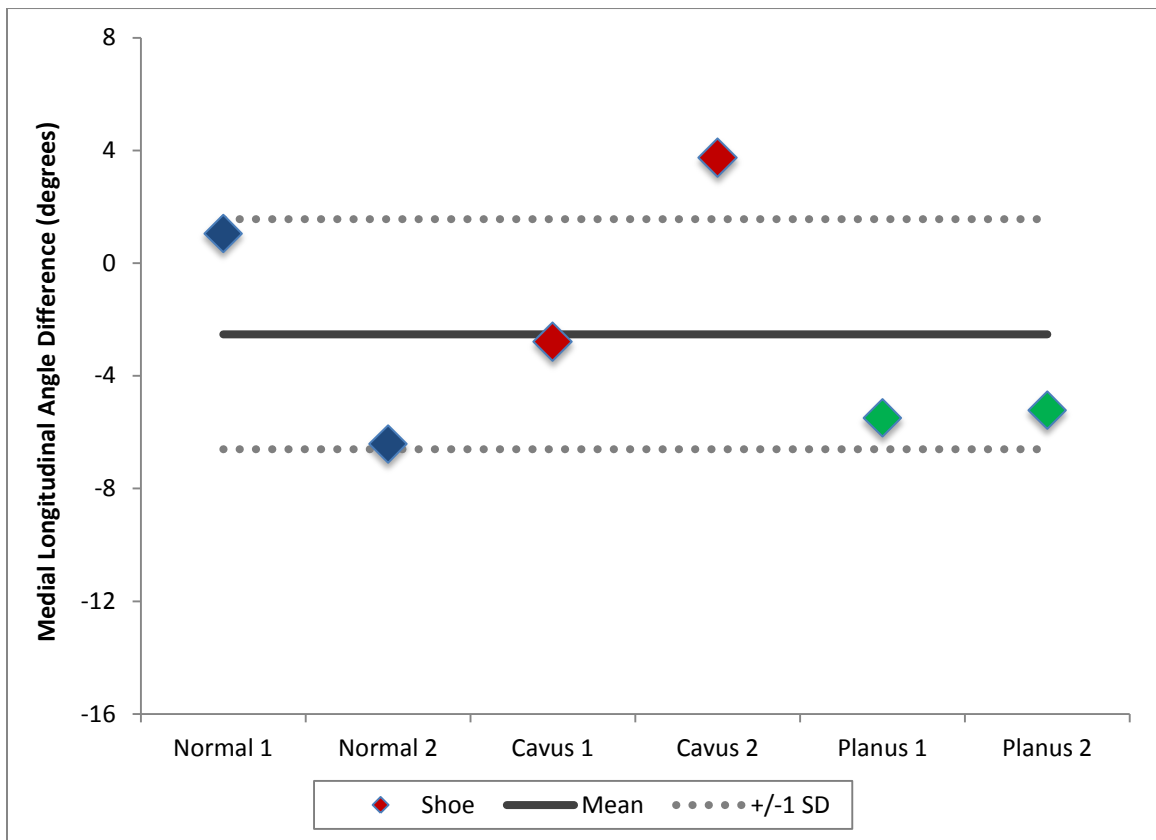


**Figure 3.4: MLA angle differences with subjects in a neutral cushioning shoe compared with no shoe at the instant of foot-flat in dynamic walking gait. Data points are shown in blue, red and green for normal, pes cavus and pes planus foot types, respectively.**

### 3.4 DISCUSSION

The purpose of this study was to measure the medial longitudinal arch angle at the instant of foot-flat during dynamic walking gait for two conditions – barefoot and wearing neutral cushioning running shoes. Results show that the medial longitudinal arch (MLA) angles of all three foot types have a large amount of variability when comparing barefoot angles between groups, indicating an obvious difference in arch structure between each foot type. The normal group showed the smallest mean MLA angle measure which was not consistent with our hypothesis. It was predicted that the cavus group would demonstrate the smallest mean arch angle of the three participant groups. The cavus group was expected to show a smaller angle (or greater arch height) due to the definition of a cavus foot – excessive inversion at the subtalar joint and supination of the forefoot at the transverse tarsal joint (Franco, 1987). Combining this definition and the angle measure derived by Tome et al. (2006), it was expected that the medial process of the calcaneus would be more in-line with the navicular tuberosity and first metatarsal head, thereby calculating a smaller angle, but this was not the case. An explanation for this measure may be the proportion of the vector magnitudes used for the MLA angle calculation, perhaps indicating a difference in overall cavus foot structure, described in section 2.3.

The study hypothesis was supported on one hand, as the results demonstrated the largest mean MLA angle occurred in the planus group. This was expected since pes planus subjects were expected to show the lowest navicular height, an everted calcaneus and excessive pronation occurring of the forefoot and therefore, the greatest MLA angle (Franco, 1987).

MLA angle differences of the six subjects demonstrated a mean decrease with the neutral cushioning running shoe. Though this angle decrease is consistent with the hypothesis, statistical analyses showed that the mean angle differences for all six subjects was not statistically significant ( $p > 0.05$ ) between the two conditions. When looking at the mean differences within groups, only the planus group demonstrated a significant angle change from barefoot to the running shoe ( $p < 0.05$ ). Both planus subjects showed a decrease in MLA angle when wearing the running shoes, indicating an increase in arch height with respect to the barefoot condition. These results are in contrast to those

discovered from a study performed by Molloy et al. (2009) who measured plantar pressure distributions for 75 participants (40 low-arched, 35 high-arched) across three conditions (non-shod, motion control running shoes and cushioning running shoes) during treadmill walking. The low-arched group showed an increase in modified arch index with the cushioning shoe compared with no shoe. The modified arch index is a measure of mean plantar contact area of the midfoot divided by that of the entire foot; therefore, this increase in measure indicates a greater amount of pronation occurring at the midfoot. In the present study, the cushioning shoe gave added support for the planus participants, therefore elevating the arch slightly and restricting its ability to elongate during flatfoot of stance phase. This finding may indicate less movement of the medial midfoot and thus, a slightly smaller degree of pronation for patients with pes planus.

Inconsistencies in the data may be attributed to variability in arch height and structure within each group. The clinician's assessment of each participant's arch height and foot function may not reflect the actual arch angle measurement of the participants, which is likely because of the variability in the anatomy of the foot from person to person. Since this is the first study to measure the arch angle using RSA, additional data may support other trends between foot types. It was thought that a total of six participants overall would have shown a trend in the results; however, only two subjects from each foot type were analyzed and this was not sufficient to show significant trends between pathologies. Another contributing factor to a limited trend in the data is because of the type of running shoe used for this study, neutral cushion, as it is typically given to normal or high-arched individuals who require maximum shock absorption, which is the main goal of this running shoe type. A more significant trend and consistent support of the medial longitudinal arch may have been seen with the use of other running shoe types such as a stability or motion control shoe. Such a comparison was done by Molloy et al. (2009) who measured plantar pressure using New Balance shoes - cushioning (model 880) or motion control (model 1122), and compared the modified arch index (explained previously) in both high and low-arched subjects. The low-arched group showed a decrease in modified arch index from cushioning to motion control shoe, meaning the latter demonstrated decreased pronation at the midfoot. This would be an interesting study going forward using markerless RSA.

Future analysis may include using this same method (markerless RSA) to show the differences in other types of footwear, such as looking at the differences in running shoe types – stability, motion control and perhaps a minimalist running shoe (both low support and low cushion) and compare how they may change the medial longitudinal arch during dynamic gait.

### 3.5 REFERENCES

- Allen, A.-M. (2009). *Development and Validation of a Markerless Radiostereometric Analysis (RSA) System*. London, Canada: Western University.
- Franco, A. H. (1987). Pes Cavus and Pes Planus - Analyses and Treatment. *Physical Therapy*, 67(5), 688-694.
- Gefen, A., Megido-Ravid, M., Itzchak, Y., & Arcan, A. (2000). Biomechanical Analysis of the Three-Dimensional Foot Structure During Gait: A Basic Tool for Clinical Applications. *Journal of Biomechanical Engineering*, 122, 630-639.
- Hamill, J., & Knutzen, K. M. (2003). *Biomechanical Basis of Human Movement: Second Edition*. Baltimore: Lippincott Williams & Wilkins.
- Jenkyn, T. R., Anas, K., & Nichol, A. (2009, March). Foot Segment Kinematics During Normal Walking Using a Multisegment Model of the Foot and Ankle Complex. *Journal of Biomechanical Engineering*, 131, 1-7.
- Kedgley, A., & Jenkyn, T. R. (2009b). RSA calibration accuracy of a fluoroscopy-based system using nonorthogonal images for measuring functional kinematics. *Medical physics*, 36(7), 3176-3180.
- Molloy, J. M., Christie, D. S., Teyhen, D. S., Yeykal, N. S., Tragord, B. S., Neal, M. S., . . . McPoil, T. (2009). Effect of Running Shoe Type on the Distribution and Magnitude of Plantar Pressures in Individuals with Low- or High-Arched Feet. *Journal of the American Podiatric Medical Association*, 99(4), 330-338.
- Norden, M., & Frankel, V. H. (2001). *Basic Biomechanics of the Musculoskeletal System: Third Edition*. Baltimore: Lippincott Williams & Wilkins.
- Tome, J., Nawoczenski, D. A., Flemister, A., & Houck, J. (2006). Comparison of Foot Kinematics Between Subjects with Posterior Tibialis Tendon Dysfunction and Healthy Controls. *Journal of Orthopaedic & Sports Physical Therapy*, 36(9), 635-644.
- Wrbaskic, N., & Dowlin, J. (2007). An investigation into the deformable characteristics of the human foot using fluoroscopic imaging. *Clinical Biomechanics*(22), 230-238.

## **CHAPTER 4 – FOAM CASTED HARD AND SOFT ORTHOTICS, PLASTER HARD AND SOFT ORTHOTICS AND PFO COMPARED WITH BAREFOOT WALKING**

### **4.1 INTRODUCTION**

A functional relationship exists between the structure of the medial longitudinal arch of the foot and the biomechanics of the lower limb. Common foot pathologies such as pes planus (flat foot) and pes cavus (high arch) can slightly alter the rest of the body's biomechanics and cause people to acquire musculoskeletal problems associated with their lower back, upper and lower legs, as well as cause general foot pain and discomfort (Edelstein & Bruckner, 2002). These problems are thought to occur in part because of an uneven distribution of weight on the feet. In the extremely high arched foot characteristic of pes cavus, weight-bearing is distributed unevenly along the lateral border of the foot. People with pes planus often demonstrate a flat-footed gait with no toe-off, typically associated with a large plantar weight-bearing surface with the main source of weight-bearing on the first and second metatarsals (Franco, 1987). With normally arched feet, weight-bearing that is distributed evenly on all five metatarsals.

The functional foot orthosis, or orthotic, is a conservative treatment for many musculoskeletal disorders including pes planus and pes cavus. It is commonly thought that orthotics mechanically change the positions and motions of the foot bones by applying forces or restraining the plantar surface. However, the main function of an orthotic device is to provide a change in body mechanics in an attempt to readjust the foot into a more accurate weight-bearing position (Franco, 1987).

Custom orthotics are generally prescribed by a physician and then casted and fitted by a pedorthist. They are made of both subortholen (hard) and plastazote (soft) thermoplastic materials, both having benefits for different musculoskeletal disorders. Patients are casted typically in the subtalar joint neutral position. The subtalar joint (STJ) is the articulation between the talus and the calcaneus and its neutral position is defined as the position where the joint is neither supinated nor pronated (Pierrynowski & Smith, 1997; Elveru et al., 1988). The STJ is the most widely used reference point for the clinical measurement of the relationship of rearfoot to forefoot, and subtalar joint neutral



is considered to be the ideal weight-bearing position. The goal of orthotics is to help the foot achieve a position close to that of the subtalar joint neutral (STN) position during walking gait. In doing so, the position and stress on the medial longitudinal arch (MLA) changes. For the pes planus group, the midfoot will be less pronated, and for the pes cavus group, the rearfoot will be less inverted. The results of these changes are thought to cause an increase in arch height in both groups, but by a much smaller magnitude for the pes cavus foot.

Custom foot orthotics are quite expensive and are not always covered by extended health insurance plans; therefore, people may purchase off-the-shelf devices that have minimal padding, non-custom support to alleviate minor pain in the foot or lower limb. An example of an off-the-shelf device is the proprioceptive feedback-type orthotic (PFO, Barefoot Science, Mississauga, ON, Canada). The model studied in this research is called the Barefoot Science Arch Activation Foot Strengthening System™. The design of this device, with a soft dimple under the middle of the plantar surface of the forefoot, is supposed to encourage the intrinsic muscles of the foot to contract during gait. The stabilized foot and improved muscle function is supposed to facilitate optimal foot bone alignment, and therefore develop a higher, more shock absorbing MLA.

In the literature, measuring the MLA during dynamic, weight-bearing activities such as walking has been accomplished with multi-segment foot models and optical motion. These models allow for the direct tracking of the motion of the midfoot relative to the rearfoot or forefoot (Tome et al., 2006; Jenkyn & Nicol, 2007). In a study performed by Tome et al. (2006), researchers added a reflective marker on the navicular tuberosity to calculate an angle in three dimensions spanning from the calcaneus, navicular and first metatarsal. This measurement was used to quantify the change in the MLA angle in patients with posterior tibialis tendon dysfunction. A larger angle represented a lower arch, whereas a smaller angle represented a higher arch. Error exists due to skin motion artifact when using external, skin mounted markers and this relative movement of the underlying bone has ranged from 2.3 to 4.4 degrees in the foot (Jenkyn & Nicol, 2007). To avoid skin motion artifact error, the current study uses the method of radiostereometric analysis (RSA) and fluoroscopy to directly measure the skeletal kinematics of the foot.

The purpose of this study was to determine how five different types of orthotics affected the medial longitudinal arch during dynamic gait using markerless RSA. It was hypothesized that the hard/firm orthotics will have the greatest effect on the arch, showing a smaller MLA angle than the soft orthotics. It is also hypothesized that the PFO will demonstrate even less of a change than the soft orthotic, therefore having the greatest arch angle in comparison with all the other devices.

## **4.2 METHODS**

Six female participants were chosen for this study, two from each pathology group – normally arched, pes planus and pes cavus. Participants were casted by the pedorthist using both foam box and traditional plaster casting methods described in section 1.4.2. Five orthotic devices were studied for each participant: plastazote (soft) and subortholen (firm) plaster casted orthotics, plastazote and subortholen foam casted orthotics, as well as a proprioceptive feedback type orthotic (PFO). The hard orthotic (subortholen), shown in Figure 4.1(b), was made of a 3mm RCH-500 shell layered with 55 durometer EVA and a 25 durometer EVA top cover. The soft orthotic was fabricated with 4mm Plastazote shell layered with 35 durometer EVA and a 25 durometer top cover (Figure 4.1(a)). The four custom-made orthoses were constructed with an aggressive support for the medial longitudinal arch for all study volunteers in order to demonstrate the near maximum amount of support that is typically provided to patients. The fifth orthotic was an over-the-counter device, a proprioceptive feedback-type orthotic (PFO) that is designed to quickly and safely strengthen the intrinsic muscles of the foot to restore healthy foot function, optimizing comfort and performance (Figure 4.1(c)).



**Figure 4.1:** (a) Custom soft material (plastazote) orthotic, (b) custom hard material (subortholen) orthotic, and (c) proprioceptive feedback-type orthotic (PFO) with different foam inserts.

Prior to testing, the pedorthist assured that the orthotics fit properly into the correct size of neutral cushioning running shoes (New Balance Canada Inc.; Mississauga, Ontario, CA), with multiples sizes available to fit every participant. This type of shoe was chosen since a neutral cushion running shoe is supposed to provide extra cushioning but little support, unlike a stability or motion control shoe. Pedorthists recommend patients use neutral cushion shoes with orthotics since the orthotics are custom made to provide the amount of support they will need and therefore they do not need additional support that other running shoes may provide. The volunteers were asked to walk along the platform past the laterally placed fluoroscope at their preferred pace, placing their left foot with the heel aligned with a mark on the platform (specific to each testing day). The fluoroscope recorded the left foot from heel strike to toe off at 30 frames per second (Figure 4.2(a)).

Before and after data collection, the fluoroscopes were calibrated with a calibration frame (Figure 4.2(b)) designed by Kedgley (2009c), the laboratory coordinate system  $x$ ,  $y$  and  $z$  represented by tape in red, green and blue, respectively. Following testing, a distortion grid was placed on the image intensifier of each fluoroscope in order to correct for pin cushion distortion. The position of the beads on both the calibration and

distortion images were manually located using the custom written software described in Section 1.2 (MATLAB; The MathWorks, Natick, MA, USA). Following distortion correction of the calibration image(s), a series of custom algorithms written by Allen (2009) determined the location of both x-ray foci, in addition to the sixteen fluoroscope parameters used to recreate the experimental set-up, also described in section 1.2.

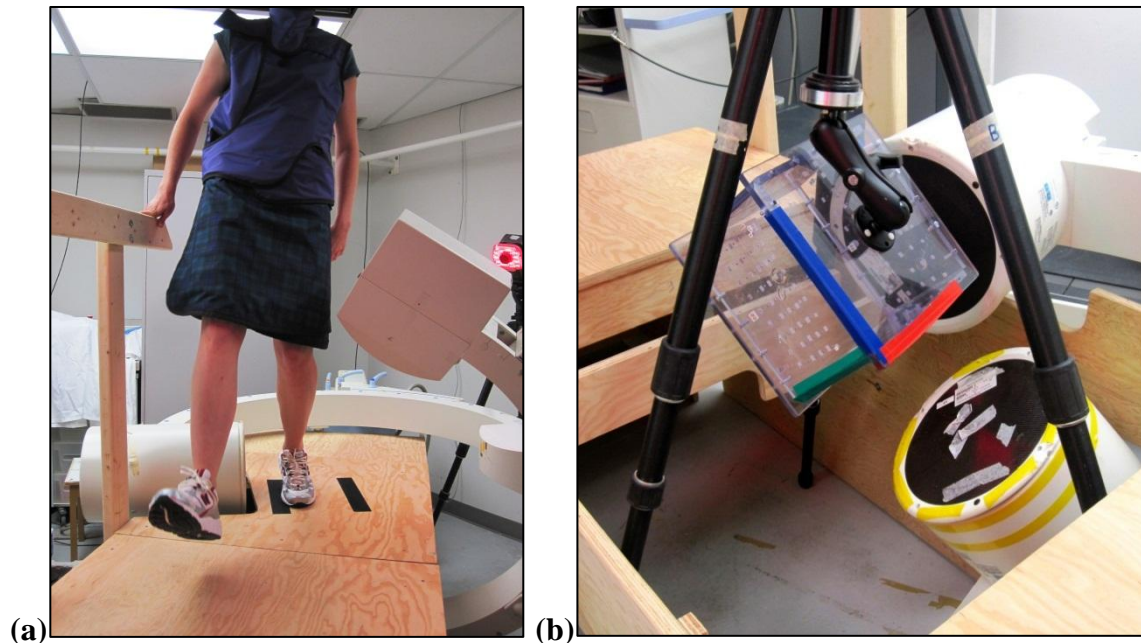


**Figure 4.2: (a) Participant walking on wooden platform during data collection (left), and (b) calibration of both fluoroscopes with a calibration frame with axes x, y, z, denoted by red, green and blue, respectively (right).**

The fluoroscopes were synchronised by collecting the dynamic x-ray videos for each fluoroscope simultaneously with the same computer hardware (ViewCast Corporation; Plano, TX, USA). All frames were extracted for each condition and converted from MPEG video format to TIFF format (tagged image file format). Four frames at the flatfoot phase of stance phase were then matched to assure full weight-bearing stance of the left foot.

Image matching (Section 1.2.2) was completed for each condition and all six participants. Following matching, custom written RhinoScript (Rhinceros; Robert McNeel & Associates, Seattle, WA, USA) was used to export the locations of five bony landmarks into a spreadsheet. Custom written MATLAB code was then used to determine the angle of the MLA by calculating the dot product between two vectors from

the navicular tuberosity to the medial process of the calcaneus and the first metatarsal head. The changes in arch angle with the various orthotics were compared with respect to barefoot walking to quantify the level of support provided by the orthotics compared with no support.

Statistical analysis was performed using SPSS (IBM Corporation, Armonk, New York, USA). A repeated measures analysis of variance test (ANOVA) was used to detect any statistical differences in the measured arch angle for the five conditions, comparing the mean differences between orthotics and barefoot walking. Where appropriate, Tukey's post-hoc analyses were used to evaluate statistical differences. Statistical significance was set at  $p < 0.05$ .

### 4.3 RESULTS

The average medial longitudinal arch (MLA) angle differences with respect to barefoot walking are compared in Figure 4.3 for the five orthotic conditions. The conditions graphed in Figure 4.3 show arch angle differences both above and below zero, which represents the barefoot MLA angle for each subject. Figure 4.4 demonstrates identical results but in a bar graph, showing the change in angles of the five orthotic conditions from barefoot walking. An increase in angle results in a greater MLA angle than the barefoot condition and therefore, a decrease in arch height. Similarly, a decrease in angle represents a smaller MLA compared with barefoot walking, meaning an increase in arch height, which is the ultimate goal of the orthotics. Three subjects showed a decrease in arch angle with most of the orthotics (one cavus and two planus participants) with one planus participant showing a very large decrease with the foam hard orthotic ( $-19.4^\circ$ ). The two normal participants both demonstrated some increases in arch angle when walking with orthotics.

Differences in MLA angles are summarized in Table 4.1 along with the means and standard deviations for each foot type. For the normal group, the foam casted soft orthotic provided the largest MLA angle change of  $4.22^\circ \pm 1.9^\circ$ , indicating an angle increase (decrease in arch height). The smallest change for the normal group occurred with the plaster cast hard orthotic, also showing a slight angle increase of  $1.25^\circ \pm 1.5^\circ$ . It

should be noted that in the normally arched group, most of the angle changes for both subjects were in the positive direction for all conditions compared with barefoot.

The greatest decrease in MLA angle for the cavus group occurred with the foam casted soft material orthotic with a mean angle difference of  $-3.16^{\circ} \pm 1.4^{\circ}$  whereas this foot type showed an increase in MLA angle with the plaster casted hard orthotic of  $2.99^{\circ} \pm 4.2^{\circ}$ , resulting in a lower arch height with this device. The mean differences in arch angles were negative for the pes planus group for all five devices, showing a decrease in arch angle. The greatest angle decrease was found with the foam casted hard orthotic ( $-11.7^{\circ} \pm 7.7^{\circ}$ ) and the smallest change occurring with the PFO device ( $-2.60^{\circ} \pm 5.4^{\circ}$ ).

These results showed no significant differences when comparing the mean MLA angle changes with the barefoot condition for all participants ( $p > 0.05$ ). Additionally, there were no significant effects between any devices when comparing within each pathological group ( $p > 0.05$ ).

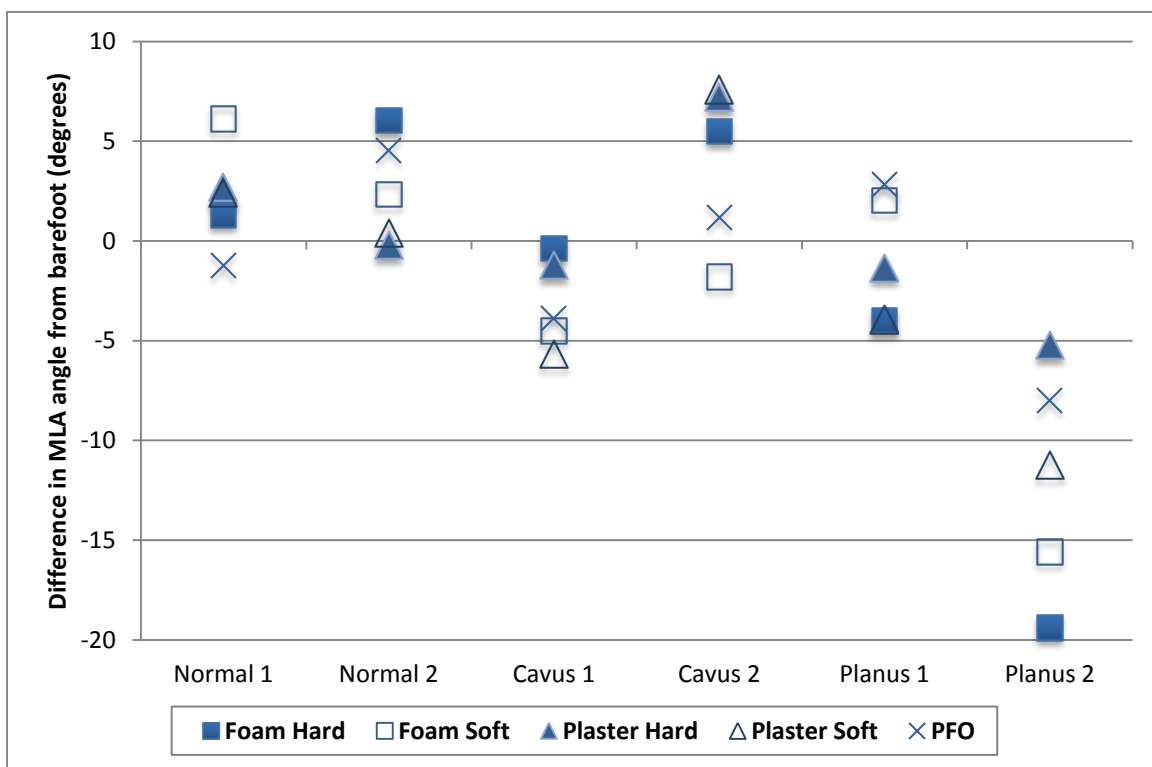


**Figure 4.3: A comparison of MLA angle differences while walking with five orthotic conditions compared to barefoot walking.**

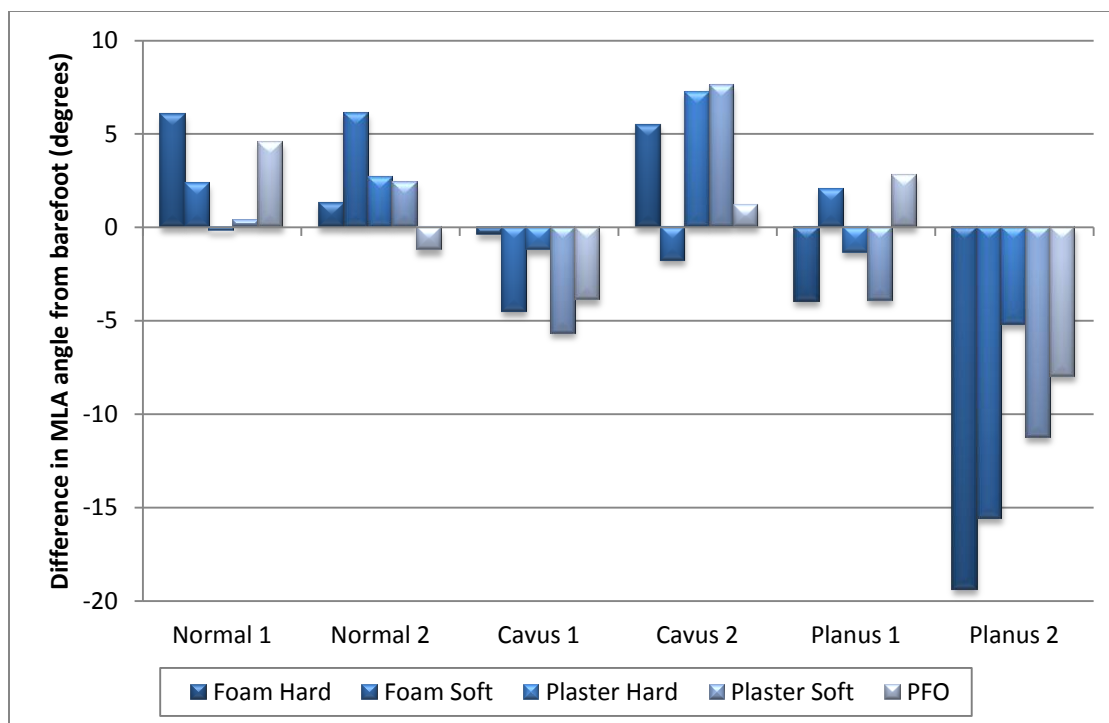


**Figure 4.4:** Comparison of MLA angle changes from barefoot walking for five conditions – foam casted hard and soft orthotics, plaster casted hard and soft orthotics, and PFO.

**Table 4.1:** MLA angle differences from barefoot walking of five different conditions along with the mean and standard deviation, separated by foot type.

<b>Normal</b>	<b>Normal 1</b>	<b>Normal 2</b>	<b>Mean</b>	<b>SD</b>
Foam Hard	1.3	6.0	<b>3.7</b>	2.4
Foam Soft	6.1	2.3	<b>4.2</b>	1.9
Plaster Hard	2.7	-0.2	<b>1.2</b>	1.5
Plaster Soft	2.4	0.4	<b>1.4</b>	1.0
PFO	-1.2	4.5	<b>1.7</b>	2.9
<b>Cavus</b>	<b>Cavus 1</b>	<b>Cavus 2</b>	<b>Mean</b>	<b>SD</b>
Foam Hard	-0.4	5.5	<b>2.6</b>	2.9
Foam Soft	-4.5	-1.8	<b>-3.2</b>	1.4
Plaster Hard	-1.2	7.2	<b>3.0</b>	4.2
Plaster Soft	-5.7	7.6	<b>1.0</b>	6.6
PFO	-3.9	1.2	<b>-1.4</b>	2.5
<b>Planus</b>	<b>Planus 1</b>	<b>Planus 2</b>	<b>Mean</b>	<b>SD</b>
Foam Hard	-4.0	-19.4	<b>-11.7</b>	7.7
Foam Soft	2.0	-15.6	<b>-6.8</b>	8.8
Plaster Hard	-1.3	-5.2	<b>-3.3</b>	1.9
Plaster Soft	-3.9	-11.2	<b>-7.6</b>	3.7
PFO	2.8	-8.0	<b>-2.6</b>	5.4

#### 4.4 DISCUSSION

The purpose of this study was to determine the effect of five different types of orthotic devices on the medial longitudinal arch (MLA) during dynamic gait. The results of the study, acquired using markerless fluoroscopic RSA, were not consistently supported with the hypothesis since the hard orthotics (both foam and plaster casted) did not have a significant effect on the MLA angle for all individuals. However, the foam casted hard orthotic did result in the greatest effect for the planus group participants, showing the largest angle decrease, indicating the greatest arch height increase. Though these results were not statistically significant, this finding is clinically relevant for this individual since the goal for the hard orthotic is to provide the greatest restriction to the arch during gait. This restriction is intended to limit the elongation of the arch in the sagittal plane but also includes restricting movement in the frontal and transverse planes, such as eversion and abduction, which lead to increased pronation of the midfoot – a significant movement in patients with pes planus (Hamill & Knutzen, 2003; Franco, 1987).

The secondary hypothesis was consistent for the planus group as well, as the PFO device showed the smallest mean decrease in arch angle compared with the other orthotics; however, this finding was not statistically significant. Similar to the first hypothesis, this result was not supported among the other two groups. Although the fourth highest insert for the PFO device was used (second highest), this type of orthotic did not provide the same rigid arch support as a custom made device. This may be because the goal of the PFO is to work like an exercise program and restore healthy foot function by strengthening the foot. The device is supposed to stimulate the intrinsic muscles of the foot with consistent use, however, there have been no previous investigations performed on this device. The support of the PFO device is accomplished with a dome contour under the distal arch area of the foot, whereas custom orthotic devices are fabricated to support the entire arch in addition to controlling rearfoot motion. Since the data was collected upon first trial with every device, there was no time for the foot to strengthen with the PFO. This improvement in muscle function likely occurs gradually and with consistent use of the device and therefore, no obvious trend or significant change was observed comparing this device to barefoot walking.



Normal group participants showed an increase in arch angle for most of the conditions, indicating a decrease in arch height with the orthotic conditions. The magnitudes of these angle increases were fairly small, the greatest mean increase occurred with the foam casted soft orthotic (4.2°). Although none of the normally arched participants had an abnormal pathology affecting the foot or lower limb, a decrease in arch angle was still expected with the custom orthotics. These custom devices were fabricated with a somewhat aggressive arch support and therefore should have demonstrated a restriction in arch elongation for the normal group. The structure of the medial longitudinal arch in a normal foot is flexible and provides ideal elastic properties to absorb shock during gait (Saltzman et al., 1995). The orthotics may be taking on some of that shock absorption, perhaps allowing the intrinsic muscles of the foot and arch to relax, therefore demonstrating a drop in arch height (or an increase in arch angle).

The cavus group also showed small mean arch changes (less than 4 degrees) with the orthotics, even more so than the normally arched group, with no particular type of device showing an obvious trend. This was expected in terms of angle magnitude, as the pes cavus foot is naturally more rigid and has less overall motion (Franco, 1987). Similar to the normal group, the foam casted soft orthotic also had the greatest effect on the cavus group but instead, caused a small decrease in arch angle, restricting arch elongation. A small decrease in angle was also shown in the PFO device; however, the remaining orthotics showed a slight increase in arch angle (approximately 1-3°). This magnitude in change is very small, as mentioned above, and was expected from a pes cavus type foot as it is quite rigid so not much motion is expected. As mentioned above, this angle increase may indicate the orthotic was absorbing some of the shock that the arch would normally attenuate during gait, allowing the arch to relax and elongate, causing a greater arch angle.

Although there was no statistical significance in any of the orthotic conditions when compared to barefoot walking, this is likely due to the low participant numbers in each foot pathology group. Two subjects per group did not show an obvious trend in MLA angle changes, nor did the subjects show a trend in absolute MLA angles between foot types. The cavus and planus group had similar MLA angles – a surprising result given the cavus group has the highest arch height; therefore, this was expected to

translate into a smaller calculated MLA angle. Since this was not the case, the proportion of the two vectors was calculated from which the angle was formed (as described in section 2.3). The mean magnitude of the vector from the navicular tuberosity to the medial process of the calcaneus, normalized to foot length, was significantly greater in the pes cavus group compared with the mean vector magnitudes of the other two pathological groups. The rearfoot of a pes cavus is inverted, and the forefoot is supinated at the transverse tarsal joint, as defined by Franco (1987). This finding of a greater vector length between the navicular and the calcaneus indicates that the calcaneus is perhaps in a slightly different position than expected – perhaps less inverted than previously thought. The osseous structure of a larger sample of pes cavus patients should be investigated further to determine if there is a trend in foot structure that is causing this longer vector that is resulting in a greater than expected MLA angle.

Strengths of this study include the consistency of evaluating and casting every participant using the same clinician. Additionally, the evaluation performed by the clinician was completed in a regular clinical setting. Keeping the clinician consistent eliminates any error to do with slight differences in examination style and casting technique. When testing each participant with the fluoroscopes, the order for which they completed each orthotic condition was completely randomized. Additionally, the shoes used with the orthotics were controlled by using neutral cushioning shoes by New Balance, model 882 (New Balance Canada Inc., Mississauga, Ontario, CA), available to all participants. These shoes were used as per the recommendation by the clinician since there is little arch support built into the structure of the shoe.

Though some of the subjects may have used orthotics in the past, there was no adjustment period for the study participants, meaning they had not previously worn the specific orthotics tested for this study. With no period for the subject to get used to the orthotics, the participants' gait may have been slightly altered, possibly contributing to inconsistent results. Additionally, with no adjustment period, the muscles of the foot and lower limb were not able to strengthen or get accustomed to any of the devices, perhaps contributing to lack of significant differences in the data. No previous studies have been performed on this PFO device, therefore future work might include an analysis of the

PFO device to see if everyday use would increase foot strength, reflecting a decrease in arch angle during barefoot walking after six months of use.

#### 4.5 REFERENCES

- Allen, A.-M. (2009). *Development and Validation of a Markerless Radiostereometric Analysis (RSA) System*. London, Canada: Western University.
- Edelstein, J. E., & Bruckner, J. (2002). *Orthotics: A Comprehensive Clinical Approach*. SLACK Incorporated.
- Elveru, R. A., Rothstein, J. M., Lamb, R. L., & Riddle, D. L. (1988). Methods for Taking Subtalar Joint Measurements. A Clinical Report. *Physical Therapy*, 68, 678-682.
- Franco, A. H. (1987). Pes Cavus and Pes Planus - Analyses and Treatment. *Physical Therapy*, 67(5), 688-694.
- Hamill, J., & Knutzen, K. M. (2003). *Biomechanical Basis of Human Movement: Second Edition*. Baltimore: Lippincott Williams & Wilkins.
- Jenkyn, T., & Nicol, A. (2007). A multi-segment kinematic model of the foot with a novel definition of forefoot motion for use in clinical gait analysis during walking. *Journal of Biomechanics*(40), 3271-3278.
- Kedgley, A. (2009c). *Development of a Fluoroscopic Radiostereometric analysis system with an application to glenohumeral joint kinematics*. London, ON: School of Graduate and Postdoctoral Studies, Western University.
- Pierrynowski, M. R., & Smith, S. B. (1997). Effect of Patient Position on the Consistency of Placing the Rearfoot at the Subtalar Neutral. *Journal of the American Podiatric Medical Association*, 87(9), 399-406.
- Saltzman, C. L., Nawoczenski, D. A., & Talbot, K. D. (1995). Measurement of the Medial Longitudinal Arch. *Archives of Physical Medicine and Rehabilitation*, 76(1), 45-49.
- Tome, J., Nawoczenski, D. A., Flemister, A., & Houck, J. (2006). Comparison of Foot Kinematics Between Subjects with Posterior Tibialis Tendon Dysfunction and Healthy Controls. *Journal of Orthopaedic & Sports Physical Therapy*, 36(9), 635-644.

## **CHAPTER 5 – TWO-DIMENSIONAL VERSUS THREE-DIMENSIONAL ANALYSIS**

### **5.1 INTRODUCTION**

Foot structure plays a vital role in human locomotion as it is the body's connection with the ground. One of the more important and highly variable structural characteristics of the human foot is the medial longitudinal arch, which provides necessary shock absorption for the foot during gait and other activities (Saltzman et al., 1995). Variations in the structure of the arch as well as the corresponding gait problems that accompany abnormal arch height are often treated with foot orthoses or orthotics.

Custom foot orthotics are most commonly prescribed by a certified Canadian pedorthist for foot pathologies such as pes planus (low arch or flat foot) and pes cavus (high arch). These common pathologies may contribute to additional musculoskeletal problems associated with the lower back, upper and lower legs, as well as general foot pain and discomfort (Edelstein & Bruckner, 2002). These symptoms are generally the result of a malalignment of the foot, and compensatory gait mechanisms that follow. Therefore, the main function of an orthotic device is to provide support for the plantar aspect of the foot in an attempt to readjust the foot into a more accurate weight-bearing position (Franco, 1987).

Though patients treated with foot orthotics may be relieved of foot pain and other symptoms, the changes in foot structure and function are not quantified; therefore, how each individual is affected by orthotics is only speculated by a clinician. Quantifying the kinematics of the foot is difficult to accomplish as the motions between the joints are very small in comparison to the rest of the body. Because of these small ranges of motion, performing a normal gait analysis using optical motion capture with a standard marker set does not reveal anything about the specific foot joints (Jenkyn & Nicol, 2007).

In order to quantify these small motions of the foot, radiographic measurements have been used to measure skeletal kinematics, typically in two-dimensional studies. A few of the investigations calculated the calcaneal-first metatarsal angle (CI-MT1), a medial longitudinal arch measure that used single plane videofluoroscopy during normal gait (Saltzman et al., 1995; Wearing, Urry, Perlman, Smeathers, & Dubois, 1998). The

same angle calculation, denoted as CIMA or CFMA, was later implemented to measure the arch using lateral x-ray images in order to classify normal and flat-arched foot posture (Murley, Menz, & Landorf, 2009).

It has always been thought that there are limitations to completing an analysis in two dimensions as it does not quantify out of plane rotation, but the question still remains – how similar is the CFMA measure in comparison to a true three-dimensional analysis? Three-dimensional analyses are the gold standard in kinematic research since the motions of the body are fundamentally three-dimensional; therefore, it is necessary to be able to quantify the motions of a joint in all three anatomical planes to fully characterize the motion. Markerless radiostereometric analysis (RSA) has been used and validated in the WOQIL lab for the shoulder, and has since been used for the foot to compare the biomechanical or anatomical effects of various orthotic devices (Chapter 4).

The purpose of this study is to compare a two-dimensional radiographic analysis of the medial longitudinal arch with the previously completed analysis using a three-dimensional method. The two-dimensional analysis will measure CFMA angle in the lateral fluoroscopic view whereas the three-dimensional analysis will measure the MLA angle by digitizing bony landmarks using markerless RSA. It was hypothesized that the arch angles calculated would be different from 2D to 3D for each foot type, but that the changes between the calculated 2D and 3D angles would be consistent across all conditions for each participant.

## **5.2 METHODS**

Six females participated in the study (mean 27.3 years of age), two of each foot type: normal arch, pes cavus (high arch) and pes planus (low arch). Each participant was assessed by a certified Canadian pedorthist in order for them to fit the required specifications of each foot type. The participants had to fit the requirements to be considered part of a pathological group, with no evidence of other foot problems such as hallux valgus. Other exclusion criteria were previous foot or ankle fractures as well as rigid pes planus, meaning the arch was absent in both seated and standing positions.

The participants were asked to walk along a wooden platform in front of the laterally placed fluoroscope at their preferred pace. In order for both the lateral and the

anterior posterior fluoroscopes to capture the foot in motion, the subjects were asked to align their left heel with a mark on the platform (specific to each testing day). The two-dimensional analysis was calculated from the fluoroscope that captured the lateral view of the foot.

Four conditions were compared for this study including barefoot walking and walking with three devices: foam casted hard orthotic, foam casted soft orthotic and a proprioceptive feedback-type orthotic (PFO, Barefoot Science, Mississauga, Ontario, Canada). Walking trials were performed until a good view of the foot was recorded to make sure the calcaneus, navicular and base of the first metatarsal were visible in both fluoroscopes at the instant of foot-flat during stance phase of gait.

Prior to testing, fluoroscopic images were taken of a calibration frame designed by Kedgley (2009c) such that both fiducial and control points were visible. Following testing, a distortion grid was placed on the image intensifier of each fluoroscope in order to correct for pin cushion distortion. The fluoroscopes were calibrated and corrected for distortion for each testing date.

A custom written algorithm described in Section 1.2 was used to locate the position of the beads in both the calibration and distortion grid images (MATLAB; The MathWorks, Natick, MA, USA). After correcting the calibration image(s) for distortion, additional custom algorithms were used to determine the location of both x-ray foci, as well as the calibration parameters used to recreate the experimental set-up, also described in section 1.2 (Allen, 2009). Each fluoroscope recorded at 30 frames per second and was synchronized to one another using specialized hardware. All frames were extracted to TIFF format (tagged image file format) from the dynamic fluoroscopy video for all four conditions. Four images at the instant of foot-flat during stance phase were evaluated in order to represent where the foot would be bearing the most weight during gait, and the measurements from these images were averaged to represent the arch angle measure for each participant and each condition.

To obtain three-dimensional (3D) data, the matching process was completed for the four conditions, similar to section 4.2. Following matching, custom written RhinoScript, developed by Allen (2009), was implemented (Rhinceros, Robert McNeel & Associates, Seattle, WA, USA) and used to export the locations of the bony landmarks

designated in OsiriX (Figure 5.1(a)) into an Excel spreadsheet (Microsoft Corporation, Washington, US). Three bony landmarks were exported from the calcaneus – the medial process, sustentaculum tali and the lateral cuboid surface, as well as one from both the first metatarsal head and navicular tuberosity.

Custom written MATLAB code was then used to determine the angle of the medial longitudinal arch by calculating the dot product of the 3D vectors from the navicular tuberosity to the medial process of the calcaneus and first metatarsal head (section 1.3.2.2).

For the two-dimensional (2D) analysis, custom MATLAB code was written and implemented to calculate the angle of the medial arch (Appendices B2 & B3). For each frame in the lateral fluoroscope view, two landmarks were identified on the plantar aspect of the calcaneus, at the most posterior and anterior surfaces. These landmarks were then connected with a line (Figure 5.1(b)). A second line was then created from two points on the dorsal aspect of the first metatarsal and then the angle between these two lines was calculated, represented in blue in Figure 5.1b. This calcaneal-first metatarsal angle (CFMA) defined the convexity of the medial longitudinal arch as described by Murley et al. (2009).

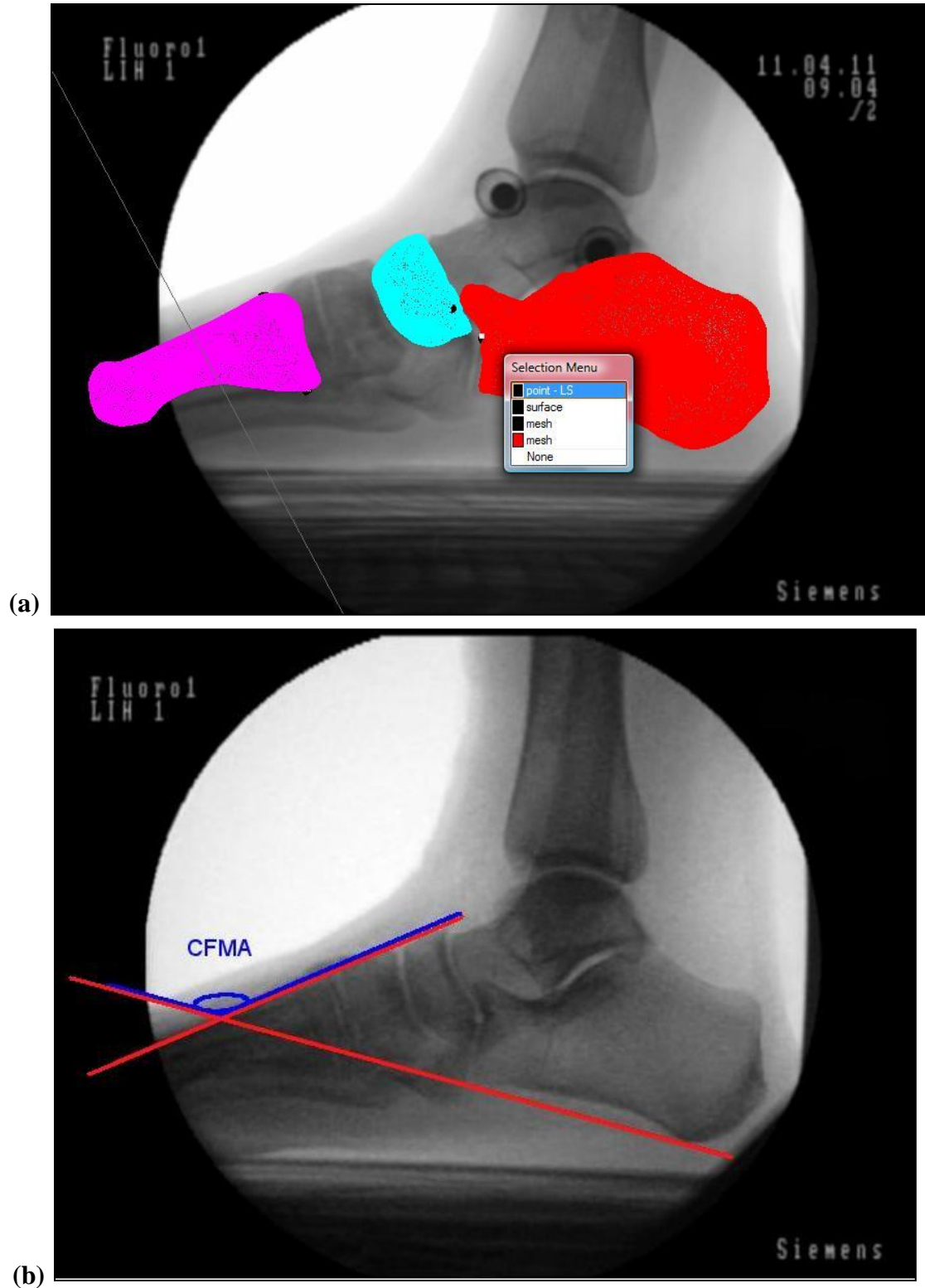


**Figure 5.1: Lateral fluoroscopic view of the foot showing (a) the process of selecting bony landmarks following matching process in Rhinoceros using script 'ExportPoints.rvb', and (b) the calcaneal-first metatarsal angle calculation (CFMA) defined by Murley et al. (2009).**

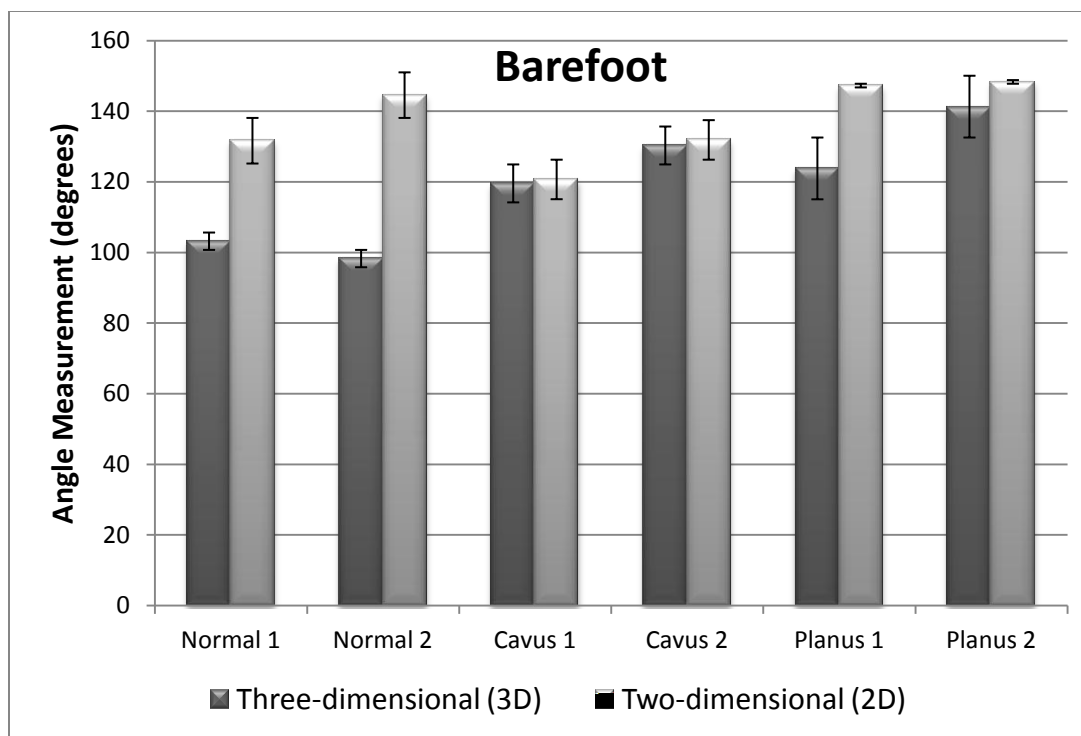


### 5.3 RESULTS

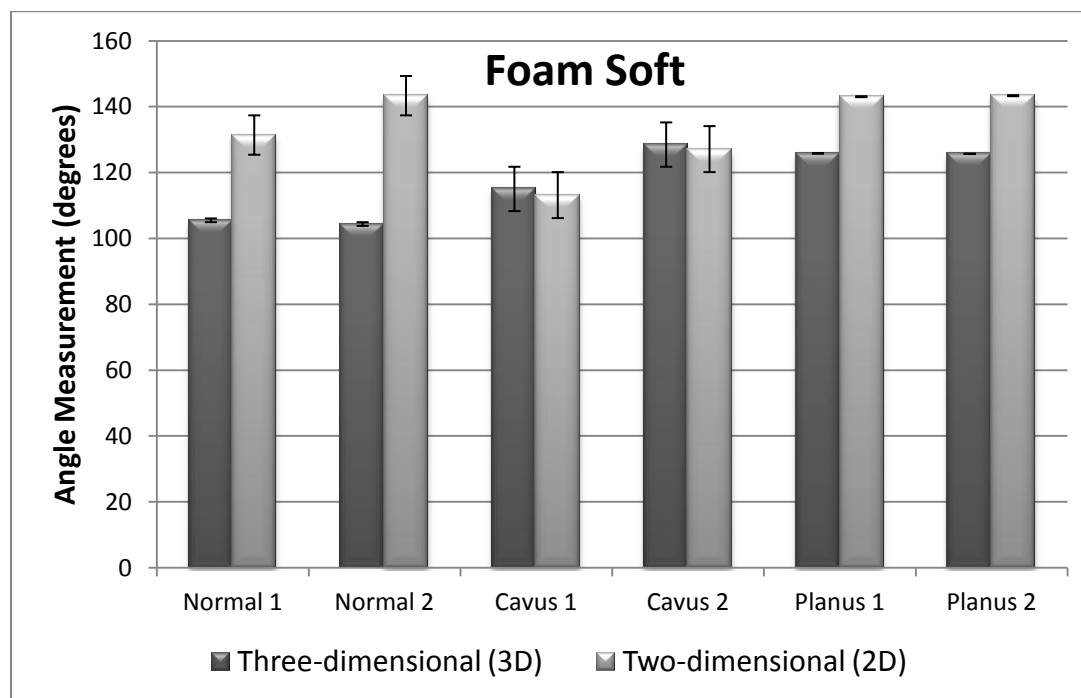
The differences between the three-dimensional (3D) MLA angle and the two-dimensional CFMA are compared by condition in Figures 5.1 to 5.4. Overall, the differences between the two analyses were the largest in the normal group and the smallest in the cavus group for all four conditions. The differences between the MLA and CFMA angles are listed in Table 5.1, as well as the mean and standard deviation of each subject. As hypothesized, differences did exist between analyses; however, comparing measured differences within each participant, the values were similar between conditions with low standard deviations ( $2.1^{\circ}$  to  $5.0^{\circ}$ ). These similarities can be seen in Figures 5.6 to 5.8, which use column graphs to compare the mean differences between analyses for each foot type, with all conditions displayed.

Table 5.2 shows the mean of each condition within each foot type, as well as the mean and standard deviations of the differences for both participants in each group. The normal group had the greatest difference between analyses with a mean of  $-33.0^{\circ} \pm 10.2^{\circ}$ , the planus group showed a mean difference of  $-16.6^{\circ} \pm 4.52^{\circ}$  and the cavus had the smallest difference between the 2D and 3D analyses with a mean of  $1.95^{\circ} \pm 2.60^{\circ}$ .

Bland-Altman (Bland & Altman, 1986) plots for normal, pes cavus and pes planus are shown in Figures 5.9, 5.10 and 5.11, respectively. The horizontal axis in each plot is the mean angle of the two measures (MLA and CFMA). The vertical axis represents the difference of the two measures (i.e. MLA-CFMA). The mean difference between the two types of measurement for each of the four conditions is shown as a solid horizontal line with the dotted horizontal lines representing  $\pm 2$  standard deviations (SD) from the mean. The mean difference between 3D and 2D measures, as mentioned previously, was  $-33^{\circ}$  for the normal foot type,  $-2^{\circ}$  for the pes cavus foot type and  $-17^{\circ}$  for the planus foot type.



**Figure 5.2:** Comparison of two- and three-dimensional analyses of six participants in the barefoot condition. Error bars for each subject are represented by the standard deviation of each foot type.



**Figure 5.3:** Comparison of two- and three-dimensional analyses of six participants in the foam casted soft orthotic condition. Error bars for each subject are represented by the standard deviation of each foot type.

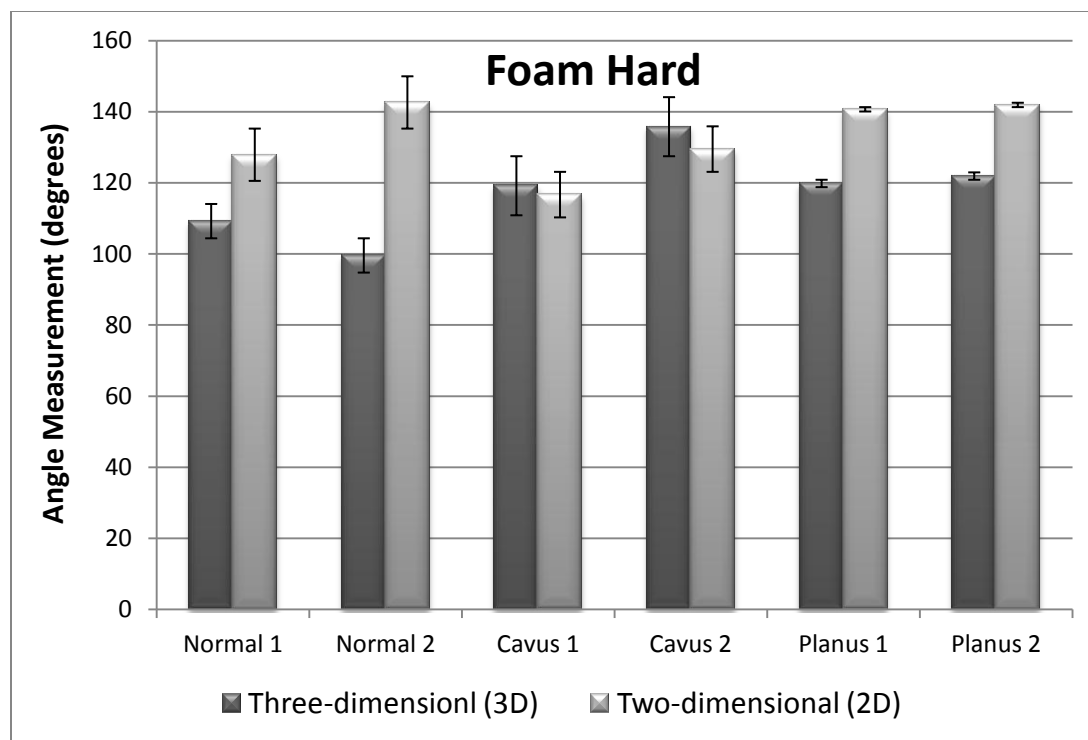


**Figure 5.4:** Comparison of two- and three-dimensional analyses of six participants in the foam casted hard orthotic condition. Error bars for each subject are represented by the standard deviation of each foot type.

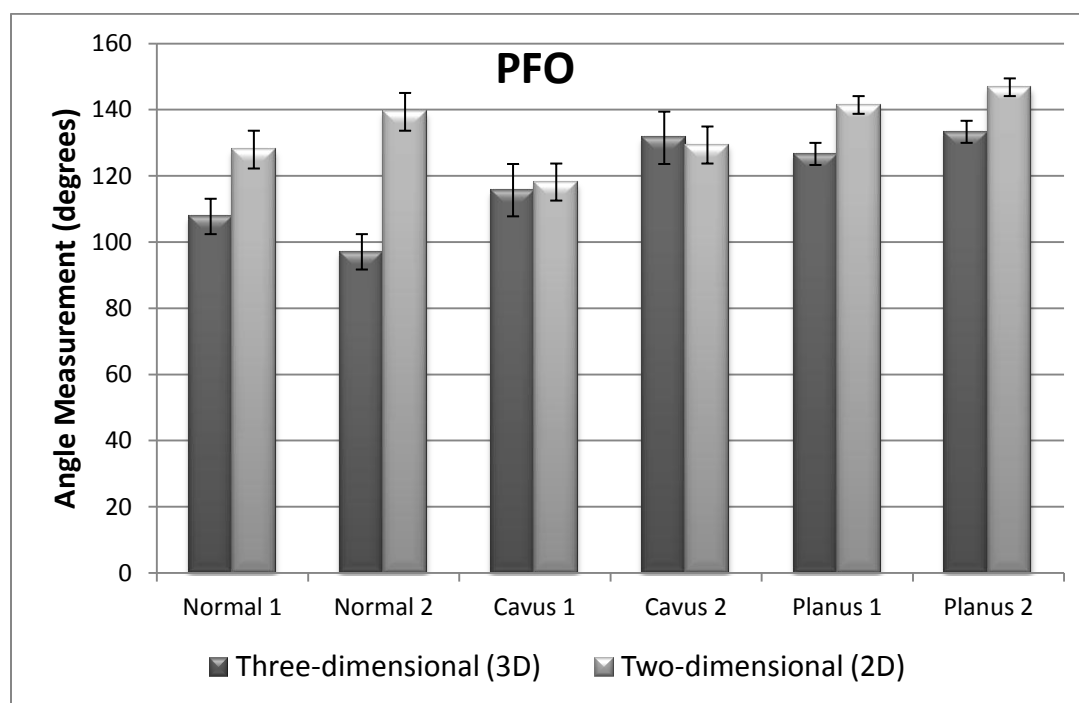


**Figure 5.5:** Comparison of two- and three-dimensional analyses of six participants in the PFO condition. Error bars for each subject are represented by the standard deviation of each foot type.

**Table 5.1: Differences between 3D and 2D arch angle analyses for each subject ( $\Delta\theta$ )**

<b>Delta Theta <math>\theta</math></b>	<b>Normal</b>	<b>Normal</b>	<b>Cavus</b>	<b>Cavus</b>	<b>Planus</b>	<b>Planus</b>
<b>Barefoot</b>	-28	-46	-0.1	-1.6	-22	-7.5
<b>Foam Soft</b>	-26	-39	-0.4	1.6	-16	-18
<b>Foam Hard</b>	-19	-43	4.8	6.6	-21	-20
<b>PFO</b>	-20	-42	1.4	3.3	-14	-14
<b>Mean</b>	<b>-23.3</b>	<b>-42.6</b>	<b>1.4</b>	<b>2.5</b>	<b>-18.1</b>	<b>-15.1</b>
<b>SD</b>	4.0	2.6	2.1	2.9	3.4	5.0

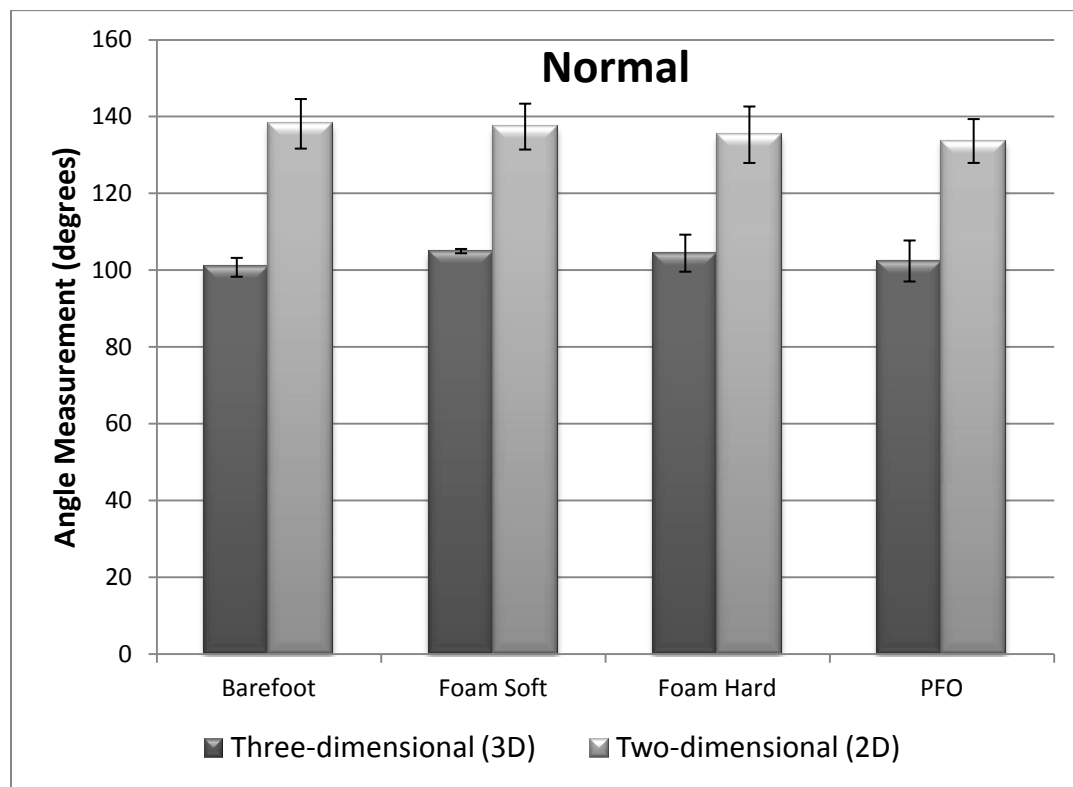


**Figure 5.6: Comparison of 3D and 2D analyses of calculated mean MLA and CFMA angles (respectively) in the normal group. Error bars for each subject are represented by the standard deviation of that condition between the two subjects.**

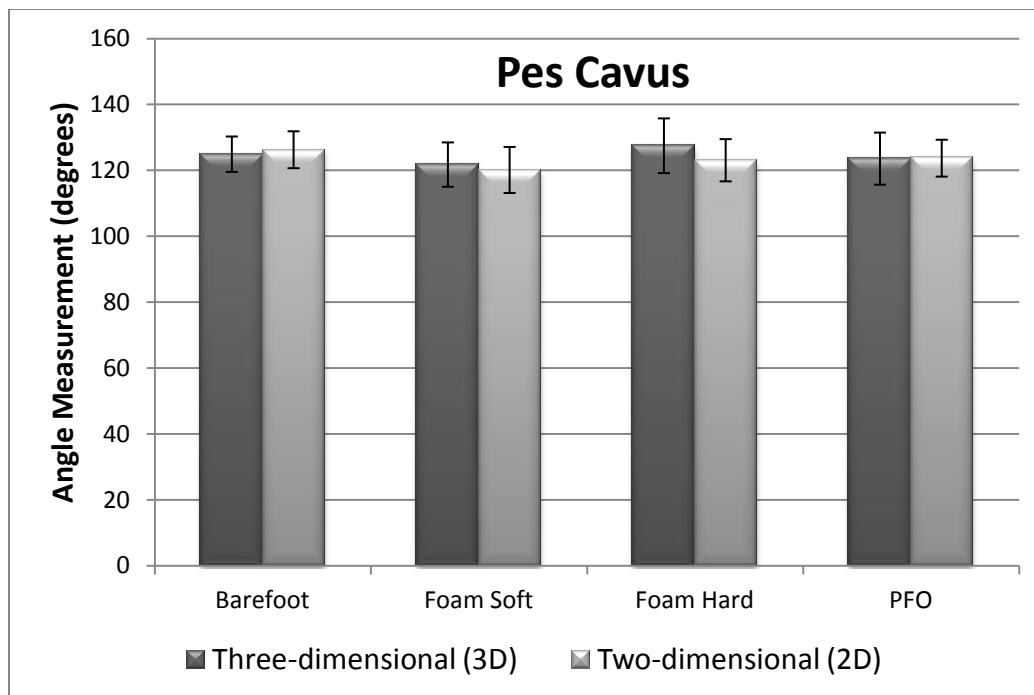


**Figure 5.7:** Comparison of 3D and 2D analyses of calculated MLA and CFMA angles (respectively) for the cavus group. Error bars for each subject are represented by the standard deviation of that condition between the two subjects.

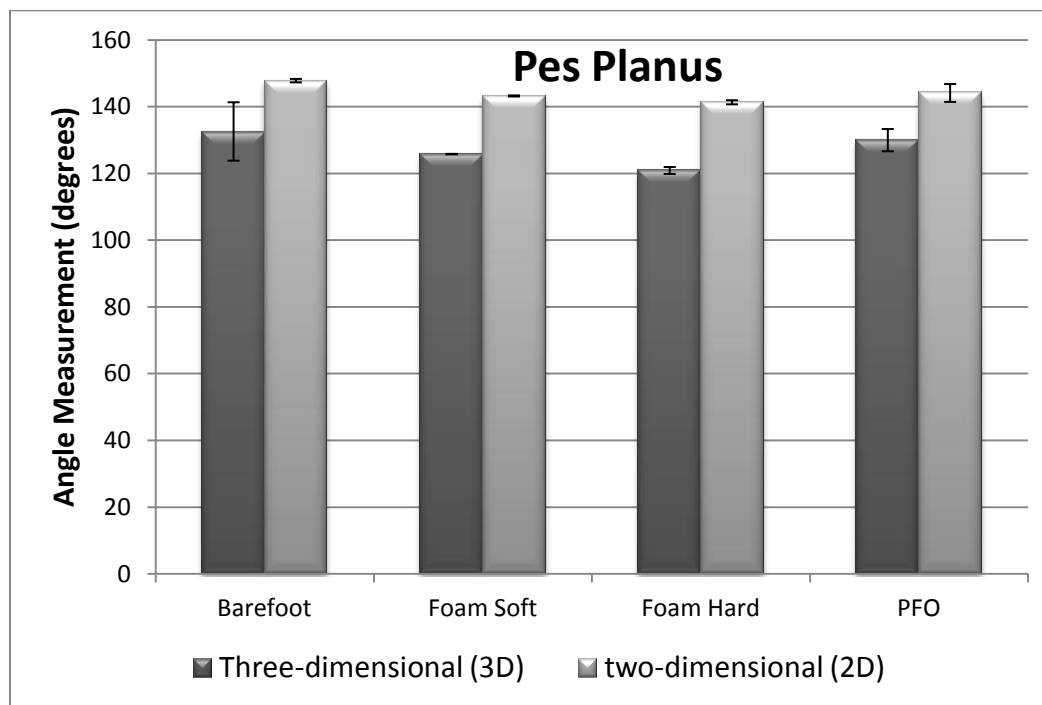


**Figure 5.8:** Comparison of 3D and 2D analyses of calculated MLA and CFMA angles (respectively) for the planus group. Error bars for each subject are represented by the standard deviation of that condition between the two subjects.

**Table 5.2: Mean differences, overall mean and standard deviation of all conditions within each pathological group between 3D and 2D analyses ( $\Delta\theta$ ).**

	<b>Normal</b>	<b>Cavus</b>	<b>Planus</b>
Barefoot	-37	-0.8	-15
Foam Soft	-32	0.6	-17
Foam Hard	-31	5.7	-21
PFO	-31	2.3	-14
<b>Mean</b>	<b>-33.0</b>	<b>1.95</b>	<b>-16.6</b>
<b>SD</b>	<b>10.2</b>	<b>2.60</b>	<b>4.52</b>

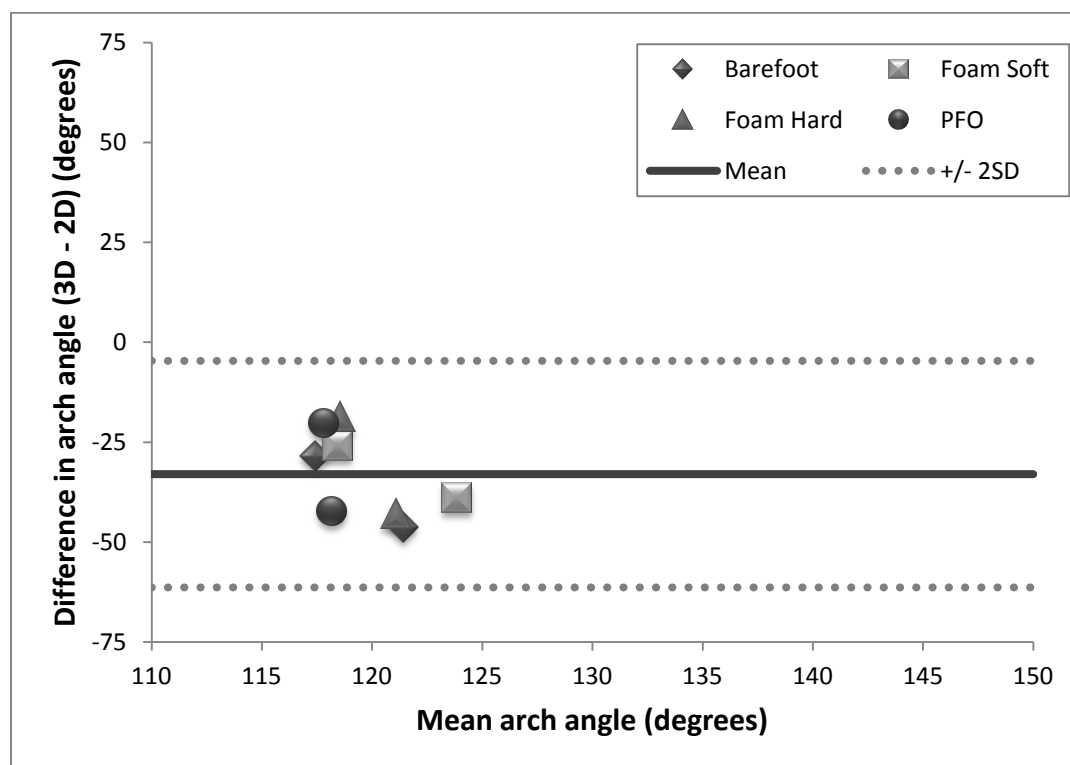


**Figure 5.9: Bland-Altman plot for both subjects of normal foot type. The mean difference in arch angle is represented by the solid line, with  $\pm 2SD$  represented by the dotted lines.**

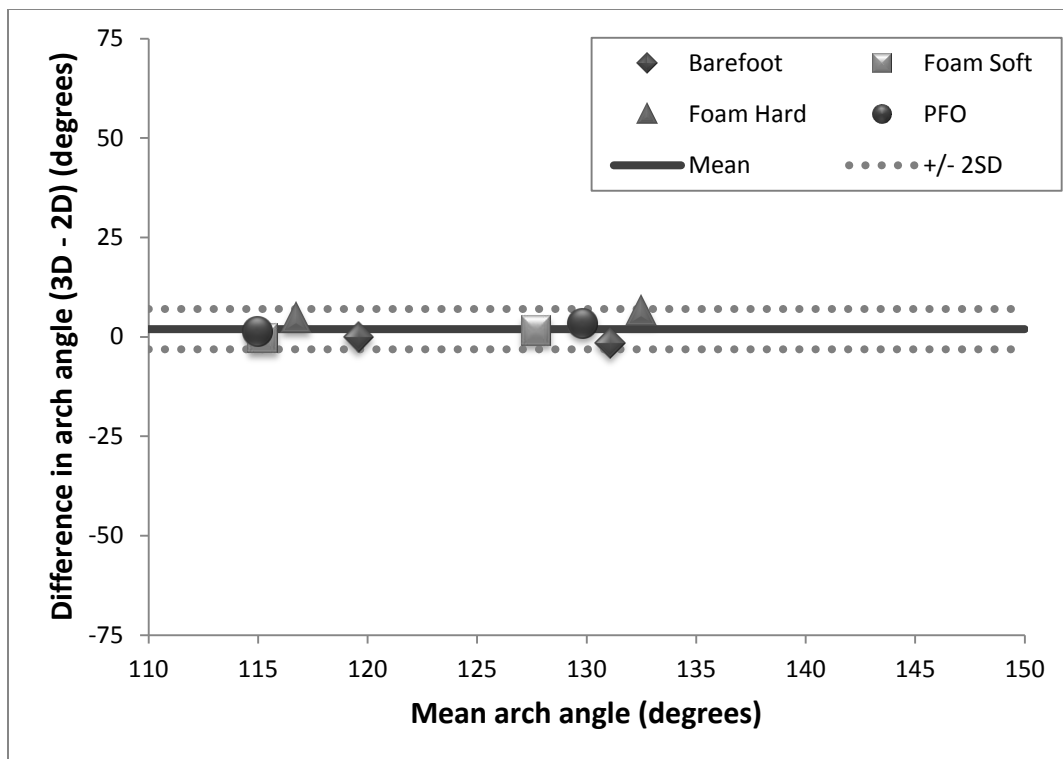


Figure 5.10: Bland-Altman plot for both subjects of pes cavus foot type. The mean difference in arch angle is represented by the solid line, with  $\pm 2SD$  represented by the dotted lines.

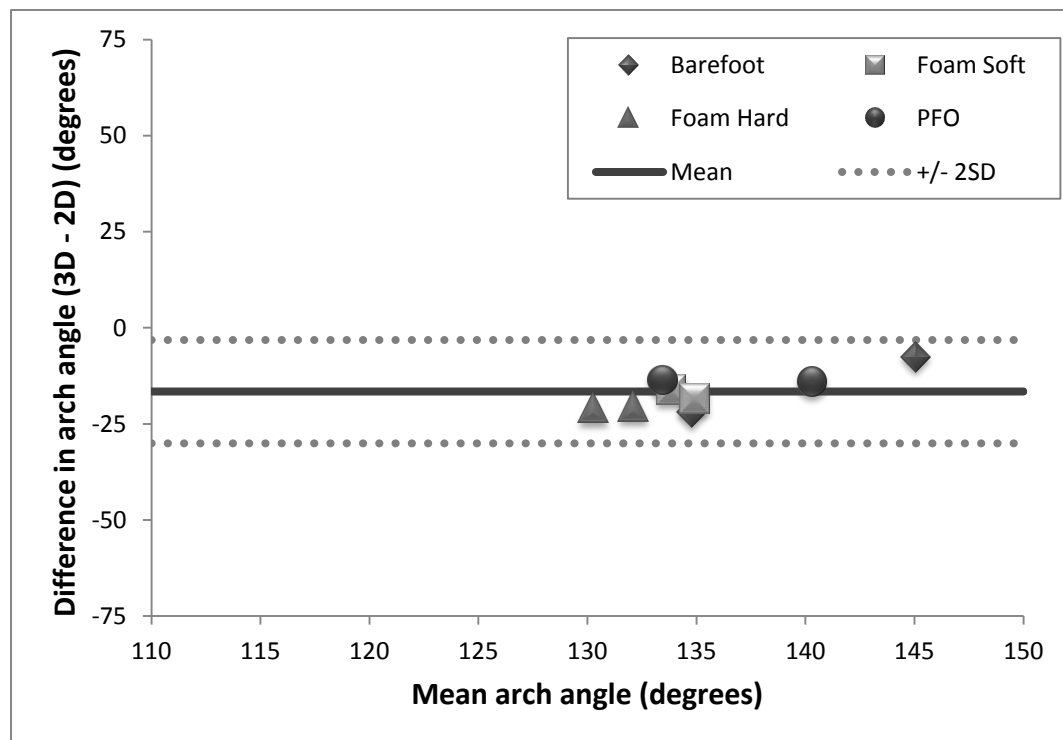


Figure 5.11: Bland-Altman plot for both subjects of pes planus foot type. The mean difference in arch angle is represented by the solid line, with  $\pm 2SD$  represented by the dotted lines.

## 5.4 DISCUSSION

The purpose of this study was to compare a two-dimensional (2D) radiographic analysis of the medial longitudinal arch with previous three-dimensional (3D) analysis completed in this research (Chapter 4). The 2D analysis measured the calcaneal-first metatarsal angle (CFMA) from a lateral fluoroscopic image whereas the 3D analysis measured the medial longitudinal arch (MLA) angle by digitizing bony landmarks using markerless fRSA. The results were consistent with the hypothesis as the 2D and 3D analyses demonstrated obvious differences for two of the three foot types. This finding indicates that the bones that make up the MLA angle are positioned in the coronal and transverse planes and cannot be quantified with a lateral 2D analysis. This finding was also suggested by Wearing et al. (1998) who used single plane fluoroscopy to measure this same arch angle (CFMA) in patients with unilateral heel pain as well as an asymptomatic control group. The findings suggested foot structure was not associated to chronic plantar fasciitis; however, investigators suggested there was undoubtedly motion in three-dimensions that was not represented by this two-dimensional analysis.

The mean difference between 3D and 2D measures, as mentioned previously, was  $-33^\circ$  for the normal foot type and  $-17^\circ$  for the planus foot type. This indicated that the 2D measure over-estimates the MLA angle in-vivo. Unlike the normal and planus plots, the cavus group shows a mean difference of  $2.0^\circ$ , which is close to zero, indicating the 2D MLA angle measure is a good estimate of the 3D angle. This means that when performing a 2D analysis of the medial longitudinal arch, the measured angle is the closest for a pes cavus (high-arch) patient. This also indicates that the cavus foot type has the least amount of out-of-plane positioning during gait, or the least motion in the frontal and transverse planes. Additionally, this finding may indicate that the positions of the three bony landmarks digitized in the 3D analysis (first metatarsal head, navicular tuberosity and medial process of the calcaneus) lie on the sagittal plane.

The agreement between MLA angle measurement techniques was also seen using the Bland-Altman plots, where the mean difference in the cavus group was 2.0 degrees, with the limits of agreement being -3.1 and 7.0 degrees. Thus, the 2D analysis may be -3.1 degrees below or 7.0 degrees above the measure from the 3D analysis - a range of 9.9 degrees. With additional sets of data for this foot type, along with repeatability measures,



more can be concluded and perhaps true quantities established to know if the 2D analysis can replace the 3D for this foot type.

The mean differences of the normal and planus groups are approximately  $-33^\circ$  and  $-17^\circ$ , respectively; therefore, the 2D analysis cannot be used in place of the 3D method. This finding was supported by the hypothesis since the 2D measurement was not expected to reflect arch positioning out of the sagittal plane. Little agreement exists between the two methods for these two foot types; however, a correlation may still be present. Since the intervals are wide in both cases, further analysis with a larger sample size may show a high correlation (r value) when plotting the 2D and 3D values against each other. This analysis may result in a known difference value that can be used as to relate one method to the other.

The results are also consistent with the hypothesis as the calculated differences across the conditions are consistent within each subject. The mean standard deviation for the four conditions among all subjects is 3.3 degrees. This finding indicates that the two analyses are both quantifying a change in the arch height, and that change is mostly proportional to one another no matter the walking condition.

This study is a comparison of two different radiographic arch angle measurements used in the literature – 2D (Murley et al., 2009) and 3D (Tome et al., 2006) analyses. Two-dimensional analyses are not capable of capturing out of plane motion; therefore, a three-dimensional analysis is required if positioning of the foot in all three anatomical planes are to be measured. However, if there was some way of correlating the two analyses with a proportion or known difference, the need for a 3D analysis may not exist, reducing both radiation for study participants and post-processing time for investigators. This study shows that there is some correlation between analyses, but that the proportion changes with different foot types.

One limitation that may have contributed to inconsistent results is the number of subjects per pathological group. Though six subjects total were compared, only two subjects of each foot type were processed. Though the cavus and planus groups showed a fairly low standard deviation of differences overall, the normal group was quite variable which may not have been as apparent had there been more subjects. Another potential reason for the variability in the results can be attributed to the position of the foot with

respect to the lateral fluoroscope – the foot may not have been precisely in the sagittal plane with respect to the image intensifier, therefore the 2D image might show a slightly angled view of that CFMA angle. The positioning for a true lateral image of the foot was attempted for each trial, but even a few degrees off could have changed the proportion of the differences between analyses.

With additional subjects added to the analyses, this comparison would provide additional insight on the validity of the 2D arch angle measurement using a lateral radiographic image. If this method can be proven to be an accurate representation of the medial longitudinal arch height and corresponding movements during gait, then three-dimensional analyses would no longer be required. Most importantly, this would also mean less radiation exposure for patients by using one fluoroscope instead of two as well as no CT scan required for the patient. Eliminating the need for a 3D analysis means substantially less time required to process the data as there would be no need for the experimental set-up recreation or creation of a 3D model to complete the lengthy matching process for markerless fRSA.

## 5.5 REFERENCES

- Allen, A.-M. (2009). *Development and Validation of a Markerless Radiostereometric Analysis (RSA) System*. London, Canada: Western University.
- Bland, J., & Altman, D. (1986). Statistical methods for assessing agreement between two methods of clinical measurement. *Lancet*, *i*, 307-310.
- Edelstein, J. E., & Bruckner, J. (2002). *Orthotics: A Comprehensive Clinical Approach*. SLACK Incorporated.
- Franco, A. H. (1987). Pes Cavus and Pes Planus - Analyses and Treatment. *Physical Therapy*, *67*(5), 688-694.
- Jenkyn, T., & Nicol, A. (2007). A multi-segment kinematic model of the foot with a novel definition of forefoot motion for use in clinical gait analysis during walking. *Journal of Biomechanics*(40), 3271-3278.
- Kedgley, A. (2009c). *Development of a Fluoroscopic Radiostereometric analysis system with an application to glenohumeral joint kinematics*. London, ON: School of Graduate and Postdoctoral Studies, Western University.
- Murley, G. S., Menz, H. B., & Landorf, K. B. (2009). A protocol for classifying normal- and flat-arched foot posture for research studies using clinical and radiographic measurements. *Journal of Foot and Ankle Research*, *2*(22), 1-13.
- Saltzman, C. L., Nawoczenski, D. A., & Talbot, K. D. (1995). Measurement of the Medial Longitudinal Arch. *Archives of Physical Medicine and Rehabilitation*, *76*(1), 45-49.
- Tome, J., Nawoczenski, D. A., Flemister, A., & Houck, J. (2006). Comparison of Foot Kinematics Between Subjects with Posterior Tibialis Tendon Dysfunction and Healthy Controls. *Journal of Orthopaedic & Sports Physical Therapy*, *36*(9), 635-644.
- Wearing, S. C., Urry, S., Perlman, P., Smeathers, J., & Dubois, P. (1998, November). Sagittal Plane Motion of the Human Arch During Gait: A Videofluoroscopic Analysis. *Foot & Ankle International*, *19*(11), 738-742.
- Xiong, S., Goonetilleke, R. S., Witana, C. P., Weerasinghe, T. W., & Au, E. Y. (2010). Foot Arch Characterization: A Review, A New Metric, and a Comparison. *Journal of the American Podiatric Medical Association*, *100*(1), 14-24.

## CHAPTER 6 – GENERAL DISCUSSION AND CONCLUSIONS

### 6.1 SUMMARY

Markerless fluoroscopic radiostereometric analysis (markerless fRSA) was previously validated using the glenohumeral joint at the Wolf Orthopaedic Quantitative Imaging Laboratory (WOQIL) at Western University by Anne-Marie Allen (2009). The primary objective of this work was to design a way to quantify the change of the medial longitudinal arch of the foot through various conditions in-vivo while using this validated fRSA method. A literature review that outlines the background information on skeletal kinematic measurement techniques, the fRSA study validation, as well as relevant clinical information is described in Chapter 1.

This system consists of two 9-inch C arm fluoroscopes, positioned at approximately 120° to one another. A wooden platform was designed and manufactured for study participants to stand and walk on during data collection. It was designed and fabricated in order to capture simultaneous lateral and anterior posterior fluoroscopy videos of the left foot. Calibration of this fRSA system as well as image digitization is performed using custom-written code created in MATLAB (Kedgley, 2009c). Distortion correction of the calibration images is completed by using a global approach polynomial fit to the positions of the stainless steel beads on a plexiglass grid to the face of the image intensifier. The remaining calibration parameters are calculated using additional custom MATLAB algorithms (Allen, 2009) and then the experimental set-up is recreated in solid modelling software called Rhinoceros. The three bones of interest are segmented in a DICOM viewer called OsiriX, and imported into the recreated experimental set-up to be matched frame by frame. For each bone, the three-dimensional coordinates of the digitized bony landmarks are exported into a spreadsheet using custom-written RhinoScript (Allen, 2009). The medial longitudinal arch is calculated between the medial process of the calcaneus, the navicular tuberosity and the head of the first metatarsal, similar to that calculated by Tome et al. (2006) who used optical motion capture. The angle calculation between these three points for this research was completed using custom-written MATLAB code, 'MLA\_Kinematics.m'. A two-dimensional angle, the

calcaneal-first metatarsal angle, was also calculated using custom-written MATLAB code in order to compare results with the three-dimensional analysis.

All studies involved participants from the Fowler Kennedy Sports Medicine Clinic on Western University's campus. A certified pedorthist recruited patients that fit into one of three foot types: pes cavus (high arch), pes planus (low arch) and normal arch. Participants were assessed on their foot structure and their gait function, and then casted by the same clinician using both foam box and plaster casting methods to make custom foot orthotics.

The first study investigates static barefoot, shoe and subtalar neutral position and is outlined in Chapter 2. The purpose of this study was to quantify the angle of the medial longitudinal arch (MLA) in static stance and show the effect of the subtalar neutral position on arch height. It was hypothesized that the arch angle would decrease slightly in the shoed condition and even more in the subtalar neutral position as compared with the barefoot condition. Sixteen subjects were tested for this analysis, 6 from the normally arched group, 5 pes planus and 5 pes cavus. The mean MLA angles with the neutral cushioning running shoe were not significantly different from the barefoot condition. When the clinician placed the participants in the subtalar neutral position, the MLA angle decreased for all subjects and the change in angle was statistically significant. Therefore, the hypothesis of this study held true since the MLA angle decrease was greater in the subtalar neutral position than the running shoe as compared with static barefoot stance. The mean arch angles in barefoot walking were smallest in the normal group which was not coincident with the hypothesis. This unexpected result led to an interesting finding when comparing the magnitude of vector NTMP normalized to foot length between foot types – it was found to be significantly larger in the cavus foot type when comparing means between planus and normal groups. This finding may be the reason for the larger than expected MLA angles in the cavus group, as it was expected that the cavus group would have the smallest angle compared with all the groups because of their highest observed arch height.

Chapter 3 described the dynamic application of markerless fluoroscopic RSA by comparing barefoot walking gait to walking with neutral cushioning running shoes. The purpose of this study was to determine the change in medial longitudinal arch kinematics

when changing from barefoot to shoed conditions during dynamic walking. It was hypothesized that the arch angle would decrease with the addition of neutral cushioning running shoes as compared with the no shoe condition. It was also hypothesized that the cavus and planus groups would show the smallest and largest mean arch angles, respectively. Six female participants were tested for this study: 2 normal arch, 2 pes planus and 2 pes cavus. The neutral cushion running shoes used were controlled for each subject – New Balance Model 882. The mean MLA arch angles increased slightly in the normal and cavus groups with the use of the running shoes; however, both subjects in the planus group demonstrated a decrease in MLA angle in neutral running shoes compared with walking barefoot. Therefore, the hypothesis was only partially proven among those in the pes planus group, and these results were statistically significant. The mean arch angles in barefoot walking were smallest in the normal group which was not coincident with the hypothesis; however, the largest MLA angle was seen in the pes planus group which was hypothesized prior to testing.

The third study used the same six female subjects (two from each pathological group) to compare five different foot orthoses (orthotics) as described in Chapter 4. The purpose of this study was to use markerless fluoroscopic RSA to determine how different types of orthotics affect the angle of the medial longitudinal arch (MLA) during dynamic gait. It was hypothesized that the hard orthotics would have the greatest effect on the arch, showing a smaller MLA angle than the soft orthotics, and therefore the greatest angle change from barefoot walking. It was also hypothesized that the proprioceptive feedback-type orthotic (PFO) would demonstrate the smallest change overall, therefore measuring the largest arch angle in comparison with the other devices. Results were variable between subject groups as well as individuals. Though there were no significant differences between any of the devices as compared with barefoot walking, the planus group showed the largest mean angle decrease from barefoot with the use of the foam casted hard orthotic which was expected, meaning an increase in arch height. The variability in data was likely due to the small sample size used for this particular study in each pathological group.

These three-dimensional (3D) analyses on the foot using markerless fRSA gives an angle between two vectors – from the navicular tuberosity to the first metatarsal and

calcaneus. Therefore this angle, used in a previous study while observing the foot segments with optical motion capture (Tome et al., 2006), is represented in three dimensions. Previous two-dimensional analyses looking at the MLA of the foot by calculating the calcaneal-first metatarsal angle (CFMA) is a simpler method (Murley et al., 2009), but does not capture any motion out of the sagittal plane when looking at a lateral radiographic image. The purpose of this final study was to compare the results of two- and three-dimensional analyses for four conditions: barefoot, foam casted hard orthotic, foam casted soft orthotic and PFO. It was hypothesized that the arch angles calculated would be different from 2D to 3D but that the changes between the calculated angles would be the consistent across all conditions for each participant. Six female participants, two from each pathological group, were used for this comparison. The two-dimensional analysis measures the CFMA angle in the lateral fluoroscopic view whereas the three-dimensional analysis will measure the MLA angle by digitizing bony landmarks using markerless fRSA. There was an obvious difference between the two analyses and this difference varied depending on foot type. The normal group showed the largest standard deviation from the mean when comparing the difference between analyses for all conditions within the same study participants. The two cavus participants showed the smallest deviation from the mean difference and also demonstrated the smallest mean difference overall, with a mean difference between analyses of less than two degrees. Therefore, the two-dimensional cavus CFMA angle measurement is close to achieving an agreement between the two analyses and therefore close to representing the actual MLA angle measurement in three dimensions. The hypothesis was proven as the differences between the calculated angles were consistent across conditions when looking at the four conditions for each individual.

## **6.2 STRENGTHS AND LIMITATIONS**

The strengths and limitations have been mentioned in each of the study's respective chapters; however, since the primary goal for this thesis was to quantify the skeletal kinematics of the medial longitudinal arch during dynamic gait, there are some overall strengths and limitations to be mentioned. An overall limitation of the method used for these studies is that it is invasive. For measurements to be obtained, radiation

must be used to acquire the desired fluoroscopic images and computed tomography (CT) scans. Therefore, study participants are exposed to more radiation than they would be normally. A second limitation is the amount of time required to complete post-processing of the images. For each testing date, the user must manually digitize the calibration and distortion grid images and with the output parameters, recreate the experimental set-up. The next step is to import the 3D model of the bone(s) (which is done separately for each participant) in order to match the bones' silhouettes to both fluoroscopic images. Once the bones reflect their exact position in three dimensions, the locations of the bony landmarks are then exported, and the matching process is repeated for the next frame.

An additional limitation specific to the equipment used for these studies is the size of the fluoroscopic image. The capture volume is quite small from using a 9-inch diameter fluoroscopic image intensifier for data collection. When limiting the visible region of the foot, it is more difficult to ensure all the bony landmarks are in the field of view for the bone matching process, also limiting participants by foot size. Since both the first metatarsal (forefoot to midfoot) and calcaneus (rearfoot) are required for matching both images for this experimental protocol, assuring the participant walks in the exact location for both fluoroscopes poses some challenges for data collection. Furthermore, this bi-planar RSA set-up with two C-arm fluoroscopes may limit the area for the participants to walk through, which may slightly alter normal gait.

A major strength of this research is that by using markerless RSA, the use of tantalum beads is not required to track skeletal motion; therefore, this procedure is much less invasive than standard RSA and can be performed on healthy and non-surgical individuals. Additionally, using fluoroscopy with RSA provides a dynamic system that may be used in ways that a conventional stereographic system cannot. Compared with a skeletal kinematic evaluation with CT scans or x-rays, the radiation dose is decreased with fluoroscopy even with two fluoroscopes and dynamic capture settings (approximately 2mSv compared to 10mSv for moving CT images). Lastly and most importantly, when compared with optical motion capture using external markers, fluoroscopic RSA shows internal bone structure, therefore eliminating error due to skin motion artifact.



### 6.3 RECOMMENDATIONS AND FUTURE DIRECTIONS

Certain recommendations can be made for the current experimental method based on the execution and findings of this thesis, such as:

- Increasing the sample size while decreasing the number of orthotics to offset costs and amount of radiation exposure. This will likely show a more significant trend in some of the dynamic studies, along with a smaller standard deviation within groups.
- Updating the current fluoroscopic equipment to larger image intensifiers and that are separate from the source components. These two items will allow for easier data collection with less restriction on space, allowing for a more natural gait and an increase in area for the participants to walk through.
- To decrease post processing time, a more automated series of algorithms could be used such as a graphical user interface (GUI) in MATLAB.
- Implementing an edge detection algorithm or using specific software to aid in the matching process. This will alleviate some of the processing time required to match each bone to each frame through the motion (Fregly, Rahman, & Banks, 2005).

Future research is required to look further into some of the above findings as well as topics related to this work. For example, an interesting finding was the length of the vector NTMP (normalized to foot length) and its difference between foot types. This distance, from the navicular to the calcaneus, is significantly longer for the cavus foot types than the normal and planus groups. This may have been the reason for the increased arch angle, when a smaller angle was expected as compared with both the normal and pes planus groups. With a larger NTMP length potentially causing a larger MLA angle, this means the orientation of the bones with respect to one another is likely different than previously thought; therefore, their position and motion during both static stance and dynamic gait should be further investigated. Similar to the findings for the 2D versus 3D analyses, motion out of the sagittal plane could perhaps be measured, showing the orientation of the rearfoot with respect to both the midfoot and forefoot in the different foot types.

Markerless fluoroscopic RSA can also be used as a method to compare and perhaps validate the multi-segment foot model developed by Jenkyn & Nicol (2007) by comparing the motions of foot segments to one another, as well as the specific movement of bones relative to one another. Additionally, comparing in-shoe pressure measurements with markerless RSA to quantify arch height would be a good measure to see how the two compare to a person's actual arch structure and weight distribution (Stolwijk, Louwerens, Nienhuis, Duysens, & Keijsers, 2011).

Though markerless fRSA is an accurate method to measure skeletal kinematics, it is somewhat invasive as it does expose people to unnecessary radiation, with half of that extra radiation coming from the need for a CT scan. Therefore, validating a method to use a standard 3D phantom bone models (Sawbones; Pacific Research Laboratories, Vashon, USA) to match fluoroscopic images would be ideal to alleviate this ethical problem. The saw bones would have to be scaled depending on the participants' foot size and type, and very specific bony landmarks would need to be chosen in order to maintain accuracy. Not only would this improve the ethical issues that this method may encounter, it would require less time commitment for each participant, as well as a shorter time spent acquiring data for the investigators.

#### **6.4 SIGNIFICANCE**

In conclusion, this work provides insight into the functionality of orthotics and presents preliminary data for the effect that orthotics have on the medial longitudinal arch for three different foot types. By examining and quantifying the height of the medial longitudinal arch with markerless fRSA, a significant difference was seen over all subjects in the subtalar joint neutral position when placed into this pose by the same clinician. As expected, neutral cushioning running shoes did not show a significant arch height increase (arch angle decrease) among any foot type. Though all groups did not show a consistent trend in arch angle differences, the pes planus participants showed a large arch angle decrease with the foam hard orthotic. The pes cavus foot type showed the greatest decrease with the foam casted soft orthotic, whereas the normal group showed angle increases with all orthotic devices. With the addition of a large sample size, a more significant trend will likely be seen among all foot types. Finally, the comparison

between the two and three-dimensional analyses was indeed different from one another. Findings suggest very little out-of-plane motion or positioning occurs for the pes cavus foot type with greater motion apparent for the pes planus and normal arch groups, showing a larger difference in calculated arch angles between the two analyses. The findings from the above work will hopefully be helpful for clinicians by increasing overall understanding of the foot and its arch kinematics under various conditions. Additionally, by investigating its skeletal kinematics in three dimensions, this study provides a new beginning for overall in-vivo research of the foot.

## 6.5 REFERENCES

- Allen, A.-M. (2009). *Development and Validation of a Markerless Radiostereometric Analysis (RSA) System*. London, Canada: Western University.
- Fregly, B. J., Rahman, H. A., & Banks, S. A. (2005, August). Theoretical Accuracy of Model-Based Shape Matching for Measuring Natural Knee Kinematics with Single-Plane Fluoroscopy. *Journal of Biomechanical Engineering*, 127, 692-699.
- Jenkyn, T., & Nicol, A. (2007). A multi-segment kinematic model of the foot with a novel definition of forefoot motion for use in clinical gait analysis during walking. *Journal of Biomechanics*(40), 3271-3278.
- Kedgley, A. (2009c). *Development of a Fluoroscopic Radiostereometric analysis system with an application to glenohumeral joint kinematics*. London, ON: School of Graduate and Postdoctoral Studies, Western University.
- Murley, G. S., Menz, H. B., & Landorf, K. B. (2009). A protocol for classifying normal- and flat-arched foot posture for research studies using clinical and radiographic measurements. *Journal of Foot and Ankle Research*, 2(22), 1-13.
- Stolwijk, N. M., Louwerens, J. W., Nienhuis, B., Duysens, J., & Keijsers, N. L. (2011, January). Plantar Pressure With and Without Custom Insoles in Patients with Common Foot Complaints. *Foot and Ankle International*, 32(1), 57-65.
- Tome, J., Nawoczenski, D. A., Flemister, A., & Houck, J. (2006). Comparison of Foot Kinematics Between Subjects with Posterior Tibialis Tendon Dysfunction and Healthy Controls. *Journal of Orthopaedic & Sports Physical Therapy*, 36(9), 635-644.

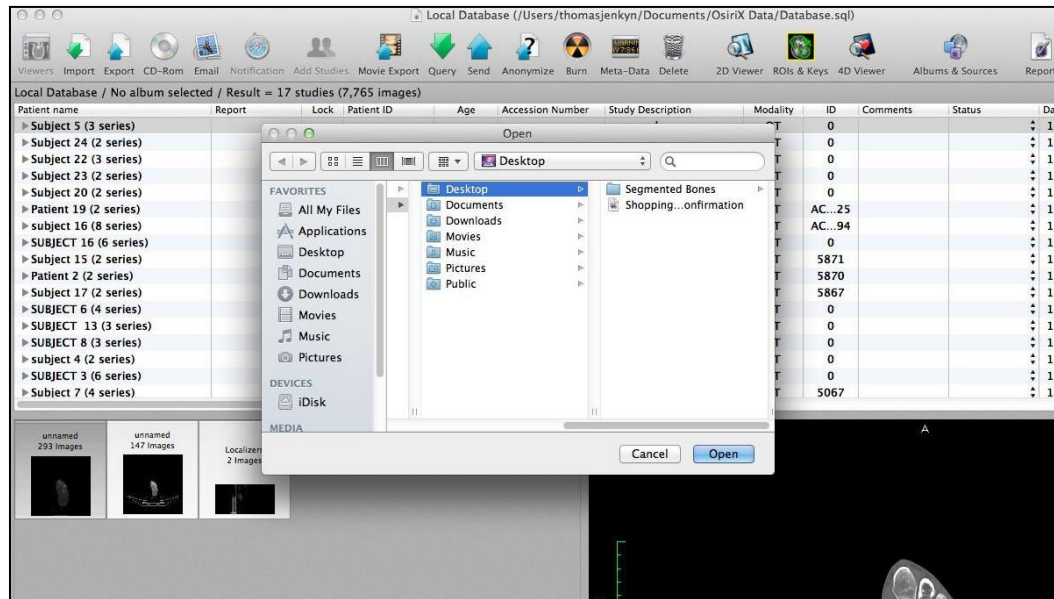
## **APPENDICES**

## APPENDIX A – SEGMENTATION USING OSIRIX

### A1. Bone Segmentation Steps – OsiriX (Pixmeo, Geneva, Switzerland)

**Note:** Do not save any work throughout this unless this guide explicitly tells you to do so. Hitting save will result in losing data that you may need in order to proceed, and may result in an error message in the process.

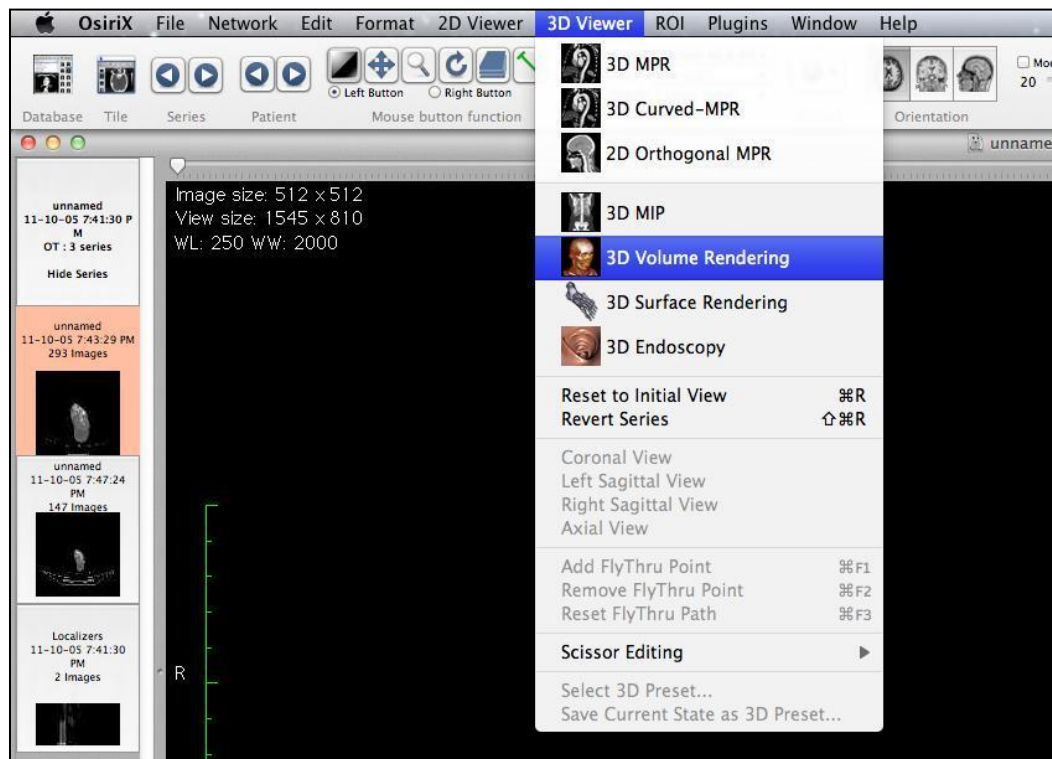
- 1) Open ‘Finder’ on the Desktop and in the Applications on the left menu bar, find OsiriX and double click to Open.
- 2) First, the CT scan files must be imported to the program and copied to the system before any manipulation can happen. Click on ‘Import’ at the top left and then select the series of CT files that you want to make into a 3D model.



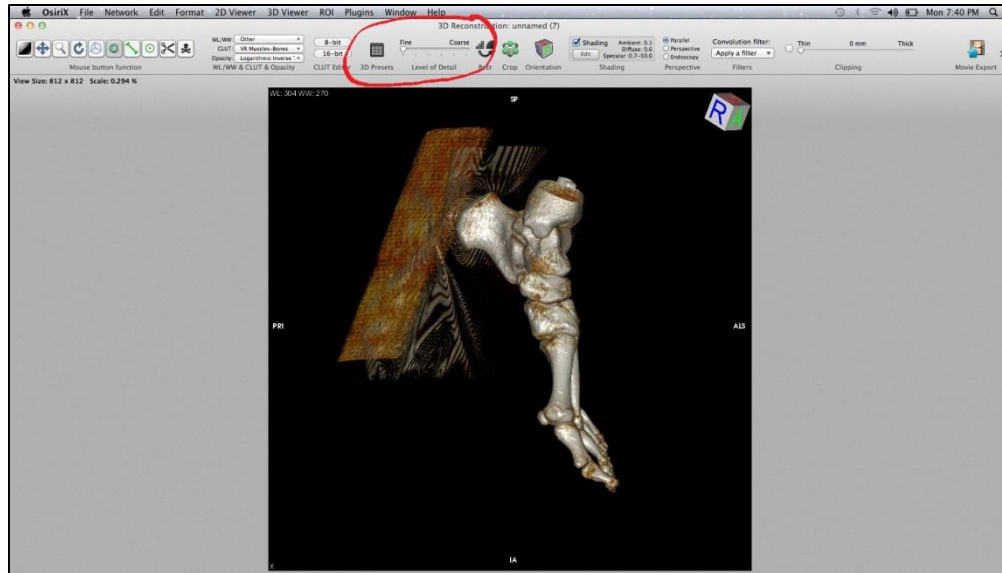
- 3) Once all the files have copied to the Local Database (above), double click the subject or patient CT whose bones you would like to segment.
- 4) The following screen will pop up > Click “I agree”.



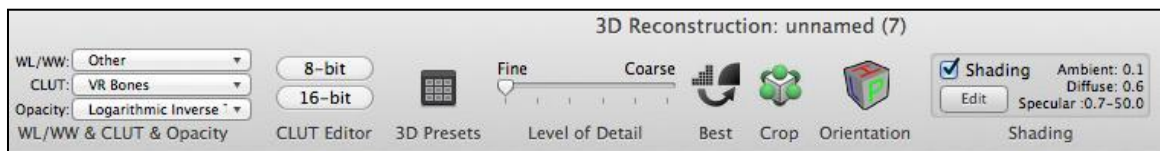
- 5) Choose the file to the left that has the most images or preview the one that appears most suitable (see highlighted pink area below). In this case, the one with the most images was the one chosen based on the slice thickness and CT properties.
- 6) Go to the top pull down menu under 3D Viewer and choose 3D Volume Rendering.



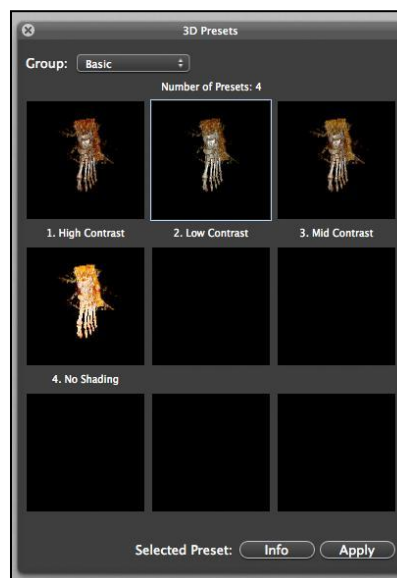
The 3D Volume Rendering window looks like the one below, with the tools in the second menu from the top.



- 7) On the second menu from the top (circled in red above), immediately change the level of detail to **FINE** (as far as it will go to the left).



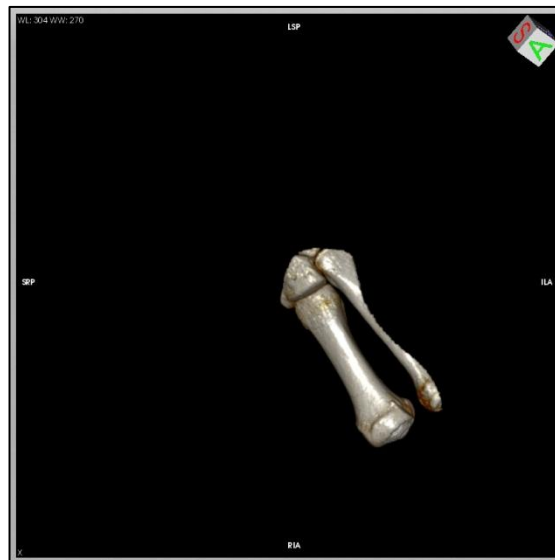
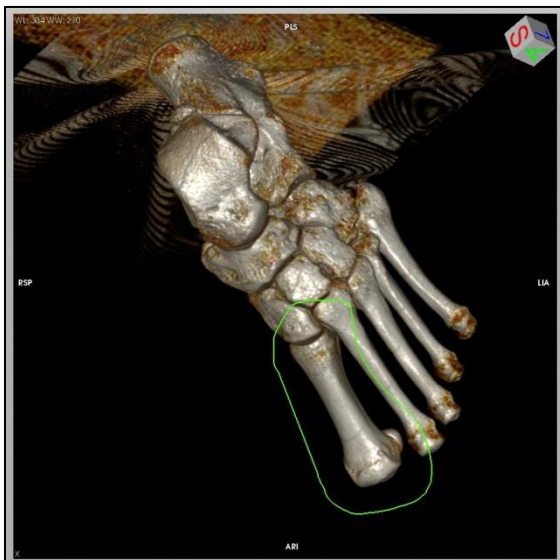
- 8) Click on the 3D presets menu to the left of that and choose the 'Basic' Group. Click on 'Low Contrast' and then click 'Apply'. This will allow for easier segmentation of the bones as there will be less visible noise and soft tissue surrounding the bone.



## 9) Description of tool functions (top left of the window in step 6):



- a. The **Poison sign** (far right) will get rid of an entire bone at once. This tool may be very useful, however, some bones may appear to be separate but in reality, there is some connection somewhere to another bone. If that's the case, this tool will remove two or more bones at one time.
- b. The **scissors** will allow you to select an area in bright green and then hitting '**Enter**' once made your selection (below) will keep what you've selected, whereas the '**Delete**' button will remove what you've selected.
  - i. It's easier to scissor around the bone you want right off the start, and press enter, and then use the delete button to eliminate the other bones that are near or touching afterwards.
  - ii. Note that the scissor function will cut everything in three dimensions from the plane you've chosen and protruding into the screen and bones behind the selection so be careful where you cut.



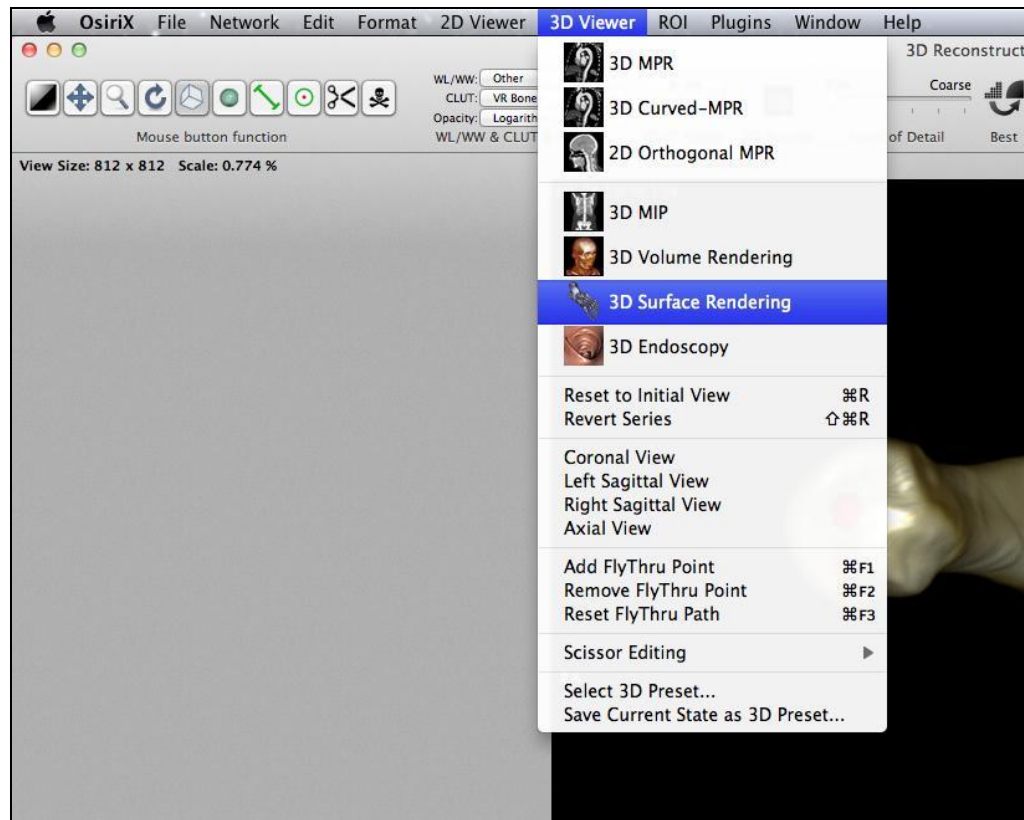
- c. The green circle with the red dot allows you to place a red sphere on the bone, marking any necessary landmarks. Try to do this as consistently as possible for each patient's CT scan, in order to compare the position of the same bony landmarks of the anatomy between subjects. These spheres will export as separate 'mesh' items, along with the single bone mesh.



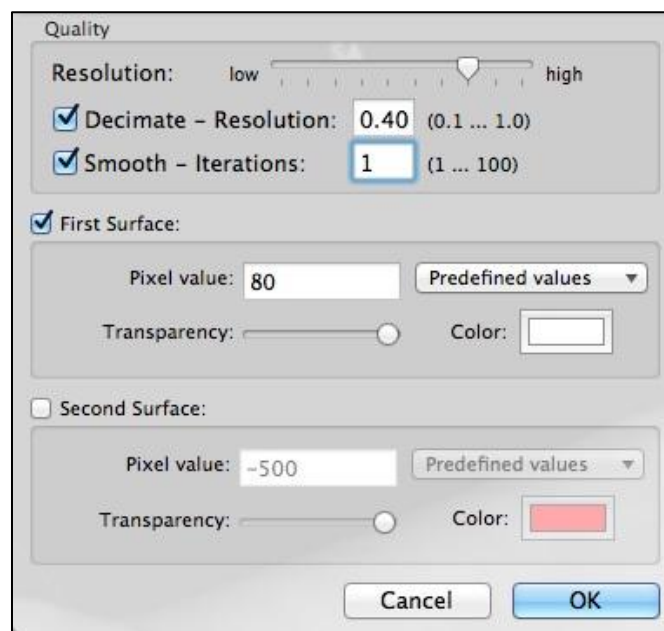
- i. You can choose to put the red points on the landmarks before or after segmentation, depending on how easily identifiable they are without the surrounding bone. For segmenting the navicular in this study, the spheres were positioned before segmentation to mark the most medial point of the tuberosity as well as the most dorsal aspect.
- d. The green line segment is a measurement tool if you want to determine the length of any two objects in two dimensions
- e. Greenish blue sphere – used to re-position the camera view, since you may be looking near the end of an extremity, the camera position may need to be changed to zoom in close on the right area.
- f. Box tool – used to rotate the model in three dimensions. The combination of these last two tools will allow you to zoom in and out and get the correct angle to use the scissor tool.
- g. Semi-circular arrow – rotates the object in the plane of view.
- h. Magnifying glass – used to zoom in and out (as well as the right click button at all times)
- i. Move function (four arrows) – left click will move the object within that plane of view. Used to reposition the object (similar to rotating the camera)
- j. Window level (black square far left) will adjust the window level and width – general CT settings. The 3D present chosen has default values for these parameters; therefore, this is not used for the purposes of this segmentation.

Note: Hold mouse over function to see what each does if you aren't sure. DO NOT hit the save button. This will create an error in the next step.

- 10) Only segment one bone at a time in the window – it is easier to crop a single bone without having to worry about what is behind it. Also, you want to export each bone separately to import into Rhinoceros.
- 11) Once the bone is segmented, the surface of the bone must be smoothed. Click on '3D Presents' similar to step 7 and in that window change the group type to: Bone CT. Select option 9 "Soft".  
Note: This setting has specific presents that show the best balance between colour and density of the bone for this thesis. If you click on 'Info', the 3D Present parameters will be shown – window length/width, the colour look up table (CLUT) and the filter used for the CT scan. These are the best surface properties for exporting the bone model to the best of the author's knowledge.
- 12) At the top menu, select the 3D Viewer drop down menu again and select the 3D Surface Rendering option (below). This will create a mesh of the segmented bone by defining a surface around its known volume. The segmented bone model can only be exported from this 3D view.



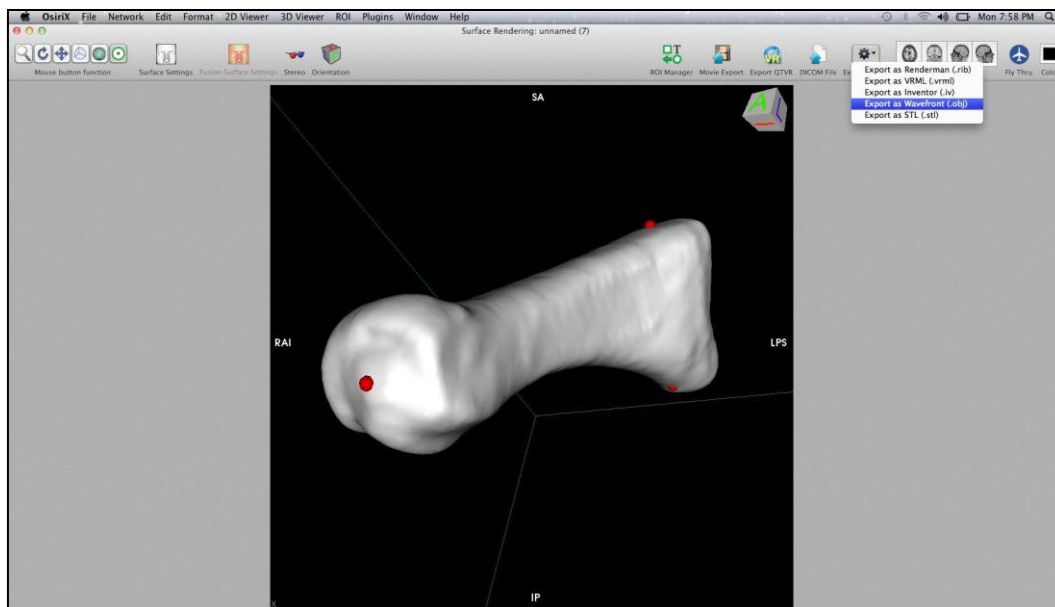
- 13) Once selected, the menu at the top of the window will pop up automatically for input regarding the desired surface settings (see below).



- a. The settings above will change depending on the patient, their bone density, as well as which bone you are working with.
- b. Move the 'Resolution' cursor to two notches to the left of high to start, and move to HIGH if that appears better.
- c. Initial settings should have 'Smooth – iterations' function to 1 (meaning less smoothing will occur at first).
- d. Initially, the Pixel Value should be set to 100 (instead of 300 by default). This setting represents the 'density' of the bone, for example, 50 for one patient made the bone too built up with sharp edges, whereas 100 created holes in the bone. The higher the pixel value, the less dense the bone – this value will need to be manipulated depending on the subject.
- e. You can also change the colour of the bone which may be a good idea to choose something that will work well in rhinoceros background.

**Important:** Once you set these values initially and they are too high (bone has holes and is not dense enough) then you cannot make it more dense by changing them in the 'surface settings' tab in the toolbar. You must close the window back to the 3D Rendering window and then start step 12 again. However, if the pixel value is started low, with a low 'Smooth' number as well, and the bone appears too dense, you can edit the surface settings by increasing the Iterations and Pixel Value gradually. I've found this to be the easiest way to get the bone looking the way you want. Start with low numbers and gradually increase them to the desired output.

- 14) The bone will now resemble the model below (example bone: first metatarsal of the left foot). From this point, the model can be exported as a 'Wavefront' or object file (.obj), which is found in the 'Export 3D-SR icon' on the Surface Rendering Menu to the right.
  - a. Select the folder you wish to save it in. The file can now be transferred to the PC of your choice so long as you have Rhinoceros on the machine for further analysis.



- 15) When closing any window, use the buttons on the top left, the red button. First, close the 3D Surface Rendering window, followed by the 3D reconstruction (volume) rendering. As long as you don't close the subject CT file (the 2D view at the beginning, that bone will remain segmented.
- 16) To start a **new** segmentation for another bone for the same patient, the last window must be closed and then the subject re-opened to start again.  
**Note:** the red spheres will not ever disappear automatically from where they were placed, even when closing the subject CT files. So you have to manually use the tool function, click on them and hit delete before adding them to the next bone.
- 17) To quit OsiriX, you have to go to the top left and click Quit OsiriX, closing the last window will not do that for you

#### Taking screen shots with a MacBook Pro

1. **Apple (Command) Key +Shift+3**  
Captures entire desktop to a file on the desktop as 'picture #'. This option lets you capture the whole screen.
2. **Apple (Command) Key +Shift+4**  
Allows you to use your mouse to select a specific part of your desktop for capture. This will turn your mouse pointer into a cross, please hold down the mouse button and drag to select the part of the screen you want. When you release the button the screenshot will "snap" that part of the screen. Press 'Esc' to release.
3. **Apple (Command) Key +Shift+4 then press Spacebar**  
Allows you to select which window to capture.

## APPENDIX B – MATLAB CODE

### B1. MLA\_KINEMATICS.M

```

% Program:          MLA_Kinematics.m
% Description:      Calculates the kinematics of the medial longitudinal
                   arch (LEFT FOOT) digitized boney landmarks in
                   conjunction with anatomical landmarks
%
%                   All with respect to the calcaneus coordinate system
% Written by:      Megan Balsdon
% Date written:    October 24, 2011
% Last modified:   March 1, 2012
%-----

% Initialize variables
endline = [0 0 0 1];
end_one = [1'];

% Obtain information about the data to be analyzed from the user
data_folder = input('Enter the name of the folder with the digitized
points: ', 's');
data_dir = ['H:\Documents\Research2 Desktop\Subject 2\' data_folder
'\'];
num_files = input('Enter the number of files to be analyzed: ');
start_file = input('Enter the value of the first file in the series:
');

for z = start_file:(start_file + num_files - 1)
    file_num = int2str(z);
    if z < 10
        data_filename = strcat('Fluoro-000', file_num, '_output.xls');
    elseif (z >= 10 && z < 100)
        data_filename = strcat('Fluoro-00', file_num, '_output.xls');
    elseif (z >= 100 && z < 1000)
        data_filename = strcat('Fluoro-0', file_num, '_output.xls');
    else
        data_filename = strcat('Fluoro-0', file_num, '_output.xls');
    end
    digi_landmarks = xlsread([data_dir,data_filename],1);

% Define Calcaneus Coordinate System
%Landmarks: ST = Sustentaculum tali, MP = Medial Process, LS = Lateral
(Anterior) Surface
LS = digi_landmarks(1,1:3);
MP = digi_landmarks(2,1:3);
ST = digi_landmarks(3,1:3);
LSMP = MP - LS;
MPST = ST - MP;
Zcal = LSMP;
Zcal_length = norm(Zcal);
Zcal = Zcal / Zcal_length;
Ycal = cross(-Zcal, MPST);
Ycal_length = norm(Ycal);
Ycal = Ycal / Ycal_length;

```

```

Xcal = cross(Zcal, Ycal);
Xcal_length = norm(Xcal);
Xcal = Xcal / Xcal_length;
origin_cal = MP;

Tcal_lab = [Xcal' Ycal' Zcal' origin_cal'];
% Add 'endline' row at the bottom of transformation matrix
Tcal_lab = cat(1, Tcal_lab, endline);

%Find NT = Navicular Tuberosity and MH = metatarsal head in Calcaneus
Coordinate System
%Other Landmarks: LC = Lateral landmark (cuboid), DA = Dorsal Aspect
%PB = Plantar aspect (base), DB = Dorsal aspect (base)

%LC = digi_landmarks(4,1:3);
NT = digi_landmarks(5,1:3);
%DA = digi_landmarks(6,1:3);
%PB = digi_landmarks(7,1:3);
%DB = digi_landmarks(8,1:3);
MH = digi_landmarks(9,1:3);

%Take inverse of T matrix and concatenate point coordinates NT & MH
Tlab_cal = inv(Tcal_lab);
Pnt_lab = cat(2, NT, end_one);
Pmh_lab = cat(2, MH, end_one);

%Find points NT & MH in terms of Calcaneus Coordinate System
Pnt_cal = Tlab_cal * Pnt_lab';
Pmh_cal = Tlab_cal * Pmh_lab';

%Remove 'end_one' from vectors to reflect true coordinates
Pnt_cal(4,:)=[];
Pmh_cal(4,:)=[];

%Create vectors from Pnt to both Pmh and MP (origin)
%in the calcaneus coordinate system

NTMP = origin_cal - Pnt_cal';
NTMH = Pmh_cal' - Pnt_cal';

NTMP_length = norm(NTMP);
NTMH_length = norm(NTMH);

%Angle Calculation using inverse cosine (degrees)
Theta = acosd((dot(NTMP, NTMH))/(NTMP_length * NTMH_length));

%Output file information

names = ['Theta(deg) ' 'NTMH' ' 'NTMP' '];
cellnames = cellstr(names);
data_filename = strrep(data_filename, 'output', 'angle');
data_write = fullfile(data_dir, data_filename);
xlswrite(data_write, cellnames);
xlswrite(data_write, Theta, 1, 'A2');

```

```

        xlswrite(data_write, NTMH_length', 1, 'B2');
        xlswrite(data_write, NTMP_length', 1, 'C2');
end

```

## B2. FIND\_POINTS.M

```

%*****
**
% Program:                Exports coordinates of four points to an Excel
sheet
%                        Points are clicked on an image in TIFF file
format
% Original written by: Angela Kedgley
% Modified by:           Megan Balsdon
% Date Modified:        June 20, 2011
%-----
---

image_type = 'i';
data_folder = input('Enter the name of the folder with the data:
','s');
image_file = input('Enter the name of the image file (FluoroA or
FluoroB): ','s');
z = input('Enter the number of the first file: ');

while ~(strcmp(image_type,'e') || strcmp(image_type,'E'))

    drawnow;
    %   image_type = input('Are there more files to be digitized? Select
Yes (y or Y) or Exit (e or E):','s');
    image_type = 'y';

    if (strcmp(image_type,'y') || strcmp(image_type,'Y'))           % There
are more files to be digitized
        file_num = int2str(z);
        if z < 10
            new_file = strcat(image_file, '-000', file_num, '.tif');
        elseif (z >= 10 && z < 100)
            new_file = strcat(image_file, '-00', file_num, '.tif');
        elseif (z >= 100 && z < 1000)
            new_file = strcat(image_file, '-000', file_num, '.tif');
        elseif (z >= 1000 && z < 10000)
            new_file = strcat(image_file, '-000', file_num, '.tif');
        else (z >= 10000)
            new_file = strcat(image_file, '-00', file_num, '.tif');
        end

        im = imread(fullfile('E:\Documents\Data\ASB Conference\',
data_folder, new_file));

        display('Select points on the image with the cursor by single-
clicking the left mouse button.');
```

```

display('Press the middle mouse button to indicate the last
point or to exit the image.');
```

```

colormap(gray(256)); image(im); axis image

names = ['point_1'; 'point_2'; 'point_3'; 'point_4'];
cellnames = cellstr(names);

display_outputs = ['point 1';
                  'point 2';
                  'point 3';
                  'point 4'];

counter = 1;
% Allow the user to select the points
for counter = 1:4
    display(display_outputs(counter,:));
    point(counter,:) = ginput(1); %
Pick the points using ginput
    if strcmp(get(gcf,'SelectionType'),'normal')
        digi_points(counter,:) = point(counter,:);
    elseif strcmp(get(gcf,'SelectionType'),'alt')
        digi_points(counter,:) = [5555 5555];
    elseif strcmp(get(gcf,'SelectionType'),'extend') %
Break out of the loop if middle mouse button is pushed
        digi_points = [5555 5555; 5555 5555; 5555 5555];
        break
    end
end

% Write the selected points to an Excel spreadsheet
if z < 10
    output_filename = strcat(image_file, '-000', file_num,
'_points.xls');
elseif (z >= 10 && z < 100)
    output_filename = strcat(image_file, '-00', file_num,
'_points.xls');
elseif (z >= 100 && z < 1000)
    output_filename = strcat(image_file, '-0', file_num,
'_points.xls');
elseif (z >= 1000 && z < 10000)
    output_filename = strcat(image_file, '-00', file_num,
'_points.xls');
else (z >= 10000)
    output_filename = strcat(image_file, '-', file_num,
'_points.xls');
end

xlswrite(fullfile('E:\Documents\Data\ASB Conference\',
data_folder, output_filename), cellnames);
xlswrite(fullfile('E:\Documents\Data\ASB Conference\',
data_folder, output_filename), digi_points, 1, 'B1');

z = z + 1;
close all; % Close all figure windows

```



```

clear points im counter digi_points output_filename;

elseif (strcmp(image_type,'e') || strcmp(image_type,'E'))
    break

else
    display('Please enter one of the available options.')
end
end

clear;

```

### B3. ANGLE\_CALC.M

```

% Program:      Angle_Calc.m
% Description:  Measures Calcaneus-First Metatarsal Angle (CFMA)
%              between two lines created from output of
%              'Find_points.m'
% Created by:   Megan Balsdon
% Date written: June 20, 2011
%-----

%Obtain excel file name from user with output points from Find_Points.m
data_folder = input('Enter the name of the folder that contains the
points files: ','s');
data_dir = ['E:\Documents\Data\ASB Conference\' data_folder '\'];

% Obtain information about a range of files if required
num_files = input('Enter the number of files to be analyzed: ');
start_file = input('Enter the value of the first file in the series:
');
data_file1 = input('Enter the start of the name of the file which
contains the object data: ','s');

i = 0;

for z = start_file:(start_file + num_files - 1)
    i = i + 1;

    if z < 10
        file_num = int2str(z);
        points_filename = strcat(data_file1, '-000', file_num,
'_points.xls');
    elseif (z >= 10 && z < 100)
        file_num = int2str(z);
        points_filename = strcat(data_file1, '-00', file_num,
'_points.xls');
    elseif (z >= 100 && z < 1000)
        file_num = int2str(z);
        points_filename = strcat(data_file1, '-0', file_num,
'_points.xls');
    elseif (z >= 1000 && z < 10000)
        file_num = int2str(z);

```

```

        points_filename = strcat(data_file1, '-00', file_num,
'_points.xls');
    else
        file_num = int2str(z);
        points_filename = strcat(data_file1, '-', file_num,
'_points.xls');
    end

    % Pixel coordinates of chosen points (x,y)
    points2use = xlsread([data_dir,points_filename],1,'B1:C4');

    % Calculating angle between two lines created from four selected
points
    line_1_x = points2use(1,1)-points2use(2,1);
    line_1_y = points2use(1,2)-points2use(2,2);
    line_2_x = points2use(3,1)-points2use(4,1);
    line_2_y = points2use(3,2)-points2use(4,2);
    line_1 = [line_1_x line_1_y];
    line_2 = [line_2_x line_2_y];
    line_1_2_product = dot(line_1, line_2);
    line_1_length = norm(line_1);
    line_2_length = norm(line_2);
    line_1_2_L = line_1_2_product/(line_1_length*line_2_length);
    line_1_u = line_1/line_1_length;
    line_2_u = line_2/line_2_length;

    if ((line_2_u(2)-line_1_u(2))<0)
        angle = -acosd(line_1_2_L);
    else
        angle = acosd(line_1_2_L);
    end

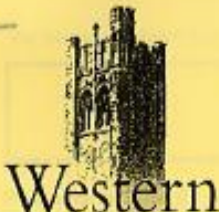
    %output_filename = strrep(points_filename, 'points', 'analyzed');
    %output_write = fullfile(data_dir, output_filename);
    output_write = fullfile(data_dir, [data_file1, '_analyzed.xls']);
    points_analyzed = [line_1 line_2 angle];
    %xlswrite(output_write, points_analyzed, 1);
    range = ['A', int2str(i)];
    xlswrite(output_write, points_analyzed, 1, range);

end

```

## APPENDIX C – ETHICS APPROVAL

The following two Appendices (C & D) are the ethics approvals that were obtained to conduct all of the clinical studies described in Chapters 2 to 5.

	<b>Office of Research Ethics</b> The University of Western Ontario Room 5150 Support Services Building, London, ON, Canada N6A 3K7 Telephone: (519) 881-3036 Fax: (519) 850-2466 Email: ethics@uwo.ca Website: www.uwo.ca/research/ethics							
	<b>Use of Human Subjects - Ethics Approval Notice</b>							
<b>Principal Investigator:</b> Dr. T.R. Jenkyn		<b>Review Level:</b> Full Board						
<b>Review Number:</b> 17353		<b>Revision Number:</b>						
<b>Review Date:</b> August 10, 2010		<b>Approved Local # of Participants:</b> 30						
<b>Protocol Title:</b> Investigation of in-vivo foot and orthotic interactions with using optical motion capture and bi-planar x-ray fluoroscopy								
<b>Department and Institution:</b> Mechanical & Materials Engineering, University of Western Ontario								
<b>Sponsor:</b> NSERC-NATURAL SCIENCES ENGINEERING RESEARCH COUNCIL								
<b>Ethics Approval Date:</b> January 11, 2011		<b>Expiry Date:</b> April 30, 2011						
<b>Documents Reviewed and Approved:</b> UWO Protocol, Letter of Information and Consent Form dated 8 Nov 2010 and Poster								
<b>Documents Received for Information:</b>								
<p>This is to notify you that The University of Western Ontario Research Ethics Board for Health Sciences Research Involving Human Subjects (HSREB) which is organized and operates according to the Tri-Council Policy Statement: Ethical Conduct of Research Involving Humans and the Health Canada/ICH Good Clinical Practice Practices: Consolidated Guidelines; and the applicable laws and regulations of Ontario has reviewed and granted approval to the above referenced revision(s) or amendment(s) on the approval date noted above. The membership of this REB also complies with the membership requirements for REB's as defined in Division 5 of the Food and Drug Regulations.</p> <p>The ethics approval for this study shall remain valid until the expiry date noted above assuming timely and acceptable responses to the HSREB's periodic requests for surveillance and monitoring information. If you require an updated approval notice prior to that time you must request it using the UWO Updated Approval Request Form.</p> <p>During the course of the research, no deviations from, or changes to, the protocol or consent form may be initiated without prior written approval from the HSREB except when necessary to eliminate immediate hazards to the subject or when the change(s) involve only logistical or administrative aspects of the study (e.g. change of monitor, telephone number). Expedited review of minor change(s) in ongoing studies will be considered. Subjects must receive a copy of the signed information/consent documentation.</p> <p>Investigators must promptly also report to the HSREB:</p> <ul style="list-style-type: none"> <li>a) changes increasing the risk to the participant(s) and/or affecting significantly the conduct of the study;</li> <li>b) all adverse and unexpected experiences or events that are both serious and unexpected;</li> <li>c) new information that may adversely affect the safety of the subjects or the conduct of the study.</li> </ul> <p>If these changes/adverse events require a change to the information/consent documentation, and/or recruitment advertisement, the newly revised information/consent documentation, and/or advertisement, must be submitted to this office for approval.</p> <p>Members of the HSREB who are named as investigators in research studies, or declare a conflict of interest, do not participate in discussion related to, nor vote on, such studies when they are presented to the HSREB.</p>								
		Chair of HSREB: Dr. Joseph Gilbert FDA Ref #: IRB 0000940						
<table border="1" style="width: 100%;"> <tr> <th colspan="3">Ethics Officer to Contact for Further Information</th> </tr> <tr> <td><input type="checkbox"/> Janice Sutherland (jsuther@uwo.ca)</td> <td><input type="checkbox"/> Elizabeth Wambolt (ewambolt@uwo.ca)</td> <td><input type="checkbox"/> Grace Kelly (grace.kelly@uwo.ca)</td> </tr> </table>			Ethics Officer to Contact for Further Information			<input type="checkbox"/> Janice Sutherland (jsuther@uwo.ca)	<input type="checkbox"/> Elizabeth Wambolt (ewambolt@uwo.ca)	<input type="checkbox"/> Grace Kelly (grace.kelly@uwo.ca)
Ethics Officer to Contact for Further Information								
<input type="checkbox"/> Janice Sutherland (jsuther@uwo.ca)	<input type="checkbox"/> Elizabeth Wambolt (ewambolt@uwo.ca)	<input type="checkbox"/> Grace Kelly (grace.kelly@uwo.ca)						
<p style="text-align: center;">This is an official document. Please retain the original in your files.</p>								
UWO HSREB Ethics Approval - Revision V 2008-07-01 (pptApprovalNoticeHSREB_REV)		cc: ORE File U-IRB Page 1 of 1						

**APPENDIX D – CRIC APPROVAL****LAWSON HEALTH RESEARCH INSTITUTE****FINAL APPROVAL NOTICE**

RESEARCH OFFICE REVIEW NO.: R-10-576

PROJECT TITLE: Investigation of in-vivo foot and orthotic interactions with using optical motion capture and bi-planar x-ray fluoroscopy.

PRINCIPAL INVESTIGATOR: Dr. Thomas Jenkyn

DATE OF REVIEW BY CRIC: March 16, 2011

Health Sciences REB#: 17353

Please be advised that the above project was reviewed by the Clinical Research Impact Committee (CRIC) and the project:

**Was Approved**

**PLEASE INFORM THE APPROPRIATE NURSING UNITS, LABORATORIES, ETC. BEFORE STARTING THIS PROTOCOL. THE RESEARCH OFFICE NUMBER MUST BE USED WHEN COMMUNICATING WITH THESE AREAS.**

Dr. David Hill  
V.P. Research  
Lawson Health Research Institute

All future correspondence concerning this study should include the Research Office Review Number and should be directed to Sherry Paiva, CRIC Liaison, LHSC, Rm. C210, Nurses Residence, South Street Hospital.

cc: Administration

## APPENDIX E – RAW DATA & STATISTICS

### E1. Static Data

<b>STATIC</b>	<b>(DEG)</b>	<b>Barefoot</b>	<b>STN</b>	<b>Shoe</b>
Normal	Subject 2	84.4	70.8	99.4
Normal	Subject 4	87.6	76.1	90.0
Normal	Subject 6	96.1	91.1	98.5
Normal	Subject 7	96.4	86.3	92.4
Normal	Subject 8	98.4	90.5	100.9
Normal	Subject 23	129.3	113.0	123.3
Cavus	Subject 3	88.3	77.8	83.5
Cavus	Subject 13	128.3	124.1	129.1
Cavus	Subject 15	101.6	88.0	96.8
Cavus	Subject 20	117.4	108.5	112.1
Cavus	Subject 22	118.8	107.9	111.6
Planus	Subject 5	104.4	93.9	94.1
Planus	Subject 16	128.4	116.6	115.2
Planus	Subject 17	135.8	122.2	140.9
Planus	Subject 19	130.9	117.2	133.1
Planus	Subject 24	139.3	120.3	133.9

### E2. Dynamic Data

<b>Foot Type &amp; Subject</b>		<b>Average Foot-flat angle (degrees)</b>						
		<b>Barefoot</b>	<b>Shoe</b>	<b>Foam Soft</b>	<b>Foam Hard</b>	<b>Plaster Soft</b>	<b>Plaster Hard</b>	<b>PFO</b>
Normal	Subject 7	98.3	91.8	104.4	99.6	100.6	101.0	97.0
Normal	Subject 6	103.2	104.2	105.5	109.2	103.6	103.0	107.7
Cavus	Subject 9	119.6	116.8	115.0	119.2	113.9	118.3	115.7
Cavus	Subject 13	130.3	134.0	128.5	135.8	137.9	137.5	131.5
Planus	Subject 16	123.8	118.3	125.8	119.8	119.9	122.5	126.6
Planus	Subject 24	141.3	136.1	125.7	121.9	130.1	136.1	133.3

### E3. Data on Vector Lengths – NTMP & NTMH (Results in Chapter 2)

NORMAL	Trial #	Barefoot	Vector Lengths (mm)		Foot Lengths (cm)	NTMH/L	NTMP/L	
			NTMH	NTMP				
	Subject 4	0	87.61	101.97	111.36	26.7	0.382	0.417
	Subject 6	0	96.05	91.98	119.93	22.9	0.402	0.524
	Subject 7	0	96.40	90.62	105.14	24.1	0.376	0.436
	Subject 8	0	98.43	106.95	88.71	28.1	0.381	0.316
	Subject 23	18	129.28	114.24	150.53	28.2	0.405	0.534
			<b>Mean</b>	<b>101.15</b>	<b>115.14</b>	26	<b>0.389</b>	<b>0.445</b>
				<b>MP/MH</b>	<b>1.14</b>			
PLANUS	Trial #	Barefoot	NTMH	NTMP	(cm)	NTMH/L	NTMP/L	
	Subject 5	1	104.44	104.86	116.23	29.7	0.353	0.391
	Subject 16	4	128.42	95.66	113.13	23.9	0.400	0.473
	Subject 17	22	135.81	97.09	130.28	26.4	0.368	0.493
	Subject 19	9	130.87	99.16	118.81	25.7	0.386	0.462
	Subject 24	2	139.29	105.22	113.13	26	0.405	0.435
			<b>Mean</b>	<b>100.40</b>	<b>118.31</b>	26.34	<b>0.382</b>	<b>0.451</b>
				<b>MP/MH</b>	<b>1.18</b>			
CAVUS	Trial #	Barefoot	NTMH	NTMP	(cm)	NTMH/L	NTMP/L	
	Subject 3	6	88.31	85.49	117.69	21.8	0.392	0.540
	Subject 13	0	128.28	91.33	162.84	23.8	0.384	0.684
	Subject 15	1	101.58	99.95	136.03	24.1	0.415	0.564
	Subject 20	23	117.42	103.11	154.30	26.5	0.389	0.582
	Subject 22	16	118.77	106.09	148.79	25.5	0.416	0.583
			<b>Mean</b>	<b>97.19</b>	<b>143.93</b>	24.34	<b>0.399</b>	<b>0.591</b>
				<b>MP/MH</b>	<b>1.48</b>			

### E4. Chapter 2 - SPSS Outputs

#### Within-Subjects Factors

Measure: MEASURE\_1

static	Dependent Variable
1	Barefoot
2	STN
3	Shoe

**Descriptive Statistics**

	Mean	Std. Deviation	N
Barefoot	111.5844	18.86623	16
STN	100.2575	17.92553	16
Shoe	109.6616	17.89939	16

**Multivariate Tests<sup>b</sup>**

Effect		Value	F	Hypothesis df	Error df	Sig.	Partial Eta Squared
static	Pillai's Trace	.905	66.508 <sup>a</sup>	2.000	14.000	.000	.905
	Wilks' Lambda	.095	66.508 <sup>a</sup>	2.000	14.000	.000	.905
	Hotelling's Trace	9.501	66.508 <sup>a</sup>	2.000	14.000	.000	.905
	Roy's Largest Root	9.501	66.508 <sup>a</sup>	2.000	14.000	.000	.905

a. Exact statistic

b. Design: Intercept

Within Subjects Design: static

**Mauchly's Test of Sphericity<sup>b</sup>**

Measure: MEASURE\_1

Within Subjects Effect	Mauchly's W	Approx. Chi-Square	df	Sig.	Epsilon <sup>a</sup>		
					Greenhouse-Geisser	Huynh-Feldt	Lower-bound
static	.575	7.747	2	.021	.702	.752	.500

Tests the null hypothesis that the error covariance matrix of the orthonormalized transformed dependent variables is proportional to an identity matrix.

a. May be used to adjust the degrees of freedom for the averaged tests of significance. Corrected tests are displayed in the Tests of Within-Subjects Effects table.

b. Design: Intercept

Within Subjects Design: static

**Estimates**

Measure: MEASURE\_1

static	Mean	Std. Error	95% Confidence Interval	
			Lower Bound	Upper Bound
1	111.584	4.717	101.531	121.638
2	100.258	4.481	90.706	109.809
3	109.662	4.475	100.124	119.200

### Pairwise Comparisons

Measure: MEASURE\_1

(I) static	(J) static	Mean Difference (I-J)	Std. Error	Sig. <sup>a</sup>	95% Confidence Interval for Difference <sup>a</sup>	
					Lower Bound	Upper Bound
1	2	11.327*	.949	.000	8.771	13.883
	3	1.923	1.714	.839	-2.694	6.540
2	1	-11.327*	.949	.000	-13.883	-8.771
	3	-9.404*	1.888	.000	-14.490	-4.318
3	1	-1.923	1.714	.839	-6.540	2.694
	2	9.404*	1.888	.000	4.318	14.490

Based on estimated marginal means

\*. The mean difference is significant at the .05 level.

a. Adjustment for multiple comparisons: Bonferroni.

### FOR BETWEEN SUBJECTS ANALYSIS

#### Between-Subjects Factors

	Value Label	N
Foot Category	1.00	6
	2.00	5
	3.00	5

#### Descriptive Statistics

Foot Category		Mean	Std. Deviation	N
Barefoot	Normal	98.6950	15.96923	6
	Planus	127.7660	13.70813	5
	Cavus	110.8700	15.84055	5
	Total	111.5844	18.86623	16
STN	Normal	87.9405	14.71900	6
	Planus	114.0311	11.48424	5
	Cavus	101.2644	18.33846	5
	Total	100.2575	17.92553	16
Shoe	Normal	100.7335	11.85030	6
	Planus	123.4241	18.96446	5
	Cavus	106.6130	17.27203	5
	Total	109.6616	17.89939	16



Multivariate Tests<sup>c</sup>

Effect		Value	F	Hypothesis df	Error df	Sig.	Partial Eta Squared
Intercept	Pillai's Trace	.986	260.131 <sup>a</sup>	3.000	11.000	.000	.986
	Wilks' Lambda	.014	260.131 <sup>a</sup>	3.000	11.000	.000	.986
	Hotelling's Trace	70.945	260.131 <sup>a</sup>	3.000	11.000	.000	.986
	Roy's Largest Root	70.945	260.131 <sup>a</sup>	3.000	11.000	.000	.986
FootType	Pillai's Trace	.655	1.950	6.000	24.000	.113	.328
	Wilks' Lambda	.427	1.945 <sup>a</sup>	6.000	22.000	.118	.347
	Hotelling's Trace	1.149	1.915	6.000	20.000	.128	.365
	Roy's Largest Root	.945	3.780 <sup>b</sup>	3.000	12.000	.040	.486

a. Exact statistic

b. The statistic is an upper bound on F that yields a lower bound on the significance level.

c. Design: Intercept + FootType

## Tests of Between-Subjects Effects

Source	Dependent Variable	Type III Sum of Squares	df	Mean Square	F	Sig.	Partial Eta Squared
Corrected Model	Barefoot	2308.594 <sup>a</sup>	2	1154.297	4.952	.025	.432
	STN	1863.876 <sup>b</sup>	2	931.938	4.099	.042	.387
	Shoe	1471.778 <sup>c</sup>	2	735.889	2.869	.093	.306
Intercept	Barefoot	200809.860	1	200809.860	861.439	.000	.985
	STN	162268.393	1	162268.393	713.632	.000	.982
	Shoe	193074.993	1	193074.993	752.832	.000	.983
FootType	Barefoot	2308.594	2	1154.297	4.952	.025	.432
	STN	1863.876	2	931.938	4.099	.042	.387
	Shoe	1471.778	2	735.889	2.869	.093	.306
Error	Barefoot	3030.426	13	233.110			
	STN	2955.992	13	227.384			
	Shoe	3334.044	13	256.465			
Total	Barefoot	204556.274	16				
	STN	165645.066	16				
	Shoe	197216.631	16				
Corrected Total	Barefoot	5339.020	15				
	STN	4819.868	15				
	Shoe	4805.821	15				

a. R Squared = .432 (Adjusted R Squared = .345)

b. R Squared = .387 (Adjusted R Squared = .292)

c. R Squared = .306 (Adjusted R Squared = .200)

## Multiple Comparisons

Tukey HSD

Dependent Variable	(I) Foot Category	(J) Foot Category	Mean Difference (I-J)	Std. Error	Sig.	95% Confidence Interval	
						Lower Bound	Upper Bound
Barefoot	Normal	Planus	-29.0710*	9.24519	.020	-53.4824	-4.6597
		Cavus	-12.1750	9.24519	.411	-36.5863	12.2364
	Planus	Normal	29.0710*	9.24519	.020	4.6597	53.4824
		Cavus	16.8960	9.65629	.225	-8.6008	42.3928
	Cavus	Normal	12.1750	9.24519	.411	-12.2364	36.5863
		Planus	-16.8960	9.65629	.225	-42.3928	8.6008
STN	Normal	Planus	-26.0906*	9.13094	.034	-50.2003	-1.9809
		Cavus	-13.3238	9.13094	.341	-37.4335	10.7858
	Planus	Normal	26.0906*	9.13094	.034	1.9809	50.2003
		Cavus	12.7667	9.53696	.400	-12.4150	37.9485
	Cavus	Normal	13.3238	9.13094	.341	-10.7858	37.4335
		Planus	-12.7667	9.53696	.400	-37.9485	12.4150
Shoe	Normal	Planus	-22.6907	9.69727	.085	-48.2957	2.9144
		Cavus	-5.8795	9.69727	.819	-31.4845	19.7256
	Planus	Normal	22.6907	9.69727	.085	-2.9144	48.2957
		Cavus	16.8112	10.12847	.257	-9.9324	43.5548
	Cavus	Normal	5.8795	9.69727	.819	-19.7256	31.4845
		Planus	-16.8112	10.12847	.257	-43.5548	9.9324

Based on observed means.

The error term is Mean Square(Error) = 256.465.

\*. The mean difference is significant at the .05 level.

**NTMP****Descriptives**

NTMP

	N	Mean	Std. Deviation	Std. Error	95% Confidence Interval for Mean		Minimum	Maximum	Between-Component Variance
					Lower Bound	Upper Bound			
Normal	5	.4453	.08897	.03979	.3348	.5558	.32	.53	
Planus	5	.4511	.03950	.01766	.4021	.5002	.39	.49	
Cavus	5	.5909	.05508	.02463	.5225	.6592	.54	.68	
Total	15	.4958	.09179	.02370	.4449	.5466	.32	.68	
Model			.06457	.01667	.4594	.5321			
Fixed Effects									
Random Effects				.04758	.2911	.7005			.00596

**Test of Homogeneity of Variances**

NTMP

Levene Statistic	df1	df2	Sig.
1.387	2	12	.287

**ANOVA**

NTMP

	Sum of Squares	df	Mean Square	F	Sig.
Between Groups	.068	2	.034	8.143	.006
Within Groups	.050	12	.004		
Total	.118	14			

### Post Hoc Tests - Multiple Comparisons

#### NTMP

#### Tukey HSD

(I) FootType	(J) FootType	Mean Difference (I-J)	Std. Error	Sig.	95% Confidence Interval	
					Lower Bound	Upper Bound
Normal	Planus	-.00580	.04084	.989	-.1148	.1032
	Cavus	-.14555*	.04084	.010	-.2545	-.0366
Planus	Normal	.00580	.04084	.989	.1032	-.1148
	Cavus	-.13975*	.04084	.013	-.2487	-.0308
Cavus	Normal	.14555*	.04084	.010	.0366	.2545
	Planus	.13975*	.04084	.013	.0308	.2487

\*. The mean difference is significant at the 0.05 level.

### E5. Chapter 3 - SPSS Outputs

#### Paired T-test – within Planus Group

##### Paired Samples Statistics

		Mean	N	Std. Deviation	Std. Error Mean
Pair 1	Barefoot	132.5465	2	12.37602	8.75117
	Shoe	127.1902	2	12.56796	8.88689

##### Paired Samples Correlations

		N	Correla tion	Sig.
Pair 1	Barefoot & Shoe	2	1.000	.000

##### Paired Samples Test

		Paired Differences					t	df	Sig. (2- taile d)
		Mean	Std. Deviati on	Std. Error Mean	95% Confidence Interval of the Difference				
					Lower	Upper			
Pair 1	Barefoot - Shoe	5.35637	.19194	.13573	3.63182	7.08093	39.465	1	.016

## APPENDIX F – CURRICULUM VITAE

### CURRICULUM VITAE MEGAN BALSDON

#### **POST-SECONDARY EDUCATION:**

Master of Engineering Science – Mechanical and Materials Engineering  
*University of Western Ontario (2009 – 2012)*

Bachelor of Science in Engineering – Biological Engineering  
*University of Guelph (2001 – 2006)*

#### **TEACHING EXPERIENCE:**

Teaching Assistant  
MME 9615/BME 9531  
Biomechanics of Human Joint Motion  
*University of Western Ontario (Fall 2010)*

Teaching Assistant  
MME 2213  
Engineering Dynamics  
*University of Western Ontario (Winter 2010 & 2011)*

#### **POSTERS & PRESENTATIONS:**

**Balsdon M.** Bushey K., Dombroski C. Jenkyn T.R. (August 2011). Investigating in-vivo motion of the medial longitudinal arch with different orthotic types using lateral fluoroscopy images during dynamic gait'. American Society of Biomechanics Conference, Long Beach, CA.

**Balsdon M.** & Bushey K. (May 2011). 'Investigations of in-vivo foot and orthotic interactions using optical motion capture and bi-planar x-ray fluoroscopy'. Foot and Ankle Symposium – Fowler Kennedy Sports Medicine Clinic, London, ON.

#### **PRESENTATIONS IN SUBMISSION:**

**Balsdon M.** Bushey K., Dombroski C. Jenkyn T.R. (for August 2012). 'Static Comparison of Subtalar Joint Neutral and Neutral Cushioning Running Shoes to Barefoot Stance using Markerless Radiostereometric Analysis'. American Society of Biomechanics Conference, Gainesville, FL.

#### **PROFESSIONAL WORK EXPERIENCE:**

Process Engineering Intern  
Engineering, Procurement and Construction Management  
*WorleyParsons Minerals & Metals, Mississauga, Ontario (November 2006 – August 2009)*